University Library

A gateway to Melbourne's research publications

Minerva Access is the Institutional Repository of The University of Melbourne

Author/s:
LaTerra, Danilo

Title:
The role of the higher order thalamus during goal-directed behavior and sensory processing

Date:
2019

Persistent Link:
https://hdl.handle.net/11343/238522

Terms and Conditions:
Terms and Conditions: Copyright in works deposited in Minerva Access is retained by the copyright owner. The work may not be altered without permission from the copyright owner. Readers may only download, print and save electronic copies of whole works for their own personal non-commercial use. Any use that exceeds these limits requires permission from the copyright owner. Attribution is essential when quoting or paraphrasing from these works.

The role of the higher order thalamus during goal-directed behavior and sensory processing

Danilo La Terra BSc. MSc.

ORCID identifier: 0000-0002-9480-0134

The Neural Networks laboratory

The Florey Institute of Neuroscience and Mental Health

The University of Melbourne

December, 2019

This thesis is being submitted in total fulfilment of the requirements of the degree of

Doctor of Philosophy

Thesis Abstract

The integration and interpretation of sensorial information is a fundamental requirement for cognition. The thalamus is the sensory gate to the cortex. With its widespread cortical and subcortical connectivity, the thalamus has the network capabilities to function as an integrator of sensory relevant information necessary to drive behavior. Higher order regions of the thalamus send extensive projections to the cortex which exert a powerful influence on cortical encoding of sensory information. However, despite both anatomical and functional evidence, this aspect of thalamic functions has remained largely overlooked likely due to the complexity of investigating thalamocortical circuits in behaving animals. The posteromedial nucleus of the thalamus (POm) is the higher order thalamic nucleus mediating somatosensation. Studies have shown that the POm can modulate sensory processing of cortical pyramidal neurons in the primary somatosensory cortex and drive the cortical plasticity thought to underlie perceptual learning. Despite these reports however, the extent to which POm can influence sensory processing remains unclear and little is known about the role of the POm during sensory-based behavior, let alone goal-directed behavior.

In this thesis, I aimed to investigate the effect of POm modulatory input on the primary somatosensory cortex during sensory encoding and goal-directed behavior and determine how this thalamic influence contributes to correct behavioral performance.

To achieve this, I used a combination of patch clamp electrophysiology, optogenetics and two-photon Ca^{2+} imaging of POm axonal projections in the forepaw area of the primary

somatosensory cortex (forepaw S1) in anaesthetized and behaving mice trained to perform a sensory based goal-directed task.

The work presented in this thesis demonstrates that the activity of POm axonal projections within forepaw S1 encodes correct goal-directed active behavior and dynamically shifts according to task requirements and brain state. In addition, by activating cortical pyramidal neurons either directly or indirectly (through GABAergic interneurons), we show that POm input can both enhance or suppress sensory responses, exerting a powerful modulatory influence over cortical sensory processing. These findings expand the known roles of the higher-order-somatosensory thalamus, from sensory encoding to action selection and flexible switching. Overall, the thalamus is not a simple relay system but mediates complex cognitive functions which are crucial to guide behavior.

Declaration

I declare the following to be true:

- This thesis comprises only original work towards the completion of the Doctor of Philosophy;

- due acknowledgement has been made in the text to all other material used;

- thesis is fewer than the maximum word limit in length;

Signed,

Preface

None of the work towards this thesis has been submitted for other qualifications. None of the work towards this thesis was carried out prior to enrolment in the degree. No third party editorial assistance was sought in preparation of this thesis.

The work presented in chapter 2 was submitted for publication to Nature Neuroscience on August 20th, 2019. In regards to this work, I acknowledge that Dr. L.M. Palmer contributed equally to designing the experiments and writing the manuscript. Chapter 3 includes unpublished material which is in the final stages of manuscript preparation for submission.

I acknowledge the financial support of the Australian Government Research Training Program Scholarship, of the National Health and Medical Research Council through the research training program scheme and the project grants (APP1086082, APP1063533, APP1085708), of the Australian Research Council (DP160103047) and of the Sylvia and Charles Viertel Charitable Foundation.

Acknowledgments

My time in the Neural Networks Laboratory has developed in me a passion for scientific discovery that I will carry for the rest of my life. For imparting this gift, for all the guidance, supervision and your contagious passion for science, I express my sincerest gratitude to my supervisor, associate professor Lucy Palmer.

I would also like to thank my PhD committee members, Dr. Verena Wimmer and Prof. Andrew Lawrence, their input to this work has been instrumental and greatly improved the quality of the experiments and the science presented here.

I would like to extend my deepest gratitude to my friends and colleagues whom I have met during this journey. Especially, I thank Luca Godenzini, who has shared with me uncountable adventures both scientific and non, including these amazing 4 years in Australia. My friend Andrew Micallef who has introduced me to the art of Python coding, among other things, and has always been available for advice and guidance. Thanks to Natasha Pracejus, your constant scientific and moral support has gotten me through the most challenging moments of my PhD.

I am extremely grateful to all my lab mates, who in a way or another have assisted with my experiments, always taking the time to help with electrophysiology, imaging, behavioral or any other technical procedure.

I would also like to thank the Florey and the SOFI community for creating a welcoming and nurturing environment for all national and international students.

Finally, my deepest gratitude goes to my family back home for their constant support without which none of this could have ever been possible. Despite the distance making things a lot more difficult, you have always put my happiness first.

Table of Contents

List of Figures

Chapter 1
General Introduction

1.1 SENSORY-PROCESSING

In the natural environment, animals must combine sensory and non-sensory information in diverse and novel ways according to changing behavioral demands. To achieve this, the brain must integrate sensory information and combine it with experience to construct representations of objects and concepts to ultimately guide behavior[1]. This cognitive function is called sensory processing, is extremely complex and requires great flexibility and computational power to process copious volumes of information at high speed. The classical view of information processing in the brain is based on a hierarchical organization. Starting from the analysis of simple attributes in primary sensory areas, sensory information becomes progressively more complex moving up the hierarchy until a multimodal sensory representation is formed, a perception. Recent findings have radically changed the view of the functional role of top-down interactions in the cortex. The function of any area of the cerebral cortex, including that of primary sensory areas, is subject to top-down influences which modulate the integration of sensory information[2]. Neurons in primary sensory areas do not only encode sensory input, but integrate it with contextual information such as reward[3], expectation[4], attention[5] and motor action[6]. Most inputs to primary sensory cortical areas originate not from primary thalamus, but from higher-order structures. These top-down inputs can carry detailed information about diverse behavioral and cognitive variables[7]. Top-down inputs project heavily to layer 1 (L1), where they synapse on interneurons, and on the apical tuft dendrites of pyramidal cells, amplifying their sensory responses, and enhancing contextually-relevant behavioral outcomes[7].

Sensory processing therefore requires the interaction between bottom-up information coming from the periphery and feed-back modulation coming from higher-order cortical and sub-cortical areas. Establishing how the activity of cortical and sub-cortical regions encode perception and behavior is a complex task and can only be achieved by analyzing brain circuits in a behavioral context[2].

1.1.1 Streams of information through the thalamus

The thalamus is located in a strategic central position and with its extensive connections with virtually every cortical and sub-cortical area, is regarded as the sensory information gate to the cortex[8,9]. The thalamus comprises a multitude of nuclei that attend to different sensory modalities and more complex functions. A number of these nuclei relays modality-specific sensory information directly from the periphery to primary sensory areas in the cortex and for this reason have been termed primary relays or first order nuclei [10]. Examples of these nuclei are the dorsolateral geniculate nucleus that receives visual inputs from the retina and the ventralis basalis nucleus that receives afferent tactile inputs from the trigeminal nucleus. Alongside the first order nuclei, the thalamus contains numerous unspecific nuclei (e.g. the pulvinar and the posteromedial nucleus), which are driven primarily by cortical inputs and to a lesser extent from peripheral sensory inputs. Together these nuclei comprise the higher order thalamus. While the goal of primary thalamic nuclei is the faithful transfer of sensory information to the cortex[11], the higher order thalamus, can act as a coincidence detector of cortical and peripheral inputs[12] and modulate the cortical encoding of sensory information[10]. Historically, the direct sensory input to the cortex passing through the first order thalamic nuclei has been termed feed-forward. Whereas, the

term feed-back has been adopted to define the modulatory input originating within the brain, from cortical areas higher in the processing hierarchy. Feed-back input can reach primary sensory areas in the cortex either passing through the higher order thalamus or directly via cortico-cortical connections[13,14].

1.1.2 Feed-forward and feed-back input targets in the cortex

The cortex is a layered structure that in humans reaches a vertical depth of 2-3 millimeters but whose surface forms the greatest portion of the brain. It generally comprises 6 layers[14] although a more phylogenetically primitive area can be found, the archicortex, which forms the hippocampus and consists only of three layers[15]. The organization of feed-forward and feed-back input within the cortex appears to follow a specific laminar distribution (Figure 1.1). The primary target of the feed-forward input is layer 4 (L4). This layer comprises small cells densely packed and for this reason has been termed the granular layer. From L4, the input then feeds forward to layer 2/3 (L2/3), which then projects down to the output layers of the cortex layer 5 (L5) and layer 6 (L6) [14]. However, Constantinople and Bruno (2013) describe an alternative pathway connecting the primary sensory thalamus directly to L5 and L6[16]. Although the anatomical organization of the feed-forward information stream in sensory cortices appears to follow a general building principle, from a functional perspective, the input separation between layers is likely less demarcated. For example, L4 is known to contain dendrites from L5 and layer 3 (L3) pyramidal neurons and these dendrites may provide alternative pathways to the "standard" input flow[14]. Conversely, feed-back input, either from the thalamus or the cortex, tends to avoid middle layers. Instead, its principal target is the outermost layer of the cortex, L1[13]. The remaining feed-

back input falls into L5 and L6. Studies in the visual cortex, where the contribution of feed-back input to visual processing is better determined, demonstrate that projections from L2/3 neurons of higher visual areas target L5 neurons of cortical areas lower in the processing chain, and this route is suggested to provide a channel for the top-down modulation of attention[14]. Similarly, higher order thalamic nuclei are a major source of feed-back input[10,11,22–26]

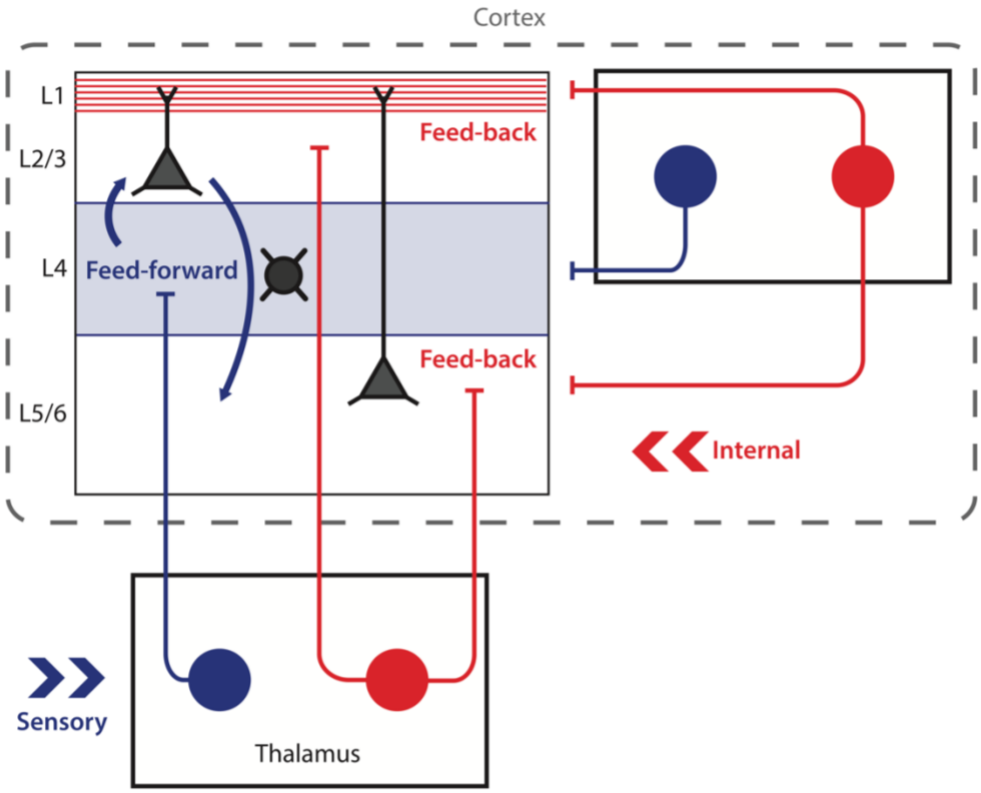

Figure 1.1| Canonical feed-forward and feed-back input connectivity in the cortex The feed-forward stream (blue) is driven by external information passing through the thalamus or through cortical sensory areas. The feed-forward input lands primarily into cortical layer 4, it then feeds forward to L2/3, which in turn projects down to the output layers of the cortex (L5 and L6). The feed-back stream (red) is internally generated from higher order cortical and thalamic regions and innervates cortical L1 and L5.

1.1.3 Cortical pyramidal neurons

Pyramidal neurons are the principal cell type in the cortex comprising approximately 70-85% of the its entire neuronal population[17]. These neurons are found solely in the cortex and reside in all cortical layers except for L1. Pyramidal neurons represent a heterogeneous neuronal population; however, some common features can be found: 1) all pyramidal cells possess a pyramidal shaped soma, 2) they are all glutamatergic excitatory neurons and present numerous spines along the length of their dendrites. 3) from the top region of the soma a primary apical dendrite extends, up to 1 mm in length, towards the upper cortical layers; this dendrite usually reaches L1 where gives off thin collateral branches. This top most region of the apical dendrite is termed tuft and is the recipient of a vast amount of modulatory inputs [18,19]. From the base of the soma, a number of basal dendrites branches off, these are usually directed laterally or downward and mainly receive feed-forward input[20]. Similarly, the axon originates from the basal region of the soma and extends out of the cortical column to other cortical or sub-cortical regions. Thus, on average, pyramidal neurons have their targets at distant locations from their soma[17].

1.1.4 Dendritic integration

The vast majority of synaptic input a pyramidal neuron receives targets its dendrites[21]. When an excitatory input reaches its dendritic target, it triggers an excitatory post-synaptic potential (EPSP). From this distal location, the EPSP must travel to the axon initial segment if it is to contribute to the neuron's action potential (AP) output. At this site, if the depolarization reaches a given voltage threshold, an AP will be initiated[22].

Since the fundamental work by Rall et al (1967), dendritic passive properties have been considered the basic mechanism of dendritic integration[23], whereas less attention was paid to dendritic active currents[24]. According to Rall's models, inputs can be integrated at least in two ways, by sublinear or linear summation. Sublinear integration takes place when two or more inputs occur in a close spatial and temporal proximity due to the diminishing driving force resulting from the membrane potential nearing the reversal potential. Conversely, linear integration occurs to spatially distributed synaptic inputs, a phenomenon that usually involves the entire dendritic tree. However, along with passive properties, dendrites are equipped with voltage and ligand-regulated ion conductances known as "active conductances". Among these, dendritic spikes are all or none voltage events[25], which differ in terms of the ionic current transferred across the membrane: Na^+, Ca^{2+} or mixed ionic current (through NMDA receptors), their spatial arrangement along the dendritic branch and their activation properties [26]. They grant dendrites the ability to increase the impact of incoming inputs performing what is known as supralinear summation, adding an extra level of complexity to the integrative capabilities of pyramidal neurons. Thus, dendritic active properties have important consequences for sensory processing and behavior [13,27–29].

1.1.5 Inhibitory networks influence cortical activity

The remaining 20-30% of cells populating the cortex is made up by interneurons, most of which are inhibitory. An organizing principle of all cortical sensory areas, is the fine inhibitory control these interneurons exert during sensory encoding[30,31]. In fact, cortical excitation and inhibition are two complementary aspects of the same neuronal process.

Even a simple sensory stimulus, like a brief tone, a whisker deflection or an odor leads to the concomitant occurrence of synaptic excitation and inhibition[31]. Inhibitory interneurons locally target other cortical neurons, both excitatory and inhibitory, and mediate their inhibitory control through the release of the neurotransmitter *gamma*-Aminobutyric acid (GABA)[32]. GABA acts on two classes of receptors, $GABA_A$ and $GABA_B$ receptors (R). $GABA_A$Rs are ionotropic channels permeable to Cl^-, they can have a strong effect on the membrane potential *in vivo* and generate a large conductance that shunts the depolarizing effect of excitatory inputs. $GABA_B$Rs are G-protein-coupled receptors which normally work via Gβγ G-protein signaling, and act on Ca channels primarily via direct inhibition of presynaptic voltage gated Ca^{2+} channels (VGCCs), without hyperpolarization[33].

In the neocortex, inhibitory inputs are provided by various interneurons; of particular note, are cells expressing the Ca^{2+} binding protein parvalbumin (PV), the vasoactive-intestinal peptide (VIP) and the peptide transmitter somatostatin (SOM)[34]. PV basket cells form strong inhibitory contacts onto the perisomatic regions of their target pyramidal neurons, exerting a tight control over the timing and magnitude of neuronal output[35]. For instance, feed-forward inhibition mediated by these interneurons rapidly truncates afferent excitation of pyramidal neurons, limiting the temporal window during which action potentials can be generated[36]. SOM interneurons largely consist of cells with axons that form contacts along pyramidal neuron dendritic arbors at distal locations[35]. The best characterized of these interneurons is the Martinotti cell, which has an axon that ramifies extensively in cortical L1, contacting the apical tufts of pyramidal neurons[37]. Notably, SOM interneurons receive facilitating feed-back excitation from neighboring pyramidal cells, which can lead to a progressive supralinear recruitment of more SOM interneurons and corresponding shunting

of excitatory activity[38]. VIP interneurons on the other hand, preferentially form synaptic contacts with other inhibitory interneurons[39–42]. VIP interneurons are predominantly found in superficial cortical layers and are innervated by local and long-range excitatory inputs as well as serotonergic and cholinergic afferents[43–46]. VIP interneurons are strongly recruited by arousing events such as the onset of motor activity[43,44]. In turn, they regulate cortical excitation and sensory response gain through inhibition of pyramidal neurons and other interneurons[43,47].

Cortical interneurons can either be activated locally, by glutamatergic inputs originating from neighboring pyramidal neurons, or by long-range projecting inputs from distal cortical and subcortical regions. The simple connectivity pattern between interneurons and local excitatory pyramidal cells forms the basis for the so-called feed-back or recurrent inhibition[31]. Conversely, excitation of cortical interneurons by long-range inputs generally results in feed-forward inhibition of pyramidal cells[30,48]. Interhemispheric inhibition is a well-documented example of long-range feed-forward inhibitory modulation[48,49]. This important function is mediated by transcallosal fibers and plays an important role in fine motor control[50], visuo-spatial attention[51] and somatosensory processing[52]. Palmer et al (2012) investigated the cellular mechanism responsible for interhemispheric inhibition in the somatosensory system. The authors demonstrated that sensory evoked inhibition was achieved by transcallosal input recruiting specific inhibitory networks in the somatosensory area contralateral to the activated cortex[48]. Interestingly, suppression of pyramidal neurons sensory evoked responses became apparent only when preceded by contralateral cortical activation[48]. It was further discovered that the inhibitory modulation was provided by the activation of post-synaptic $GABA_B$ receptors, presumably by

neurogliaform cells. This cell type is typically located in L1 and targets the distal portion of L5 apical dendrites where it conveys slow inhibition through synaptic inputs expressing $GABA_B$ receptors[48].

In a similar vein, the thalamus can have a strong inhibitory influence on cortical activity via feed-forward inhibition[30,41,53]. For example, anatomical studies indicate that PV, SST, and 5-HT neurons in somatosensory cortex (S1) receive innervation from the posteromedial nucleus of the thalamus (POm), the higher order somatosensory thalamic nucleus[41,53,54]. Input from the POm activates PV and VIP interneurons, but suppresses SST neurons[41,53]. POm input to inhibitory neurons also shows laminar specificity, with PV interneurons having the highest connection probability and response amplitude in layer 5 while VIP expressing interneurons, showing largest amplitudes in superficial layers[30]. Therefore, recurrent and feed-forward inhibition together tightly regulate the activity of excitatory pyramidal neurons (Figure 1.2).

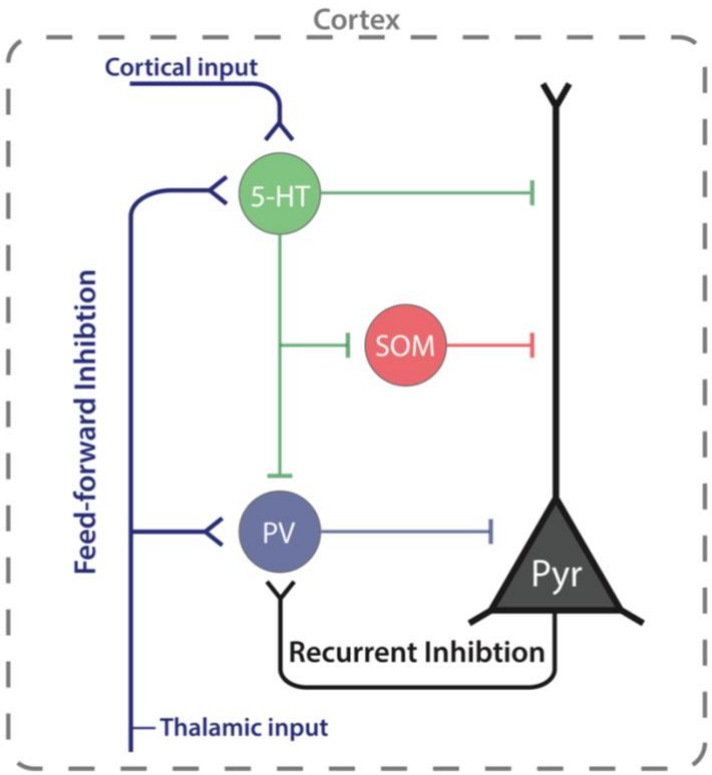

Figure 1.2| GABAergic interneurons regulate pyramidal neurons activity

Schematic illustrating the three major inhibitory interneuron types in the neocortex. Excitatory (+) and inhibitory (-) synapses are shown. Cortical interneurons can be activated locally, by glutamatergic inputs originating from neighboring pyramidal neurons. Here, a perisomatic-targeting interneuron that express parvalbumin (PV, blue) is excited by a neighboring pyramidal cell (Pyr, black) leading to recurrent inhibition, which sharply curtail the generation of somatic action potentials. Similarly, long-range projecting inputs from distal cortical and thalamic regions target serotonergic (5-HT, green) or PV interneurons which in turn shunt pyramidal neurons' activity through feed-forward inhibition. Somatostatin expressing interneurons (SOM, red) are instead more strongly modulated by feed-back input or by local 5-HT and pyramidal neurons.

1.1.6 Sparse coding of superficial cortical layers

Recordings from multiple cortical regions *in vitro* and *in vivo* have shown that L2/3 pyramidal neurons have low spontaneous and evoked firing rates, usually 1 spike per s, and selectively respond to a narrow range of sensory stimuli[55–58]. This singular mode by which superficial cortical networks process information is termed sparse coding[59–62]. In contrast, L5 pyramidal neurons encode information more densely, firing at higher frequencies (5–15 spikes per s) and responding to a wider range of stimuli[55–58]. In the sensory thalamus, spike rates are much higher compared to cortex and neurons respond to a broader range of tactile, visual and auditory stimuli[59,59,60,62]. At the first thalamocortical integration point, in cortical layer 4, this selectivity process is shaped by strong feed-forward inhibition and short integration time windows. In rat somatosensory cortex, Bruno and Sakmann[63] estimated that convergent inputs from ~85 thalamic neurons need to summate in order to drive a single L4 neuron to spike. Why would the brain have evolved such an inefficient and costly system to process information where the vast majority of cortical neurons sits idle the vast majority of time?

Several theories have been proposed. The most intuitive explanation is that sparse coding in a subset of cortical networks improves stimulus selectivity. Supporting this notion, electrophysiological studies in the whisker system have shown that correlated activity within a small subpopulation of ~5–100 cortical neurons is sufficient to signal the presence of a whisker deflection[60]. By the same token, forming associations or storing patterns in memory using local learning rules within a subset of neurons would facilitate information storage[62]. Finally, sparse coding, counterintuitively, could be an energy efficient strategy

to reduce the metabolic cost of generating APs required for neuronal signalling[64,65]. While the significance of sparse coding remains an open question, there is consensus that inhibition plays a crucial role in determining this phenomenon [59,60,62,66]. In rat primary somatosensory cortex, simultaneous activation of a subset of excitatory neurons induces strong, disynaptic, and widespread recurrent inhibition[38,67], which contributes to the sparse population responses characteristic of this cortical region. In auditory cortex, extracellular recordings show that spiking responses in awake, attending animals are suppressed compared to passive listening[68] and similarly, in the olfactory cortex precise timing between excitation and inhibition likely limits the number of evoked action potentials (1.6 per respiratory cycle) elicited by any given odor[69]. The sparsification process arises early in development. The physiological mechanisms underlying this transition are poorly understood, however they are likely linked to the onset of $GABA_A$ receptor current switch from depolarizing to hyperpolarizing and the concurrent surge in feed-forward thalamocortical inhibition, which increases greater than 10-fold[70]. Despite a body of research on this issue now spanning over decades, determining how the concerted activation of sparse ensembles of neurons leads to perception and behavior remains a fundamental question in neuroscience.

1.2 GOAL DIRECTED AND HABITUAL BEHAVIOR

From our daily experience, we know that external sensory stimuli –a smell, a sound, an image- can trigger complex goal-directed responses –dispose of rotten food, start a 100m sprint at the sound of the starter pistol, slow down at a danger sign. Sensory processing is therefore a crucial component of goal-directed behavior[71]. But what defines goal-directed

behavior and distinguishes it from different types of behavioral responses such as habits or simple Pavlovian automatic reflexes?

Surprisingly, characterizing the goal-directedness or habitual nature of an action, and the underlying neural circuits involved, has proven to be challenging, and in some cases, remains controversial. Seminal work by Dickinson and colleagues first laid out the experimental assays to classify a behavior as goal-directed or habitual based on its relationship with the outcome[72,73]. One such experimental manipulation is outcome devaluation. In these tasks, an animal learns that actions can result in the delivery of reward. For example, an animal might learn that pressing one lever will yield a food pellet, while pressing a second lever will deliver water from a spout. In the next stage of the study, the value of one outcome is altered. This change in value may be achieved by changing the animal's motivational state (e.g. altering the animal's degree of hunger or thirst) or through manipulations that alter the intrinsic value of the outcome (e.g. pairing a food with pharmacologically induced illness). The effect of this manipulation on performance of the instrumental action is then tested. Importantly, this test is performed in extinction (i.e. when no further outcomes are delivered), which ensures that instrumental behavior can only be informed by outcome knowledge learned during the initial training, as well as by any change in representation of the current value of the outcome. If the action is driven by the current desirability of the outcome, a decrease in outcome value should result in attenuation of the instrumental response, whereas an increase in value should yield an increase in performance of the action. In contrast, habitual actions, which are thought to involve no processing of outcome value, are insensitive to such manipulations. For example, an animal that continues to press a lever associated with food delivery after having eaten to satiety

would reveal its actions to be habitual, whereas a cessation of lever pressing would reflect a goal-directed evaluation[72,74,75]. In their pivotal study, Adams and Dickinson (1981) were the first to demonstrate that, after rats were trained to press a lever for sucrose, devaluing the sucrose by pairing its consumption with an aversive effect (induced by an injection of lithium chloride) caused a subsequent reduction in performance when the rats were again allowed to lever press in an extinction test. The reduction in performance suggested that the rats encoded the lever press–sucrose association during training and were able to integrate that learning with the experienced change in the value of the sucrose to alter their performance[73]. This demonstration was of central importance because, at the time, the available evidence suggested that lever-press acquisition was controlled solely by sensorimotor learning, involving a process of stimulus-response association. Adams and Dickinson's (1981) finding was the first direct evidence to contradict this view and to suggest that lower mammals, like humans [76], are capable of elaborate forms of encoding behavioral relevant information [73].

A second assay to evaluate the goal-directedness of a behavioral response involves altering the learned contingency between the action and the desired outcome. If an action is goal-directed, the lack of benefit in performing it will reduce the strength of the action-outcome relationship and thus the performance of the action itself. Conversely, a behavior that persists when its action-outcome contingency has been degraded is considered to be habitual[75]. Dickinson and colleagues (1998) provide a classic example of contingency degradation experiment[77]. In this study, hungry rats were previously pre-trained on a positive reinforcing schedule, to press two levers to obtain a food pellet, each lever associated with an equal probability of obtaining the food reward. One group of rats

received a short pre-training (4 sessions) while the second group received a long pre-training (12 sessions). During the pre-training phase, the animals formed an early action-outcome association which was followed by contingency degradation -the omission training. During contingency degradation, one of the levers, the omission lever, was reassigned to postpone the delivery of a sucrose water reward which otherwise would have been delivered after a fixed time-period from lever pressing. The prediction here was that if the behavior was goal-directed, as it turned out to be, the animal would reduce pressing on the omission lever to maximize reward gain. This experiment established that the reversal of the contingency from positive (respond to get the reward) to negative (withhold the response to get the reward) affected undertrained animals, which decreased their response to the omission lever, but not the over-trained group, suggesting that with repetition the behavior becomes habitual and hence resistant to outcome modifications[77].

1.2.1 Brain structures underlying goal-directed and habitual behavior

The goal-directed and habitual systems provide an effective machinery to navigate the uncertainty of an ever-changing environment[78–81]. Novel and complex tasks need be acquired daily; this feat can be achieved thanks to the great flexibility of the goal-directed system although with great energy expenditure. On the other hand, some of these tasks need to be performed routinely, and require precision and mastery. At this stage the habitual system comes into action, through repetition, action planning becomes reflexive, thus greatly lowering the energy demand[78–81]. Shifting between goal-directed and habitual actions is in fact essential for efficient and flexible decision making[82]. However, because they are less flexible habitual behaviors can sometimes lead to maladaptive responses.

Thus, investigating the neural circuits underlying the goal-directed and habitual system is of crucial importance to understand brain dysfunction [72,78,79].

The prelimbic region of the prefrontal cortex (PFC) has been extensively involved in goal-directed learning: Lesions of this area in rats lead to habitual behavior preventing goal-directed learning even at the earliest stages of training[80]. In humans, numerous studies have shown that a homologous region to the rat prelimbic area is the ventromedial (vm) PFC. fMRI investigations have outlined that this area of the human cortex encodes the value of expected rewards associated with specific actions[83–85]. The orbitofrontal cortex (OFC) is another cortical region critical for goal-directed behavior[78]. Lesions of the OFC impaired goal-directed behavior in mice[82], rats[86], and monkeys[87]. Importantly, Gremel and Costa (2013)[82] using simultaneous *in vivo* electrophysiological recording from the OFC and its downstream targets in the striatum showed that neuronal activity in this region correlated with goal-direct behavior, increasing in both the dorsomedial striatum (DMS) and OFC, while the dorsolateral striatum (DLS) was less engaged during goal-directed action. Both lesion and imaging studies suggest that OFC activity is required for goal-directed behavior potentially through downstream signaling to its subcortical targets in the striatum[82]. The striatum is in fact extremely important for the generation and control of motor patterns and is a key structure for both goal-directed and habitual behavior[76,78,79,81]. Numerous studies employing outcome-specific devaluation paradigms have revealed that different sub-regions of the striatum are selectively responsible for generating habitual or goal-directed actions[78]. Lesions of the DMS make mice[82] and rats[88] trained on a goal-directed task, resistant to outcome devaluation and contingency degradation protocols. On the other hand, the DLS is primarily relevant for habitual behavior[78]. Rats with lesions to this region

remained goal-directed even after extensive training. This increased sensitivity to the consequences of actions was observed both with outcome devaluation and contingency degradation procedures. Overtrained rats were unable to adjust their performance when responding caused the omission of reward delivery, whereas inactivation of DLS rendered rats sensitive to this omission contingency[89]. In addition to the dorsal striatum, three sub-cortical structures that play an important role in the motivational aspect of goal-directed and habitual behavior are the nucleus acumbens (NA) the ventral tegmental area (VTA) and the basolateral amygdala (BLS)[78]. The NA forms part of the ventral striatum and together with the VTA is one of the best characterize sub-cortical regions forming the brain's reward system[90]. The amygdala is a subregion of the limbic system, which is involved in learning and memory triggered by emotionally salient experiences such as fear or reward[91]. Lesion studies to any of these sub-cortical regions have shown impairment in goal-directed behavior[78]. Importantly, these regions are strongly interconnected among each other and with the prelimbic and orbitofrontal areas of the PFC[78] thus providing the neural circuit to support the cognitive and motivational flexibility required to acquire and execute complex goal-directed actions.

1.2.2 Thalamic function during goal-directed behavior

As far as we know the structures involved in the acquisition and execution of goal-directed actions examined so far –the prefrontal cortex, the mesolimbic system and the striatum- have no specialized peripheral receptors to gauge the motivational value of a stimulus[92]. This observation raises the question: How and where does the external sensory information meet the internal motivation in the brain?

The thalamus granted its extensive connectivity with multiple cortical and subcortical structures could potentially provide the network necessary for the binding of sensory information relevant for behavior [93]. Historically, the thalamus has been viewed as little more than a passive relay of peripheral information to the cortex having little contribution to cognition[94]. This canonical view has been challenged by numerous studies showing that the thalamus plays an active role during behavior[95–99]. An example of such work is an elegant experiment by Komura et al (2001)[100]. In this study, the authors recorded the activity of a region of the posterior thalamus strongly connected with the amygdala and the temporal cortex in rats trained to perform a delayed stimulus-reward association task. Auditory or visual stimuli were presented for 2s and, after a 1s delay, a spout automatically protruded close to the mouth of the rat. If the rat licked the spout within 2 s after the delay period, the rat could obtain a sucrose water reward. Analysis of the neural activity during the task illustrated that the posterior thalamus encoded the stimulus and its associated reward value by an increase in action potential (AP) firing time locked with the onset of the stimulus. This increase in early activity was modality specific and did not occur for unrewarded stimuli. In addition, a second long-lasting response characterized by a gradual increase in APs firing, which peaked just prior to reward delivery, predicted the reward. This late component of the thalamic response rapidly disappeared during extinction (i.e. when the reward was no longer delivered) as early as after 16 trials. These results strongly suggest that stimulus-reward related computations take place already at the level of the thalamus. Another thalamic region important for reward based behavior is the paraventricular nucleus of the thalamus (PVT)[101]. Photoinhibition of the anterior PVT projections to the nucleus accumbens and amygdala, increased or decreased, respectively,

sucrose seeking, during random reward omission but not when reward was delivered. In agreement with these findings, anatomical studies show that the thalamus receives dopaminergic inputs from the VTA and substantia nigra[102–104], which could provide the modulatory input necessary for reward related computations. Interestingly, a comparative investigation between rat's and primate's thalami has highlighted that the number of dopaminergic receptors of thalamo-projecting dopaminergic neurons is increased in higher mammals[103]. Similarly, the size of the thalamic inhibitory interneuron population targeted by these dopaminergic projections is increased[103]. These findings are insightful for two reasons: First, it is possible that in higher mammals, more complex computations could take place in the thalamus supported by a more developed local inhibitory network and the dopaminergic modulation it receives. Second, the presence of more dopamine receptors in the primate thalamus suggests that manipulations to induce dopamine specific disorders such as parkinsonism or the use of drugs which target the dopaminergic system, such as cocaine or amphetamines, which are usually tested in rodents, might be less effective, due to the rodent rudimentary thalamic dopaminergic system. Hence, these findings invite for extra caution when comparing dopaminergic specific manipulations between rodent models and humans.

In addition to the motivational drive, the smooth initiation and correct execution of an action are fundamental aspects of goal-directed behavior. It is widely accepted that these motor functions are primarily governed by the motor cortex and its cortical-striatal projections[105]. However, the motor cortex is not the only controller capable of generating movements. As emerged from studies in rodents and primates with motor cortex lesions, although dexterity is compromised in these animals, other aspects of motor control survive

remarkably intact[106–108]. In this regard, the thalamus has been shown to contribute to both the correct execution and initiation of motor actions in rodents[109] . Furthermore, specific thalamic regions might be involved in different aspects of the performance of a learned action[109–111]. Examples of such thalamic nuclei are: the parafascicular (PF) and ventroposterior (VP) nucleus[109]. Optogenetic inactivation of PF thalamostriatal projections in the dorsal striatum was sufficient to hinder the initiation of a sequence of movements in mice trained to perform a sequence of lever presses to obtain a reward. Interestingly, once the sequence was initiated, PF terminal inactivation was ineffective to halt the behavioral performance. Conversely, optogenetic axonal inactivation of striatal projecting neurons from the VP nucleus, including the ventroposterior medial (VPM) and posterior medial (POm) nuclei, significantly perturbed both the initiation and execution of the sequence of goal-directed movements[109]. Taken together these findings suggest that the thalamus might play a far richer role in the generation and execution of goal-directed actions which requires further investigation.

1.2.3 Thalamic modulation of cortical activity underlies goal-directed attention

Recent work has highlighted another interesting aspect of thalamic activity, its role in attentional allocation[112]. This cognitive function is required for goal-directed selection and amplification of sensory signals across distributed cortical networks. The thalamus, especially the higher order thalamus, seems to be crucial for carrying out this task[112]. The medial dorsal thalamus (MD) and the pulvinar are particularly important examples in this regard[97,99,113]. The nucleus MD is heavily connected with the PFC and in both rodents and

primates, lesions of this nucleus leads to working memory impairment resembling PFC damage[114–116]. By focusing on the mouse MD in a task in which animals maintained abstract rules during a delay, Schmitt et al (2017) interrogated the role of MD in both sustaining attention and in PFC function[113]. Although MD neurons showed little tuning specificity for the task rule, the sustained input from this nucleus to the PFC was necessary to maintain rule representation by amplifying the activity of rule specific PFC cortical neurons. Similarly, the pulvinar is a fundamental controller of visual attention[99,112]. Given its extensive connectivity within all visual areas, several studies in nonhuman primates have suggested that the pulvinar may regulate activity across these cortical areas during attentional control[117,118]. Saalmann et al (2012) trained macaques on a visuo-spatial attention task in which a spatial cue signaled the location of a subsequent target flanked by distracter stimuli. Simultaneous electrophysiological recordings from multiple visual areas and the pulvinar showed that the higher order visual thalamus synchronized activity between interconnected cortical areas according to attentional allocation[99]. Thus, this study provided the first direct evidence for a thalamic role in coordinating functional interactions across cortical areas. However, while thalamic synchronization and amplification of cortical activity might be useful to achieve certain behavioral outputs, desynchronization and suppression of cortical activity may be equally important and have a strong impact on sensory processing[68,95,119,120]. An example is provided by the rodent barrel cortex, the somatosensory cortical region responsible for whiskers touch sensation[121]. In the barrel cortex, thalamic input increases during active whisking leading to desynchronization of cortical activity[121] which in turn is correlated with a reduction in sensory encoding of cortical pyramidal neurons[122]. Similar findings have been reported in the rodent auditory

cortex, where engaging in an auditory task, which involved the selection and nose poking into one of three nose ports in an operant chamber, reduced sensory encoding of the task relevant auditory cue as compared to passively hearing the same cue[68]. Although preliminary, these findings suggest that thalamic input, by modulating cortical activity, may play a critical role in controlling the functional connectivity and state within and across cortical areas in a task-dependent and flexible way.

1.2.4 Goal-directed/habitual behavior implications for cognitive dysfunction

Dysfunctions of the goal-directed/habitual system have been linked to a number of neuropsychiatric disorders ranging from addiction[123], binge-eating disorder[124], obsessive-compulsive disorder (OCD)[125], schizophrenia[126] and Parkinson's disease (PD)[81]. Imaging studies indicate that abnormal activity of the cortico-striatal circuit involved in goal-directed/habitual behavior is a common feature among these disorders[78,81] . In PD patients, dopamine depletion leads to an over-inhibition of habitual movements[127,128]. In this state of the PD pathology, an excessive inhibitory output of the basal ganglia motor circuit onto the thalamo–cortical, premotor and prefrontal areas results in excessive inhibition of the cortical motor regions and consequent reduction of a range of normally automatic movements -such as blinking, arm swinging, turning in bed, handwriting and making facial expressions-[127,128]. A more profound understanding of the neuronal circuits involved in PD would undoubtedly help the development of more targeted pharmacological treatments. In this regard an interesting case is reversal learning. Reversal learning plays an important part in affective processing and emotional regulation[129]. In healthy individuals, reversal

learning activates the ventral striatum as well as the OFC and the ventrolateral PFC[129]. Reversal learning is impaired in individuals with PD when on dopaminergic medication but not when tested off medication. fMRI investigations have shown that this impairment may be associated with a levodopa-induced disruption of the NA physiological state. In fact, the function of the NA can be disrupted by doses of levodopa that are titrated to improve motor function[130].

Similar to PD, abnormally increased activity and metabolism during resting state were found in the OFC, anterior cingulate cortex, striatum, and thalamus of OCD patients[131–133]. A standard animal model of OCD is the Sapap3-KO mouse, whose behavior is characterized by stereotypic self-grooming[134]. In these mice, grooming continues to the point that the animal develops skin lesions. This grooming behavior may be comparable to the compulsive hand-washing seen in OCD patients. These mice lack SAPAP3, a protein abundant at excitatory synapses that maintains their normal functioning. The absence of SAPAP3 in the dorsal striatum underlies the behavioral phenotype of anxiety and compulsive grooming in Sapap3-KO mice, which not only links these OCD-like behaviors to circuits that control goal-directed and habitual behaviors, but also further links this animal model to OCD patients, who show basal ganglia abnormalities.

In Schizophrenic patients, functional abnormalities in the goal-directed/habitual circuits have been suggested to cause the emergence of negative symptoms[135]. Abnormal activity is found in the striato-thalamo-cortical circuit, which sends modulatory ascending inputs to the PFC and in the limbic-ventral-striatopallidal circuit, which is a key component for the translation of motivation into action. The hypothesis is that a generalized hypofunction of these structures would underlie the behavioral manifestations of apathy, anhedonia,

affective flattening and attentional impairment typical of the Schizophrenic pathology[135]. Parallels have also been drawn between eating-disorders characterized by an exacerbated obsessive-compulsive component such as anorexia nervosa[124] and addictive disorders such as substance dependence[136], both disorders sharing similarities in the inability to cease behaviors despite the adverse consequences. The emerging picture, as expected given the wide range of behaviors controlled by the goal-directed/habitual system, is that circuit dysfunction results in a wide range of disorders characterized by a high degree of comorbidity. Importantly, only the functional investigation of these disorders in animal models will make possible to identify the underlying circuit dysfunction and expedite the design of better psychotherapeutic strategies.

1.3 THE HIGHER ORDER SOMATOSENSORY THALAMUS

The somatosensory system provides an elegant model for studying the neural circuits involved in sensory processing and goal-directed behavior[1]. Although the gold-standard for this type of research has usually been the monkey[1,2], thanks to technological advancement and its genetic versatility, the mouse has become a powerful tool to investigate even the most complex aspects of behavior ranging from working memory, decision making, attention and learning[96,113,137–139].

1.3.1 The mouse forepaw somatosensory system

Even though mice preferentially use their whiskers for spatial navigation and detecting objects[140,141], their forepaws are also extremely important for tactile sensation and have received little attention[142,143]. At the periphery, touching to the glabrous skin of the forepaw

is transduced into electrical action potentials by a wide variety of myelinated sensory afferents, which are Aα, Aβ, Aδ fibers[144]. These neurons synapse in the dorsal horn of the spinal cord and ascend to the cuneate nucleus (CN). Ascending sensory projections from the CN travel across the midline of the brainstem to reach the ventral posterior lateral nucleus (VPL) within the thalamus. The VPL relays to the forepaw and hindpaw regions of the primary somatosensory cortex (S1), while the ventral posterior medial nucleus (VPM) relays to the whisker region of S1. VPL cortical projections follow the standard cortical distribution of feed-forward thalamic input, primarily targeting L4 of the forepaw area (forepaw) of S1[16]. These projections synapse onto principal pyramidal neurons in S1 forming columnar somatosensory maps termed barrels. These structures are particularly prominent for the whisker system but a similar circuit architecture can be found in forepaw S1[145] .

1.3.2 The posteromedial nucleus of the thalamus, projections distribution

Located ventrally to the VPL nucleus in rodents, the posteromedial nucleus of the thalamus (POm) is the higher order thalamic nucleus mediating somatosensation. The POm nucleus is primarily and reciprocally connected with S1(Fig. 1.3) but also sends dense feed-back projections to motor, premotor and association areas[146–150]. The cortical distribution of POm boutons and density of projections was nicely measured by Wimmer et al (2010) using bouton specific and cytoplasmic specific fluorescent proteins[151]. Results from this study showed that POm synaptic inputs are distributed within two prevalent bands in S1, in cortical L1 and in L5. A similar input distribution was reported by Petreanu et al (2009),

who used a channelrhodopsin (ChR2) guided approach to map POm functional synaptic inputs targeting the dendritic trees of L2/3 and L5 pyramidal neurons in S1[152]. In addition, this study found that although POm input prevalently targets the tuft region of pyramidal neurons dendrites in L1, a considerable proportion of them shows a spatially heterogeneous distribution throughout the dendritic tree. In addition, the POm nucleus can be divided into an anterior and a posterior part according to calbindin immunoreactivity[153], with axon fibers of anterior POm neurons being preferentially distributed in L5 of S1, whereas those of posterior neurons principally spread in L1 and showing wider and sparser arborisations.

1.3.3 POm nucleus receives extensive cortical and subcortical modulation

The principal driving input the POm nucleus receives originates from the primary somatosensory cortex[154,155] (S1, Fig. 1.3). Pyramidal neurons from layer 5b of S1 modulate POm activity prevalently during 'up states' resulting in an oscillatory high-low input gain[156]. POm neurons are also weakly but directly modulated by peripheral sensory inputs from the interpolar division of the spinal trigeminal nucleus[157]. Peripheral and cortical inputs can converge onto single POm neurons which are thought to act as coincidence detectors for top-down and bottom-up information[158]. The primary motor cortex (M1) is also directly and reciprocally connected with the POm nucleus [95,159]. In M1, POm projections more densely innervate superficial layers than deeper layers as compared to the projection distribution in S1 [160]. Together with the known connectivity between the POm and the striatum[109], this cortico-thalamo-striatal loop could provide the circuit for the integration and execution of sensory-motor commands.

Another interesting line of research has investigated the top-down modulatory input from the medial prefrontal cortex (mPFC) to the higher somatosensory thalamus[161]. The mPFC does not directly project to POm, instead exerts its modulatory influence indirectly via the activation of the zona incerta, a sub-thalamic region populated by GABAergic neurons which in turn strongly dampens POm activity. Through this disynaptic circuit, the mPFC could potentially control the flow of somatosensory information already at the level of the thalamus[161]. Finally, a few reports have highlighted that POm neuron responses are subject to cholinergic modulation from the brainstem[162] and a very recent study has shown that the superior colliculus, which plays a key role in attention, modulates sensory processing in somatosensory cortex via a powerful disynaptic pathway through the POm[163]. Owing such an extensive cortical and sub-cortical connectivity, the POm nucleus is well positioned to regulate fundamental aspects of sensory information processing necessary to guide behavior.

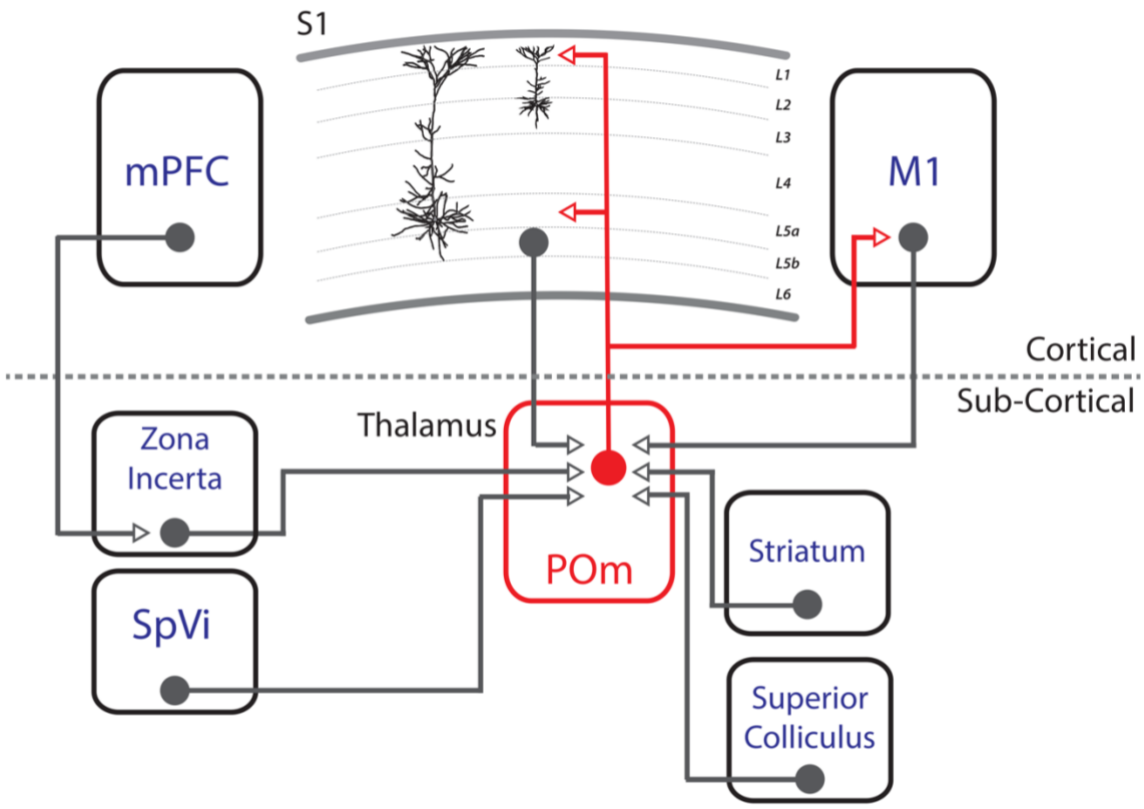

Figure 1.3| Primary cortical and subcortical projections to the POm nucleus
Schematics illustrating the extensive cortical and sub-cortical connections from and to the posteromedial nucleus (POm). POm projects to L5a and L1 (hollow-red-arrowhead). POm receive its major driving input from L5b of S1 (hollow-grey-arrowhead). The primary motor cortex (M1) and medial prefrontal cortex (mPFC) directly or indirectly modulate POm activity. Subcortical structures connected to the POm include the Zona Incerta, the interpolar division of the spinal trigeminal nucleus (SpVi), the striatum and Superior Colliculus. Example L2/3 and L5 pyramidal neurons are shown.

1.3.4 POm influence on cortical activity

The rodent barrel cortex (BC), given its well-characterized anatomy, has served as the main model region to investigate the functional contribution of POm input to sensory processing[12,27,121,152,156,164–166]. Using a combination of whisker stimulation and optogenetic activation of POm axonal projections in BC, studies have revealed that the prevalent effect of POm input in the cortex is excitatory, contributing to the enhancement of sensory responses in both L5 and L2/3 pyramidal neurons[166,167]. Through this mechanism, the POm is thought to extend the responsiveness of principal pyramidal neurons thus facilitating the integration of behaviorally relevant inputs[166]. In a similar line of research, seminal work by Gambino et al (2014) showed that POm input mediates long term potentiation (LTP) of BC pyramidal neurons evoked by rhythmic whisker stimulation[27]. A follow up investigation later revealed that the LTP effect resulted from a complex network interaction in BC initiated by the POm input[164]. POm directly excites VIP interneurons which in turn inhibit SOM interneurons finally releasing principal cells from inhibition. This thalamocortical circuit, which was required to drive cortical plasticity in BC, is also crucial in perceptual learning involving whisker detection[42], although contrasting findings have been reported[168]. In addition to enhancing cortical activity, POm can also mediate cortical inhibition[150,169]. This finding is hardly surprising as POm input is known to target inhibitory interneurons in every layer of S1[41]. To explain these conflicting results, it is important to emphasize that POm neurons both during spontaneous and sensory stimulation, show a broad range of responses[95,120,121]. Inputs of different magnitudes or durations reaching the cortex could have a different impact on cortical processing. In awake behaving animals, on-going spiking activity of POm neurons increases from periods of quiet to active

wakefulness according to the animal's cognitive state[95]. This POm input during active whisking has important consequences for cortical sensory processing as it can desynchronize S1 cortical state[121].

1.4 AIMS OF THE THESIS

As reviewed above, a body of literature suggests that the POm nucleus, the higher order somatosensory thalamus, could play an active role during behavior. This region of the thalamus is highly interconnected with somatosensory, motor, premotor and association cortical areas. At these cortical locations, POm input modulates sensory processing, perceptual learning and possibly sensory-motor integration. Furthermore, the strong afferent drive the POm receives from the mPFC, the cholinergic system and the superior colliculus, indicate that the activity of this thalamic region is under strict attentional control and suggests its potential role in goal-directed behavior. Despite this evidence however, the role of POm cortical input during behavior remains unaddressed. In a similar vein, a few reports in awake animals have highlighted that the spiking activity of POm neurons increases in frequency during active wakefulness and locomotion. In this framework, increased POm input to the cortex could have a dramatic effect on sensory processing. This aspect of POm function also remains to be investigated.

To address these questions:

AIM.1 We sought to characterize POm input activity in forepaw S1 and its contribution to cortical sensory processing during a sensory based goal-directed behavior. To achieve this aim, we used a combination of electrophysiology, two-photon Ca^{2+}imaging and optogenetics in awake behaving mice.

AIM.2 We investigated the influence the POm nucleus has on sensory processing and spontaneous cortical activity in forepaw S1 during sustained POm input activation. To achieve this aim, we used a combination of electrophysiology and optogenetics in anaesthetized mice.

Chapter 2
Higher order thalamus encodes correct goal-directed action

Author contributions

The work presented in this chapter is currently in revision; Contribution from listed authors are as follows;

D. La Terra and **L.M. Palmer** designed the experiments. **D. La Terra** performed and analyzed all experiments. **D. La Terra** and **L.M. Palmer** wrote the manuscript.

Acknowledgments: We would like to thank **Verena Wimmer** for her POm expertise and **Ronny Bergmann**, **Viktor Bahr**, **Jens Kremkow** and **Robert Sachev** for use of their pupil-tracking software.

2.1 ABSTRACT

The thalamus is the gateway to the cortex. Cortical encoding of sensory information can therefore only be understood by considering the influence of thalamic processing of sensory input. Despite modulating sensory processing, little is known about the role of the thalamus during sensory-based behavior, let alone goal-directed behavior. Here, we use patch clamp electrophysiology and two-photon Ca^{2+} imaging to investigate the role of the posteromedial nucleus of the thalamus (POm) axonal projections in the forepaw area of the primary somatosensory cortex (forepaw S1) during sensory processing and goal-directed behavior. We demonstrate that POm axons are active during tactile stimulus and cause a NMDA-dependent response in layer 2/3 pyramidal neurons within forepaw S1, extending the sensory integration window. During tactile goal-directed behavior, activity in POm axons correlates with behavioral outcome, with more robust signaling during correct responses. This activity is important for correct performance, as photoinhibition of archaerhodopsin-expressing neurons in the POm decreased overall behavioral success. Furthermore, changing task contingency altered POm axonal activity in forepaw S1, with larger but less frequent evoked Ca^{2+} transients. Taken together, POm input to forepaw S1 enhances sensory processing in cortical pyramidal neurons and encodes correct goal-directed active behavior

2.2 INTRODUCTION

Goal-directed behavior is crucial for survival in a dynamic environment. It involves the encoding and integration of sensory information that leads to specific rewarded behaviors [1-4]. Since the thalamus sends and receives widespread innervation from almost every

cortical and subcortical structure, it is perfectly positioned to temporally coordinate the binding of information required during behavior [5-7]. Indeed, the thalamus has been shown to play a critical role in cognitive tasks such as attention [8-10], sensory perception [11,12], motor preparation and suppression [13,14] and cortical plasticity [15]. The higher order thalamus is an enigmatic class of non-specific thalamic nuclei which sends feed-back information to sensory cortical areas. Specifically, the posteromedial nucleus of the thalamus (POm) is the higher order thalamic nucleus mediating somatosensation [16,17] which is therefore primarily reciprocally connected with the primary somatosensory cortex [18] but also sends dense projections to motor, premotor and association cortices [5,19-21]. The POm has been shown to influence the encoding of somatosensory inputs [22-24] and drive cortical plasticity crucial for perceptual learning [15,25,26]. Based on these functional roles and known connectivity, the POm may play an important role during goal-directed behavior. To test this, we used patch clamp electrophysiology, two-photon Ca^{2+} imaging and optogenetics, to investigate the role of POm projections in the forepaw S1 during sensory-based goal-directed behavior.

2.3 MATERIAL AND METHODS

All procedures were approved by the Florey Institute of Neuroscience and Mental Health Animal Care and Ethics Committee and followed the guidelines of the Australian Code of Practice for the Care and Use of Animals for Scientific Purposes.

Mice. Wild type C57BL/6 female mice (PN30 - PN80) were used in this study. Mice were housed in groups of 6 in a 12:12 natural light/dark cycle. All behavioral tests were performed during the light phase.

Virus injection. All surgical procedures were conducted under isoflurane anesthesia (~1-2% in O2). Body temperature was maintained at ~36 °C and the depth of anesthesia was monitored throughout the experiment. Mice (~PN30 - 40) were placed in a stereotaxic frame (Narishige) and eye ointment was applied to the eye to prevent dehydration. The skin was disinfected with ethanol 70% and betadine before lidocaine (1%, wt/vol) was topically applied to the wound edges for additional local anesthesia. An incision in the skin (10 mm) was made to expose the skull and a small craniotomy (~0.5 × 0.5 mm) was made over the left posteromedial (POm) complex of the thalamus using the following stereotaxic coordinates: rostrocaudal (RC), −1.7 mm; mediolateral (ML), −1.25 mm; dorsoventral (DV), −3.00 mm from bregma. Virus (60 nl, AAV1.Syn.GCaMP6f.WPRE.SV40; AAV1.CAG.ArchT.GFP.WPRE.SV40; or AAV1.hSyn.ChR2(H134R)-eYFP.WPRE.hGH) was slowly injected from a glass pipette (Wiretrol, Drummond) for at least 5 min using an oil hydraulic manipulator system (MMO-220A, Narishige). The skin was then sutured and Meloxicam (3mg / Kg) was injected intraperitoneally (i.p.) for additional post-operative analgesia and anti-inflammatory action. Mice were then returned to their home cage for recovery.

Chronic cranial window surgery. Mice previously injected with the Ca^{2+} indicator GCaMP6f were anaesthetized (isoflurane, ~1-2 % in O2, vol/vol) and body temperature was maintained at ~36 °C and the depth of anesthesia was monitored throughout the experiment. Eye ointment was applied to prevent dehydration and the top of the head was disinfected with ethanol 70 % and betadine and lidocaine (1 %, wt/vol) was topically applied for additional local anesthesia. The skin covering the skull was removed, and a craniotomy was performed over the left forepaw area of the primary somatosensory cortex (centered at coordinates: RC, 0 mm; ML, -2.3 mm; from bregma). The dura was left intact and a circular coverslip (3 mm diameter) was placed over the open craniotomy and seal-attached to the skull with acrylic glue. A custom-made aluminum head bar (2 x 1 x 0.1 cm) was then attached to the skull for head-fixation using dental cement (C&B metabond, Parkell Inc). Meloxicam (3 mg / Kg) was injected i.p. for additional post-operative analgesia and anti-inflammatory action. Mice were then returned to their cages to recover until behavioral training (~ 2 weeks).

Habituation and behavior. Mice were trained to perform a goal-directed tactile task using a custom made behavioral platform [45]. A three to four day habituation period preceded the beginning of the operant conditioning. During this period mice were handled and acclimatized to the behavioral setup. Mice were head restrained for incremental periods of time until habituated to head restraint. To maximize task engagement, a day prior to the beginning of behavioral training, mice were water restricted (1 ml/day of 10% sucrose water) and from this day onward this water regimen was maintained until the end of the experiment. Behavioral sessions lasted ~ 300 trials during which the mice typically

obtained their daily water intake (1 ml per day) otherwise extra water was supplemented. Ca^{2+} imaging was performed following this habituation phase for naïve data.

Behavioral platform: Mice were head-fixed to the recording frame and their paws rested unaided on either an active (contralateral) or inactive (ipsilateral) rod coupled to a stepper motor driven by an Arduino Uno microprocessor. The stepper motor delivered a pure frequency forepaw tactile stimulus (500 ms, 200 Hz). A water port was used to deliver a water reward (10ul, 10% sucrose water) and licking frequency was recorded via a custom-made piezo-based lick sensor attached to the lick port. All behavioral tests were carried out in the dark while the animal behaviour was monitored with an infrared sensitive camera (Microsoft lifecam). During the first training sessions, mice were habituated to tactile stimulus and reward delivery (typically 1-2 sessions). To establish an association between stimulus and reward, mice were able to self-initiate a trial by licking the water port which instantaneously triggered both stimulus and reward. After this habituation phase, operant conditioning was performed. **Action goal-directed task**: Background white noise (~40 DB) was played for the duration of each trial to signify task onset and mask non-task related sounds. Tactile stimulation (200 Hz, 500 ms) was delivered after a 3-sec baseline period. Following stimulus presentation, mice were given a 1.5 sec interval to report the detection of the tactile stimulus by licking the lickport (response epoch), after which reward was made available and cued by an auditory sound (400 Hz, 200 ms). Mice were then given a 2-sec time window to retrieve the reward after which the trial terminated followed by an inter trial interval (ITI) of randomized duration (between 4 – 7 sec). Only correct responses (licks during the response epoch) were rewarded (HIT) while failure to report stimulus

detection was considered an incorrect response (MISS). Trials with no tactile stimulation (catch trials) were randomly interleaved with stimulus trials. Licking within the response epoch during a catch trial was considered a false alarm (FA) and punished with a timeout of incremental duration (2 - 7 sec) while withhold licking was the correct response which was not rewarded, correct rejection (CR). Implementing catch trials and randomized ITI ensured that animals could not solve the task by adopting a time-based strategy. To facilitate learning, during the first training session the frequency of stimulus/catch trials was set to 90 / 10 %, respectively. The frequency of catch trials was progressively increased up to 40 % and maintained at this ratio until mice could reliably perform at expert level (≥ 80 correct response rate). On average, mice reached expert level within 4.38 ± 0.37 training sessions. **Action-suppression goal-directed task**: Background white noise (~40 DB) was played for the duration of each trial to signify task onset and mask non-task related sounds. As in the action goal-directed task, tactile stimulation (200 Hz, 500 ms) was delivered after a 3-sec baseline period. However, following stimulus presentation, mice were trained to withhold their licking for a 1.5-sec interval. Mice were then given a 2-sec time window to retrieve the reward after which the trial terminated followed by an inter trial interval (ITI) of randomized duration (between 4 – 7 sec). Correct suppression of licking during this epoch was rewarded with sucrose water (10 µl, 10 %). Conversely, if mice licked during this interval (early lick) no reward was delivered and the trial was aborted. Catch trials were used as in the action goal-directed task. Mice learned to reliably suppress licking (≥ 80 % correct response rate) after an average 6 ± 0.85 training sessions (Extended Data Fig. 2.6). **Behavioral switching.** Recordings were performed as mice transitioned from the goal-directed task to the action-suppression task (see above). On average mouse

performance returned to chance level after 2.25 ± 0.47 training sessions on the action suppression task, at which point recordings were performed.

Two photon Ca^{2+} imaging. Imaging of POm axons in forepaw S1 expressing the Ca^{2+} indicator GCaMP6f was performed in awake behaving mice through a chronic cranial window approximately 3 weeks after virus injection. Head-fixed mice were placed under a two-photon microscope (Thorlabs A-scope) and POm axons located 48 ± 6.8 µm below the pia surface were excited using a Ti:Sapphire laser (SpectraPhysics MaiTai Deepsee) tuned to λ = 940 nm and passed through a 16x water immersion objective (Nikon, 0.8 NA). GaAsP photomultiplier tubes (Hamamatsu) were used for detection. The field of view spanned 512 x 512 pixels and images were acquired at 30 Hz. To minimize photo-damage, the excitation power was adjusted online to the minimal value sufficient to record Ca^{2+} transients and the number of imaged trials for a given field of view (FOV) was restricted to a maximum of 40. During each trial, animal behaviour was monitored with an infrared sensitive camera (Microsoft Lifecam). Forepaw position on the tactile stimulator was analyzed post-hoc and any trials where the forepaw was not in contact with the stimulation apparatus were removed from further analysis.

Cannula implant and photo-inactivation of POm complex. For optical inactivation of the POm complex, mice (n = 9) were injected ipsilaterally into the left POm with the inhibitory opsin AAV1.CAG.ArchT.GFP.WPRE.SV40 (60 nl). Following virus injection, a custom-made fiber optic cannula (FT400EMT, 400 um 0.39 NA, 2.5 mm fiber, Thorlabs) was slowly lowered down the injection track using a stereotaxic arm until the desired depth

was reached (2.5 mm from pia). Dental cement (C&B metabond, Parkell Inc) was then applied around the edges of the cannula to secure it to the skull and left to dry for ~ 5 minutes. The same dental cement was used to attach a custom-made aluminum head bar (2 x 1 x 0.1 cm) to the skull for head-fixation. Meloxicam (3 mg/Kg) was injected i.p. for additional post-operative analgesia and anti-inflammatory action. Mice were then returned to their cages to recover until behavioral training (~ 3 weeks).

Behavioral procedures: After recovery, mice were trained on the Action goal-direct task (see Habituation and Behaviour). All behavioral procedures were performed using the Bpod behavioral platform (Bpod State Machine r1, Sanworks). Once mice reached expert level (≥ 80% correct response rate), an optogenetic experimental session was performed. Photo-inactivation of the POm complex was achieved by delivering a light pulse (565 nm, 2-sec, 5 mW) through a 400 µm optical fiber (FT400EMT, Thorlabs) directly inserted into the cannula (FT400EMT, 400 um 0.39 NA, 2.5 mm fiber, Thorlabs). The light pulse was delivered 500 ms prior to stimulus onset to ensure inactivation of the POm complex. A LED light source (LEDD1B, Thorlabs) coupled to a 565 nm LED filter (M565F3, Thorlabs) was used to generate the photo-stimulus while forepaw stimulation (500 ms, 200 Hz) was provided by a stepper motor (Precision Microdrives). A custom-made light shield was placed over the animal's head to prevent scattered light from entering the animal visual field. During a typical experimental session (~300 trials), LED-ON and LED-OFF trials were randomly interleaved at a rate of 50% each. Custom routines in Matlab were used to operate the behavioral platform and data acquisition. For control experiments, mice (n = 9)

were stereotaxically injected into their left POm (see virus injections) with AAV1-PAM MuseeGFP (60 nl) and experiments carried out as above.

Pupil tracking and analysis. To monitor engagement during the task, pupil tracking was performed in a subset of mice (n = 6) previously trained on the Action goal-directed task for the ArchT experiments (see above). Pupil tracking was performed when mice were expert on both the Action task and the Action-Suppression task (see Habituation and Behaviour). Pupil tracking was also performed during the transition between these tasks (switching) when their correct response rate dropped to chance level (~50 %). Mice were head-fixed and the right eye illuminated with infrared light (850 nm LED, Thorlabs). This illumination did not affect pupil diameter. Behavioral sessions were performed on the same apparatus used for two photon imaging inside an aluminum soundproof optical enclosure. However, some illumination (3.48 lux) was provided as we found that the pupil became maximally dilated and a-dynamic in complete darkness**.** An IR sensitive camera (Basler aCA1300-200 um) mounting a 50 mm lens (Kowa 50mm / F2.8) was used to image pupil dynamics at 15 frames per second. Frames were triggered externally using an Arduino microprocessor connected to a Bpod (Bpod State Machine r1, Sanworks) which was then used to operate the behavioral paradigm. Changes in pupil diameter were recorded and measured online using custom routines kindly provided by Bahr, Kremkow, Sachdev and colleagues [46].

In vivo whole cell recordings and photo-stimulation of POm axons in forepaw S1. Approximately three weeks after stereotaxic injection of AAV1.hSyn.ChR2(H134R)-

eYFP.WPRE.hGH (60 nl, see virus injection), mice (n = 10) were initially anaesthetized with isoflurane (~3 % in O2, vol/vol,) before urethane anesthesia (1.3 g/kg of body weight in 20 % saline, Sigma) was administered i.p. Body temperature was maintained at ~36 °C and the depth of anesthesia was monitored throughout the experiment and, when necessary, anesthesia was topped-up with 10 % of the initial urethane dose. Once anesthetized, lidocaine (1 %, wt/vol,) was injected around the surgical site and the mouse head was stabilized in a stereotaxic frame by a head-plate attached to the skull with dental cement (C&B metabond). A craniotomy was then performed above the forepaw area of the primary somatosensory cortex (~1.5 × 1.5 mm square, centered at coordinates: RC, 0 mm; ML, -2.3; from bregma) and the area was then submerged with rat ringer solution containing (135 mM NaCl, 5.4 mM KCl, 1.8 mM CaCl2, 1 mM MgCl2, 5 mM HEPES). In vivo whole cell patch recordings were obtained from L2/3 pyramidal neurons using pipettes with a tip resistance between 6 - 9 MΩ, filled with intracellular solution containing (in mM): 115 K gluconate, 20 KCl, 10 HEPES, 10 phosphocreatine, 4 ATP, 0.3 GTP adjusted to pH 7.3-7.4 with NaOH. Recordings were performed from the soma using a differential amplifier (BVC-700A, Dagan) and were filtered at 10 kHz. Test pulses (10 mV,10 ms) were applied to the pipette in voltage clamp and using maximal pressure the pipette was inserted at 30$_o$ degree-angle into the forepaw area of S1 to a vertical depth of 200 μm after which the positive pressure was decreased to 25-35 mbar and the pipette advanced at steps of 1μm until a cell was encountered (initial access resistance following whole-cell were typically ~50 MΩ). Because the in vivo recordings were performed blind, pyramidal neurons were identified according to their voltage response to current steps. Custom written software in Igor Pro (WaveMetrics) was used for acquisition and no correction was made for the

junction potential between the bath and pipette solutions. On occasion, holding current was applied to the neuron via the whole-cell recording pipette (~50-200 pA) to encourage the neuron to fire more action potentials required for analysis. **Stimulation:** Photo-stimulation of POm axonal terminals expressing ChR2 was achieved by coupling a LED light to a 5x objective (Olympus) to obtain a field of focus roughly the size of the craniotomy (1.5-2 mm in diameter). The objective was focused at the cortical surface and a LED light generator (OptoLED Light Source, CAIRN) was used to deliver a light pulse (10 ms, 470 nm, 60 mW). Stimuli were designed and triggered by custom built software in Igor Pro (WaveMetrics). Forepaw stimulation (500 ms, 200 Hz) was provided by a stepper motor (Precision Microdrives) coupled to a metal pole onto which the animal forepaw rested. POm axons in forepaw S1 and the contralateral forepaw were stimulated in isolation or simultaneously. Interleaved stimuli were delivered at low frequency 0.1 Hz to prevent habituation or sensitization effects.

For pharmacological modulation of NMDA receptors, MK-801 (1 mM, Tocris) was included in the intracellular solution. Typically, the effect of MK-801 became visible over the time course of 4–5min, and remained stable thereafter.

Histology. At completion of each experiment, mice were transcardially perfused with phosphate buffer (PB 0.1M) and 4% paraformaldehyde (PFA) solution. Brains were collected and post fixed overnight (~12 hrs.) in 4 % PFA at 4 ^{o}C before being cut into 200 μm coronal slices using a vibratome (Leica VT1000 Automated Vibratome) and mounted on glass slides using mounting medium containing nuclear staining dye DAPI (Fluoroshild, Sigma). Images of the brain slices were acquired using wide-field fluorescent microscopy

(Zeiss Axio Imager 2). Images were taken such that excitation light (EYFP, 555 nm; DAPI, 430 nm) was optimized below the maximum pixel saturation value for each fluorophore. To evaluate virus (GCaMP6f, ArchT and ChR2) expression profiles in the POm complex, images of brain sections were registered to the corresponding coronal plates of the Paxinos mouse brain atlas [47]. Data from out of target injections or failed viral expression were removed from further analysis.

Data analysis and statistical methods.

Ca^{2+} data. All analysis was performed using ImageJ and custom written routines in Matlab or Python. Horizontal and vertical drifts of imaging frames due to animal motion were corrected by registering each frame to a reference image based on whole-frame cross-correlation. The reference image was generated by averaging frames for a given field of view (FOV) in which motion drifts were minimal. Region of interests (ROIs) of axonal shafts or buttons were manually selected using the standard deviation of the entire imaging session (~ 6000 – 8000 frames). ROIs were selected so that each ROI represented a single POm axon. To calculate the baseline fluorescence (F_0) for each ROI, first the average baseline florescence intensity (across 60 frames prior to stimulus onset, 2 seconds) of each trial was taken. Second, the rolling median of these average baseline values was measured and used as F_0. Fluorescence traces are expressed as relative fluorescence changes, $\Delta F/F = (F - F_0)/F_0$. Only Ca^{2+}transients which were greater than 2x the baseline standard deviation $(F_0 + (2x\ s.d.))$ and above the threshold for a period longer than 200 ms were selected. The onset of a Ca^{2+} transient was defined as the time point at which a transient crossed the detection threshold $((F_0 + (2x\ s.d.))$. Average Ca^{2+} transient probability was

measured as $((\frac{\Sigma\, events}{time}) / \Sigma\, trials)$. The peak amplitude (ΔF/F) was measured as the local maxima between the event onset and offset (i.e. when the falling edge of the transient crossed the threshold again). The duration (ms) of a Ca^{2+} transient was calculated as the time between the event onset and offset. Three behaviorally relevant epochs were selected (1 second duration) for *spontaneous activity* (-2 to -1 sec, relative to stimulus onset); for *evoked activity* (0 to +1 sec, relative to stimulus onset) and for *reward activity* (+2 to +3 sec, relative to reward delivery). For probability comparisons, all ROIs were used, while only the subset of ROI with detectable events (greater than the threshold) were used to measure amplitude and duration. For direct comparison of spontaneous and evoked Ca^{2+} amplitude and duration, the subset of active axons with detectable Ca^{2+} events during these two behavioral epochs were used. Finally, to calculate the spontaneous Ca^{2+} frequency and amplitude in Action vs Switch (Fig. 5H and 5I), the entire (3s) spontaneous epoch duration was used.

Electrophysiology. During whole-cell recordings, custom-written Igor software (WaveMetrics) were used for both acquisition and analysis. A cell was selected for analysis if both ChR2-evoked and tactile-evoked subthreshold responses could be reliably measured. Net depolarization was calculated by first subtracting the baseline from raw intracellular membrane potential traces. To minimize the effect of up and down states, the baseline was measured as the mean membrane potential 20 ms before stimulus onset. Normalized traces were then split according to their stimulation protocol (forepaw stimulation; POm photoactivation; forepaw + POm photoactivation) and averaged. The magnitude of the sensory response was measured as the integral of the averaged evoked subthreshold voltage envelope (between 0 and +1 sec relative to stimulus onset). The

average action potential frequency was measured for spontaneous firing and evoked firing (between -4 to -2 sec and 0 to +1sec, relative to stimulus onset, respectively). The average peak amplitude and duration were measured as the local maxima and halfwidth of the average subthreshold voltage response between 0 and +1-sec relative to stimulus onset, respectively.

Pupil tracking. Videos of pupil tracking and animal behaviour were acquired and checked post hoc to remove potential artifacts due to sudden eyelid closing. Analysis of pupil dynamics were performed using a custom written algorithm in python. Briefly, pupil tracking for the entire session was split into single trials (11-sec duration) according to behavioral outcome. The average response profile was then calculated for each trial type for each mouse. Pupil dilation was monitored during a 4-sec baseline period preceding the beginning of each trial. The average peak diameter was measured as the local maxima of the average pupil response during the baseline epoch (-4 to 0 sec, relative to trial start), pre-stim epoch (-3 to 0 sec, relative to stimulus onset), stimulus and response epoch (0 to +2 sec, relative to stimulus onset) or post stim epoch (0 to +4 sec relative to stimulus onset).

Behavior. The correct response rate was determined as the fraction of correct trials over the total number of trials (HIT or correct suppression trials + correct rejection trials)/(stimulus trials + catch trials). Hit rate was measured as the ratio of HIT trials/stimulus trials and false alarm (FA) rate was measured as the ratio of FA trials/catch-trials. The behavioral effects of POm photo-inactivation were quantified by comparing the correct response rate of photo-inactivation (LED-ON trials) vs. control (LED-OFF) trials, typically 150 each per experimental session. The latency to first lick was calculated as the time of first lick occurrence after stimulus onset.

Statistical analysis. All statistics were performed using Prism software. The α significant level was set at 0.05. Normality of all value distributions was assessed by Shapiro-Wilk test (α = 0.05). Standard parametric tests were used only when data passed the normality test (p > 0.05). Non-parametric tests were used otherwise. Only two-sided tests were used.

2.4 RESULTS

Ca^{2+} imaging of POm axonal projections in forepaw S1 was performed in mice (p50-70) previously injected with the Ca^{2+} indicator GCaMP6f (AAV1.Syn.GCaMP6f.WPRE.SV40) into the POm nucleus (see Methods; Fig. 2.1a). Following expression, Ca^{2+} transients were recorded from POm axons that project to layer 1 of the forepaw S1 (48 ± 6.8 µm from the pia surface). These POm axons were sparsely spontaneously active in awake naive mice, generating large Ca^{2+} transients (>2 s.d of the baseline fluorescence; see Methods) at 0.08 ± 0.01 Hz (n=113 axons; Fig 2.1b). To test the POm involvement in sensory encoding, axonal Ca^{2+} transients were investigated during forepaw tactile stimulus (200 Hz, 500 ms; Fig. 2.1c). Here, POm axons significantly increased Ca^{2+} signaling above the spontaneous rate, evoking a response to 21.26 ± 2.22 % of forepaw stimuli (p < 0.0001; n = 113; Fig. 2.1d). These sensory-evoked Ca^{2+} transients were not significantly different in amplitude (1.15 ± 0.08 vs 1.12 ± 0.10 ΔF/F; p = 0.4078) nor duration (0.636 ± 0.878 vs 0.686 ± 0.142 s; p = 0.6761; n = 44 active axons, see Methods) to spontaneous events (Fig. 2.1e).

We next tested the influence of this evoked POm input on the processing of sensory information in the somatosensory cortex. Patch clamp recordings were performed from layer 2/3 (L2/3) pyramidal neurons in the forepaw S1 in urethane (1.3g/Kg) anaesthetized

mice which were previously injected with the excitatory opsin, ChannelRhodopsin2, in the POm (Fig. 2.1f). Photo-activation of POm axons with a single brief LED pulse (10 ms, 470 nm) evoked a large bi-phasic somatic sub-threshold voltage response (amplitude, 8.4 ± 1.48 mV; integral, 1.8 ± 0.27 mV·s; n = 19; Fig. 2.1g). This POm-evoked somatic voltage response was NMDA-channel dependent as including the NMDA channel blocker, iMK801 (1mM) in the patch pipette significantly decreased the peak voltage amplitude (iMK801, 3.9 ± 0.64 mV; p = 0.0262; n = 7; Fig. 2.1h-i). To investigate the effect of POm input during sensory processing, POm axons in forepaw S1 were photo-activated simultaneously with tactile stimulus delivered to the contralateral forepaw. Tactile stimulation (200 Hz, 500 ms; FP) evoked a large sub-threshold voltage response (amplitude, 12.61 ± 1.65 mV) and action potentials (1.38 ± 0.7 Hz) in L2/3 pyramidal neurons (n=19; Fig. 2.1j). When POm axons were photo-activated simultaneously with tactile stimulus (FP + POm), the evoked sub-threshold voltage response increased significantly in duration (FP, 182 ± 20 ms; FP + POm, 277 ± 32 ms; p = 0.0108; Fig. 2.1k) but not peak amplitude (FP, 12.1 ± 1.67 mV, FP + POm, 13.8 ± 2.15 mV, p = 0.2412; n = 19; Fig. Extended Data Fig. 2.1). Taken together, activation of POm input to the forepaw S1 leads to an increase in the duration of the sensory-evoked subthreshold voltage response in L2/3 pyramidal neurons, extending the period for sensory integration. This increased integrative window is NMDA dependent as including the NMDA channel blocker, iMK801, in the patch pipette prevented the increased duration of the tactile voltage response during POm photo-activation (FP, 174 ± 17 ms; FP + POm, 243 ± 60 ms; n = 7; p = 0.4692; Fig. 2.1l).

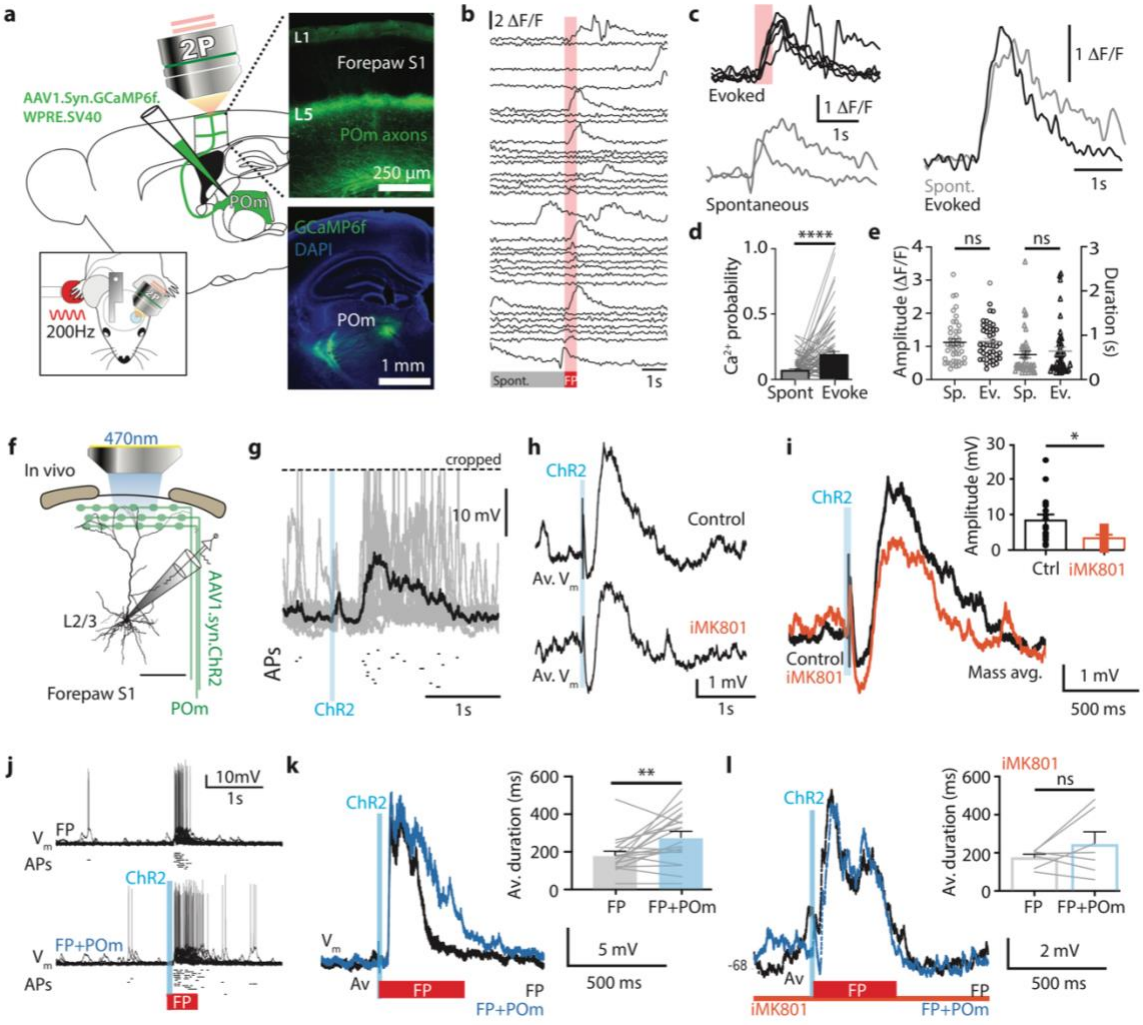

Figure 2.1| POm axonal projections in forepaw S1 encode sensory information and modulate sensory processing.

a, Experimental design. The Ca^{2+} indicator GCaMP6f was locally injected into the POm and two-photon Ca^{2+} imaging was performed from POm axons projecting to layer 1 of forepaw S1 during tactile stimulation. Post hoc fluorescence images illustrating (top) that POm primarily sends axonal projections to layer 1 and layer 5 of the forepaw S1 and (bottom) localized POm injection. **b**, Ca^{2+} traces from a representative POm axon in layer 1 of forepaw S1 in the naïve awake state during forepaw stimulation (FP; 200Hz, 500ms).

c, Left, evoked (black) and spontaneous (grey) Ca^{2+} transients from POm axon in (b). Right, Overlay of average evoked (black) and spontaneous (grey) Ca^{2+} transients. **d**, The probability of evoking a Ca^{2+} transient during forepaw stimulation versus spontaneous activity (n = 113 axons). **e**, Spontaneous (Sp.) and forepaw-stimulus evoked (Ev.) Ca^{2+} transient amplitude and duration (n = 44 axons). **f**, Experimental design. *In vivo* whole-cell patch clamp recordings were performed from L2/3 pyramidal neurons in forepaw S1 during photoactivation (460 nm, 10 ms) of ChR2-expressing POm axons. **g**, Top, Voltage responses from a typical L2/3 pyramidal neuron evoked by brief (10ms) photoactivation of POm projection axons in forepaw S1. Average, black. Bottom, Raster of evoked action potentials. **h**, Mass average voltage response from L2/3 neurons during photoactivation of ChR2 expressing POm axons in forepaw S1 during control (top, n = 19) and with the NMDA-channel blocker, MK801, included in the intracellular solution (Bottom, iMK801, n = 7). **i,** Overlay of examples in (h). Inset, Amplitude of the voltage responses in L2/3 pyramidal neurons during photoactivation of POm axons during control (black) and iMK801 (orange). **j**, Example of voltage responses in a L2/3 pyramidal neuron during forepaw stimulation alone (FP, top) and paired with photoactivation of POm axons (FP + POm; bottom). Bottom, Raster of evoked action potentials. **k**, Overlay of average evoked subthreshold voltage response from example in (j). Inset, Average duration of evoked voltage response to FP and FP+POm. **l**, Overlay of example average voltage response in a L2/3 pyramidal neuron filled with MK801 during forepaw stimulation alone (FP; black) and paired with photoactivation of POm axons (FP + POm; blue). Inset, Amplitude of the voltage responses to FP and FP + POm in L2/3 pyramidal neurons filled with MK801 (n = 7). *P < 0.05, **P < 0.01, ****P < 0.0001.

Is POm input involved in sensory-based behavior? To test this, two-photon axonal Ca^{2+} imaging was performed in mice (p50 - 70) trained in a goal-directed tactile detection task. Mice previously injected with the Ca^{2+} indicator GCaMP6f into the POm were trained to associate forepaw tactile stimulation (200 Hz, 500 ms) with a reward (see Methods; Fig. 2.2a). Here, if mice correctly responded by licking a reward port within 1.5 sec after receiving the tactile stimulus, a sucrose water reward (10% sucrose water) was delivered (HIT). We refer to this behavioral paradigm as 'action' goal-directed task. Mice rapidly learnt this task, taking on average 4.38 ± 0.37 days to reach expert level (> 80 % correct responses to tactile stimulation; Extended Data Fig. 2.2). Once expert, Ca^{2+} transients were recorded from POm axons within forepaw S1 while the mouse performed the task. During the goal-directed behavior, large Ca^{2+} transients were evoked in POm axons within S1 (amplitude, 1.26 ± 0.048 $\Delta F/F$; duration, 665 ± 35 ms; n = 199 active axons; Fig. 2.2b). Although these evoked Ca^{2+} transients were not different from those evoked in the naïve state (Extended Data Fig. 2.3), there was a two-fold increase in the number of active POm axons during HIT behavior (HIT, 90 % vs naïve, 39 %, Fig. 2.2c). Furthermore, the overall evoked activity in POm axons (n = 222) was significantly increased in rate (HIT, 37 ± 2 vs naïve, 21.3 ± 2.22 % of trials; n = 113; $p < 0.0001$; Fig. 2.2d), illustrating that during correct goal-directed behavior, POm increases the behaviorally-evoked information transferred to S1. We next assessed whether POm activity is altered during incorrect behavioral performance (MISS). Despite performing at expert level, mice missed responding to on average 12.63 ± 6.63 % of tactile stimuli. Compared to correct behavior, the probability of evoking a Ca^{2+} event in response to stimulus during these MISS trials was significantly reduced by 40 % (22.3 ± 4.4 % of trials; n = 66 axons; $p = 0.0001$; Fig. 2.2e).

Taken together, POm encodes behavioral performance, increasing the effective connectivity between POm and forepaw S1 during correct behavior in a tactile goal-directed task.

To monitor cognitive engagement during the goal-directed task, dynamic changes in pupil diameter were recorded (Fig. 2.2f). Compared with catch (no stimulus) trials, pupil dilation was significantly increased during HIT responses (0.49 ± 0.08 mm vs. 0.38 ± 0.06 mm; $p = 0.0312$; n = 6 mice; Fig. 2.2g) and peaked (0.5 ± 0.08 mm) during the delivery of the water reward (2.18 ± 0.2 s after stimulus onset). During reward delivery, maximum pupil dilation coincided with a significant increase in licking frequency (reward, 7.19 ± 0.915 Hz vs response (HIT), 5.18 ± 0.75 Hz, $p = 0.0392$; n = 8 mice; Fig. 2.2h). However, despite maximum pupil dilation and licking (motor) output, the evoked rate of POm Ca^{2+} activity was significantly reduced during reward delivery compared with stimulus presentation and behavioral response (11.3 ± 1.08 % of stimuli; $p < 0.0001$; n = 222 axons; Fig. 2.2h). This indicates that POm input does not strongly correlate with pupil dynamics during reward delivery, but preferentially conveys behaviorally relevant information to S1 during the stimulus-response epoch.

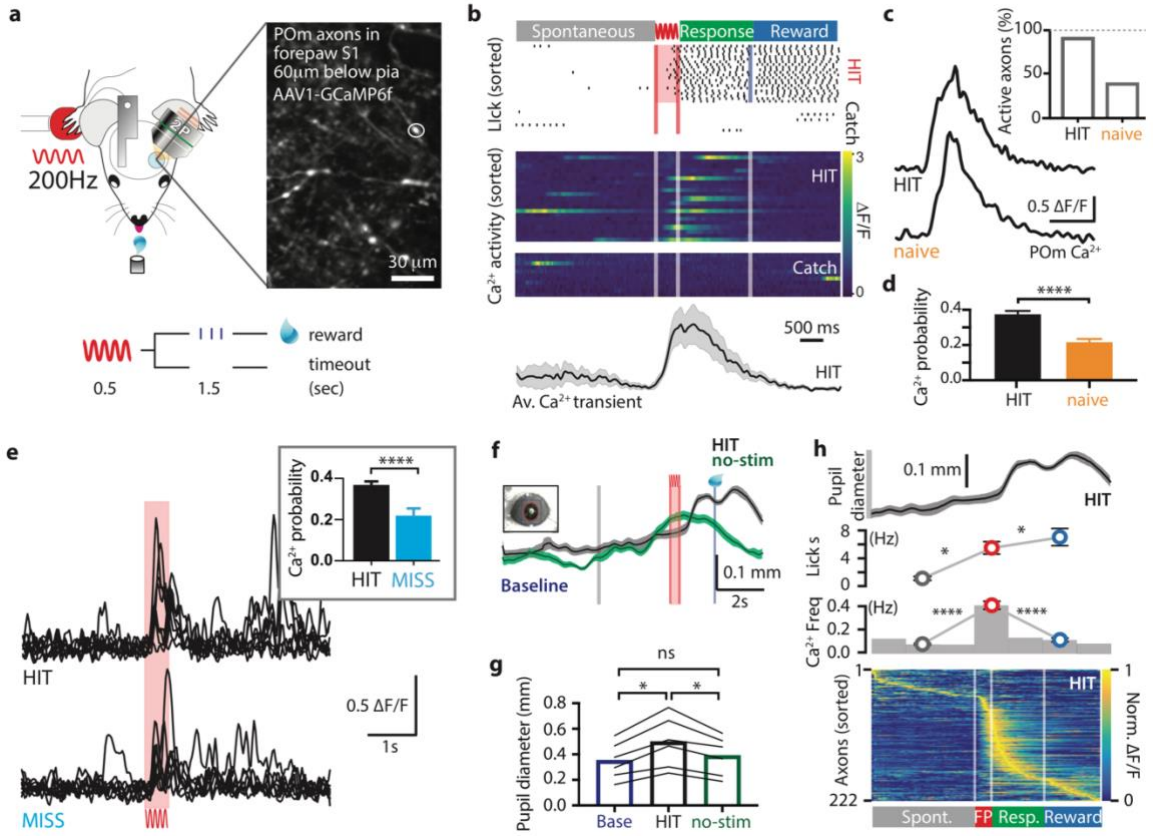

Figure 2.2| POm increases the effective connectivity with forepaw S1 during correct goal-directed behavior

a, Behavioral task design. Two-photon Ca^{2+} imaging of GCaMP6f-expressing POm axons in forepaw S1 was performed in head-restrained mice trained to report the detection of a tactile stimulus (200Hz, 500ms) by licking a reward port. Correct responses (HIT) were rewarded with sucrose water reward (10µl, 10% sucrose). **b**, Top, Raster plot showing a typical behavioral response (licks) sorted into correct HIT performance and Catch (no-stimulus) trials. Grey, spontaneous; red, tactile stimulus; green, response epoch; blue, reward epoch. Blue line, reward delivery. Middle, Ca^{2+} activity pattern during HIT and Catch trials from example POm axon in (a). Bottom, Mass average Ca^{2+} activity with SEM (shaded area) during HIT trials from axon in (a). **c**, Example of average stimulus-evoked Ca^{2+} transients during HIT trials (Top) and naïve (Bottom). Inset, The percentage of active POm axons is greater during HIT trials compared to naïve.

d, Probability of evoking a Ca^{2+} response to forepaw stimulation during correct behavior (HIT, black, n = 222) compared with naïve state (orange, n = 113 axons). **e**, Ca^{2+} responses from a representative POm axon during correct HIT (Top) and incorrect MISS (Bottom) trials. Inset, the probably of evoking a Ca^{2+} transient in the stim/response epoch during HIT and MISS behavior (n = 66 axons). **f**, Example of average pupil diameter with SEM (shaded area) during HIT (black) and Catch (no stimulus, green) trials. Grey line, start of trial; red lines, stimulus; blue line, reward delivery. **g**, Average peak pupil diameter during the stimulus/response epoch in HIT (black) and no-stim (green) trials compared with baseline (dark blue; n = 6 mice). **h**, Top, Average pupil dilation during HIT responses from (f). Grey line, start of trial. Middle, Average lick frequency during spontaneous (grey), stim/response (red) and reward (blue). Middle, Histogram of Ca^{2+} transient frequency. Bottom, Normalized average Ca^{2+} activity pattern during HIT trials for all POm axons (n = 222) sorted according to the time of peak amplitude. Data is shown as individual values or average with SEM. *P < 0.05, ****P < 0.0001.

Goal-directed behavior requires motor actions to be suppressed once they are no longer appropriate to achieve the current goal [17]. To investigate the involvement of the higher order thalamus during suppression of a previously learned goal-directed action, we performed Ca^{2+} imaging from POm axons during a modified goal-directed paradigm. Here, mice previously injected with the Ca^{2+} indicator GCaMP6f in the POm were trained in the 'action' goal-directed task (as above). Once expert (> 80 % correct responses to tactile stimulation), the behavioral paradigm was changed such that the mice only received the reward if they suppressed licking in response to the tactile stimulus (Fig. 2.3a). We refer to this behavioral paradigm as 'action-suppression' goal-directed task. Despite the enforced behavioral (licking) suppression, mice were highly engaged during the task as illustrated

by pupil tracking during the behavior. When compared with the action goal-directed task, there was no significant difference in peak pupil dilation during baseline (0.32 ± 0.05 vs 0.29 ± 0.06mm, p = 0.3121, n=6), pre-stim (0.35 ± 0.06 vs 0.31 ± 0.07mm, p = 0.2193), and post-stim (0.44 ± 0.07 vs 0.41 ± 0.09 mm; p = 0.6872; Fig 2.3b). POm projections in S1 were highly active during correct performance of the action-suppression task (Fig. 2.3c). These evoked POm Ca^{2+} transients had the same properties as those evoked during the action goal-directed task (amplitude, 1.19 ± 0.06 vs 1.26 ± 0.05 ΔF/F, p = 0.3812; duration, 623 ± 50 vs 666 ± 35 ms, p = 0.2234, n = 109/199 axons, Fig. 2.3d and e). However, during action-suppression, the probability of signaling was significantly decreased (by 34.9 %; p < 0.0001; n = 144 axons Fig. 2.3e) to a rate that was not significantly different to the evoked rate in naïve mice (24 ± 2.4% of trials; p = 0.9022). These results highlight a decrease in POm projection activity when action is suppressed, suggesting that indeed, POm encodes active behavior. Taking this into account, we again investigated the influence of behavioral performance on POm activity by directly comparing evoked Ca^{2+} activity during licking in response to stimulus presentation in correct (action goal-directed task) versus incorrect (action suppression goal-directed task) responses. Here, the lick frequency during correct behavior was significantly higher compared to incorrect behavior (5.18 ± 0.7 vs. 2.36 ± 0.4 Hz; p = 0.0109; n = 8/5 mice; Extended data fig. 2.7) but the behavior goal (licking for reward) is the same, but the outcome (obtaining the reward) differs (Fig. 2.3f). Using this comparison, POm activity is highly correlated with behavioral outcome, significantly increasing by 48.1% in evoked rate during correct opposed to incorrect performance (p < 0.0001, n = 222/79 axons, Fig. 2.3f). These results add further support to the finding that the fidelity of POm input to forepaw S1 is enhanced during correct stimulus evoked action.

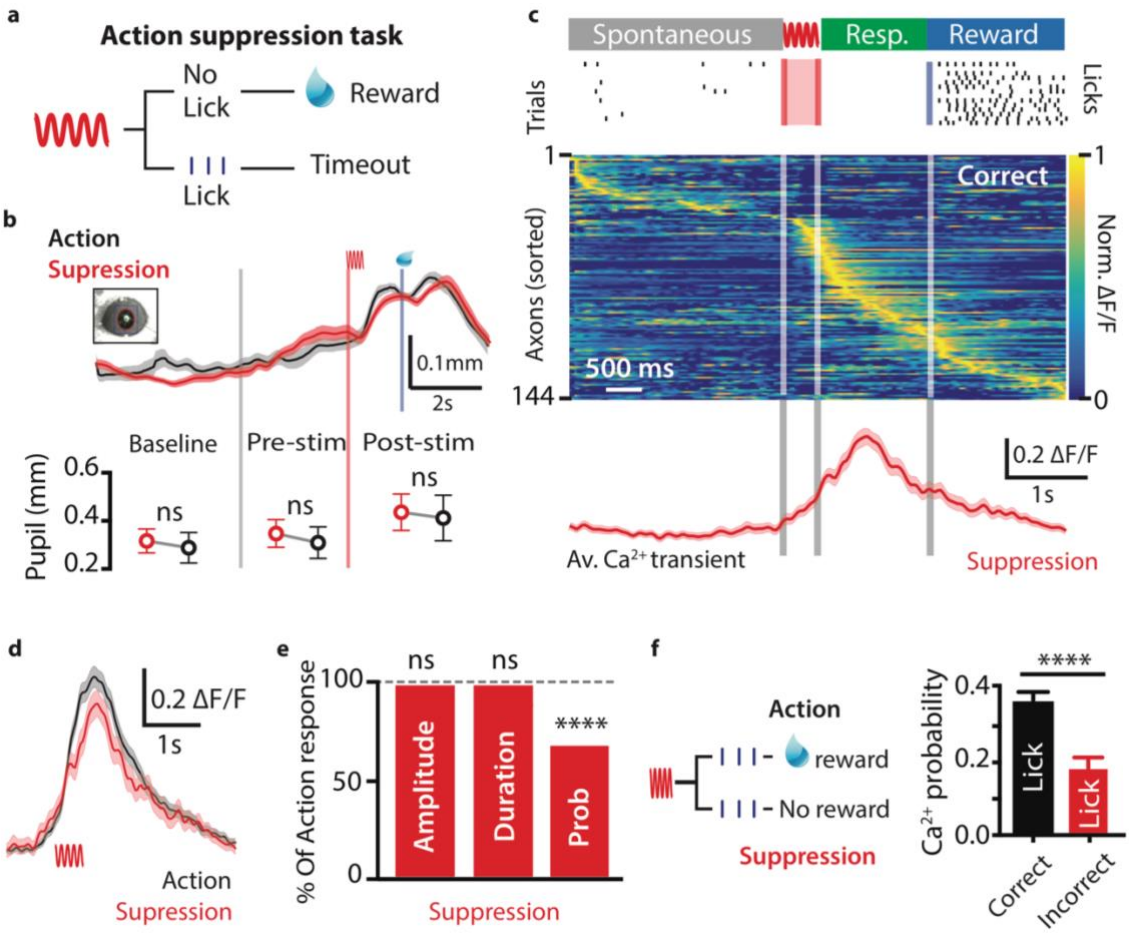

Figure 2.3| Ca^{2+} dynamics in POm axonal terminals during suppression of a goal-directed action

a, Behavioral task design. Two-photon Ca^{2+} imaging of POm axon terminals was performed in head-restrained mice trained to suppress a previously learned goal-directed action. Mice were trained to withhold licking in response to forepaw stimulation (200 Hz, 500 ms) for 1.5 seconds to get a reward (10 µl, 10 % sucrose water). **b,** Top, Average pupil diameter with SEM (shaded area) during correct performance at the 'suppression' goal-directed task (red) and 'action' goal-directed task (black). Bottom, Comparison of pupil dilation during the 'action' and 'suppression' goal-directed tasks in baseline, pre-stim and post-stim epochs (n = 6 mice). Gray line, trial start; red line, stimulus, blue line, reward delivery.

c, Top, Raster plot showing the typical licking response during correct performance of the task. Grey, spontaneous; Red, stimulus; Green, response epoch; Blue, reward epoch. Blue line, reward delivery. Middle, Average Ca^{2+} activity pattern during correct performance of the suppression task (n = 144 axons). Each row is an axon normalized to maximum fluorescence and sorted by the timing of the peak amplitude. Bottom, Mass average with SEM (shaded area) of all axons which were active in the stim/response epoch during correct performance. **d**, Overlay of mass average of evoked activity from all axons which were active in the stim/response epoch during correct performance of the 'Action' (black) and 'Suppression' (red) task. **e**, Peak Ca^{2+} amplitude, duration and probability of evoking a Ca^{2+} transient during 'Suppression' goal-directed task compared with the 'Action' task. **f**, Left, licking in response to the forepaw stimulus is rewarded in the 'Action' goal-directed task (correct), and not in the 'Suppression' task (incorrect). Right, Evoked Ca^{2+} probability during correct (black, Action goal-directed behavior (n = 222) and incorrect (Suppression goal-directed behavior, n = 79 axons) response to forepaw stimulus. Data is shown as average with SEM or as % of Action response. ****$P < 0.0001$.

How crucial is POm signaling during active goal-directed behavior? To test this, the inhibitory opsin, archaerhodopsin (ArchT, 60 nl), was unilaterally injected into the POm and a fiber-optic cannula was chronically inserted into the brain (see methods and Fig. 2.4a). Once expert at the 'action' goal-directed task (> 80 % correct; Extended Data Fig. 2.4), the POm was photo-inactivated during stimulus and behavioral response with interleaved yellow LED light (590 nm, 5 mW, 2 s, Fig. 2.4b). Here, inactivating the POm produced a significant reduction in the overall behavioral performance, with mice decreasing correct responses by on average 3.30 ± 1.29 % (n = 9; p = 0.027, Fig. 2.4c). More specifically, this decrease in performance to 79 ± 1 % was driven by a significant

decrease in the HIT rate (0.98 ± 0.006 vs 0.95 ± 0.013; n=9; p = 0.023; Fig. 2.4d). The specific effect of inactivating the POm on the active HIT response was further highlighted by no change in the rate of false alarms (0.33 ± 0.054 vs 0.34 ± 0.068; n=9; p = 0.5643; Fig. 2.4e). Furthermore, POm inactivation did not alter licking behavior as there was no significant difference in the latency to the first lick (control, 351 ± 29 ms vs ArchT, 342 ± 26 ms, n = 9, p = 0.1282, Fig. 2.4f). Influencing HIT performance by inactivating POm illustrates the importance of the higher-order thalamus in the active behavior of a goal-directed task.

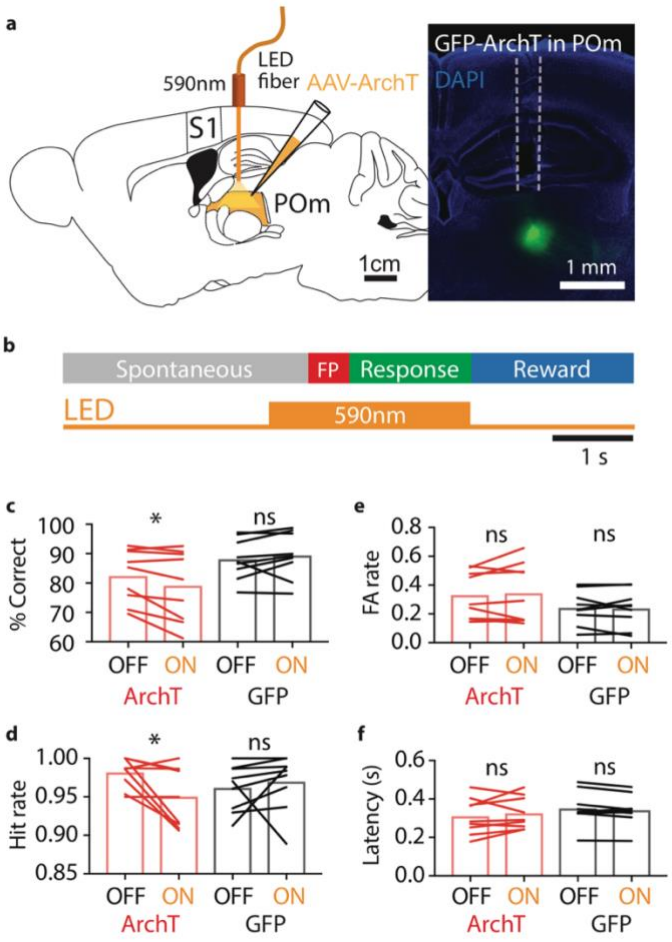

Figure 2.4| Optogenetic inactivation of the POm during the Action goal-directed task

a, Left, Experimental design. The inhibitory opsin, archaerhodopsin (ArchT) was unilaterally injected into the POm and a fiber-optic cannula was chronically inserted into the brain. Right, Localized ArchT spread in POm and fiber optic track (dotted line), bar = 1 mm.

b, The POm was photo-inactivated (590 nm, 5 mW, 2 s) during the stimulus (FP, red) and response (green) epochs in mice expert in the 'action' goal-directed task. (**c** to **e**) Behavioral performance for light OFF versus ON trials. ArchT (n = 9 mice, red), GFP control (n = 9 mice, black). Individual values are shown. *P < 0.05.

Flexible switching of behavioral motor actions in response to changing conditions is crucial for survival in a dynamic environment. To investigate the role of POm in behavioral switching, we performed Ca^{2+} imaging from POm axons in forepaw S1 as mice (n = 4) transitioned from the 'action' goal-directed task to the 'action-suppression' goal-directed task ('switching', Fig. 2.5a). On average mouse performance returned to chance level (50 % correct performance) after 2.25 ± 0.47 training sessions on the action-suppression task. During behavioral switching, pupil tracking was performed to monitor task engagement. Compared with the active goal-directed behavior, there was no significant difference in pupil dilation during baseline (0.28 ± 0.05 vs 0.30 ± 0.07mm, p = 0.6871, n = 6), pre-stim (0.29 ± 0.05 vs 0.32 ± 0.07, p = 0.4372) and post-stim epoch (0.40 ± 0.06 vs 0.43 ± 0.01; p = 0.6874; n = 6, Fig. 2.5b). Although equally engaged in the task, POm axonal Ca^{2+} signaling in forepaw S1 was altered during switching compared to expert behavior. During switching behavior, Ca^{2+} activity was evoked during stimulus presentation and behavioral response (Fig. 2.5c), however, both correct (rewarded) and incorrect (unrewarded) performance were encoded equally (probability, 15.3 ± 1.7 vs 15.1 ± 1.3 % of trials, p = 0.7401; n = 121 axons; Fig. 2.5d and e). Compared to expert behavior, POm encoding of the goal-directed task during switching was significantly reduced (by 58.6%, $p < 0.0001$; n = 121; Fig. 2.5f), however, both behaviorally evoked (amplitude, 1.45 ± 0.07 vs. 1.26 ± 0.05 $\Delta F/F$; p = 0.0072; n = 68/199 axons) and spontaneous (amplitude, 1.28 ± 0.65 vs. 1.10 ± 0.04 $\Delta F/F$; p = 0.0007; n = 102/214 axons) Ca^{2+} transients were significantly larger than expert (Fig. 2.5g). The most striking change in the activity of POm axons in forepaw S1 during the behavioral uncertainty induced by switching the response-reward contingency was the frequency of spontaneous activity, which increased significantly compared to

expert (0.12 ± 0.005 vs 0.09 ± 0.003 Hz; p = 0.0007; n = 102 / 214 axons; Fig. 2.5h). This increase in spontaneous activity per axon was further heightened by an increase in the number of POm axons which were spontaneously active (84.3 vs 61.2 %) during chance performance but not in expert mice (Fig. 2.5i). Taken together, these results indicate a profound shift in the state of POm signaling to forepaw S1, especially spontaneous signaling, as mice are flexibly adjusting their behavioral strategy during a goal-directed task.

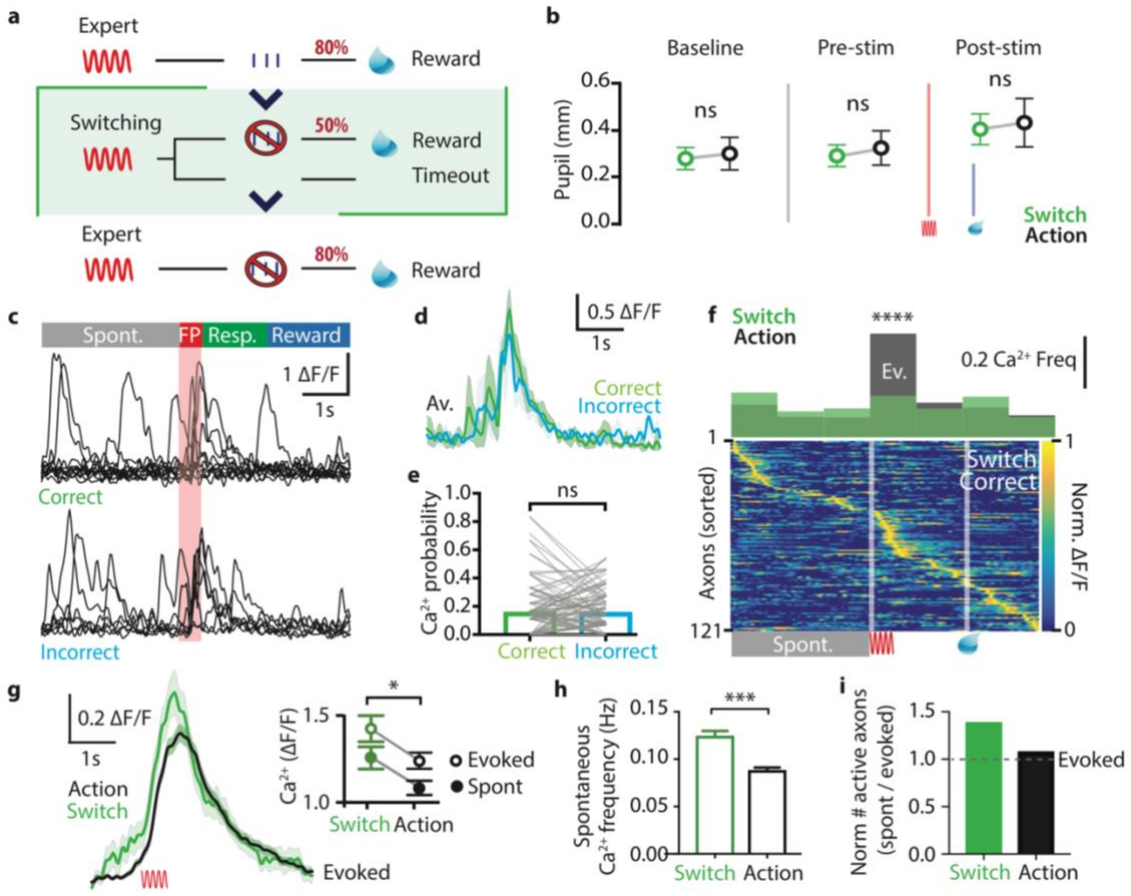

Figure 2.5| POm axons in forepaw S1 alter evoked and spontaneous Ca^{2+} activity during behavioral switching

a, Behavioral task design. Ca^{2+} imaging from POm axons in forepaw S1 was performed as mice transitioned from the 'action' goal-directed task to the 'action-suppression' goal-directed task (50 % correct performance, green). **b**, Average pupil dilation during baseline, pre-stim and post-stim during the switch (green) and 'action' task (black; n = 6). Red bar, stimulus onset; blue bar, reward delivery. **c**, Example of correct (top) and incorrect (bottom) Ca^{2+} responses in a representative POm axon. Grey, spontaneous; Red, stimulus; Green, response epoch; Blue, reward epoch. **d**, Overlay of average with SEM (shaded area) of evoked Ca^{2+} transients during correct (green) and incorrect (light blue) performance from example in (c). **e,** The probability of evoking a Ca^{2+} transient in the stim/response epoch during correct (green) and incorrect (light blue) performance.

f, Top, Histogram of Ca^{2+} transient frequency throughout switch (green) and action (black) trials. (bottom) Normalized average Ca^{2+} activity pattern during correct trials for all POm axons (n = 121) sorted according to the time of peak amplitude. **g**, Overlay of mass averages with SEM (shaded area) of evoked Ca^{2+} transients from all axons active during the stim/response epoch during correct performance in the 'Action' task (black) and Switch (green). Inset, the amplitude of the evoked (open circle) and spontaneous (solid circle) Ca^{2+} transients during switch (green) and action (black) tasks. **h**, Frequency of spontaneous Ca^{2+} events during switch (green) and action (black) goal-directed behavior. **i**, Proportion of active spontaneous POm axons normalized to number of axons with behaviorally-evoked activity during switch (green) and action (black) goal-directed behavior. Dashed line, unity 1.0 line. Error bars indicate the mean ± SEM. **P < 0.01, ***P < 0.001, ****P < 0.0001.

In summary, in awake behaving animals, POm axonal projections in forepaw S1 robustly encode sensory information generating large long-lasting Ca^{2} events in response to tactile stimulation (Fig. 2.6). Evoked Ca^{2} transients are similar during expert goal-directed behavior but changed properties during behavioral switching, increasing in amplitude and decreasing in duration (Fig. 2.6 and Extended Data Fig. 2.5). Furthermore, analysis of the evoked rate of POm Ca^{2+} activity illustrates that POm input is more robust during active behavior. Here, effective connectivity of the POm input to forepaw S1 is greatest during goal-directed action opposed to action suppression. Taken together, POm input to forepaw S1 shifts in strength and rate according to the behavioral task, thus encoding and mediating correct goal-directed action and behavioral flexibility.

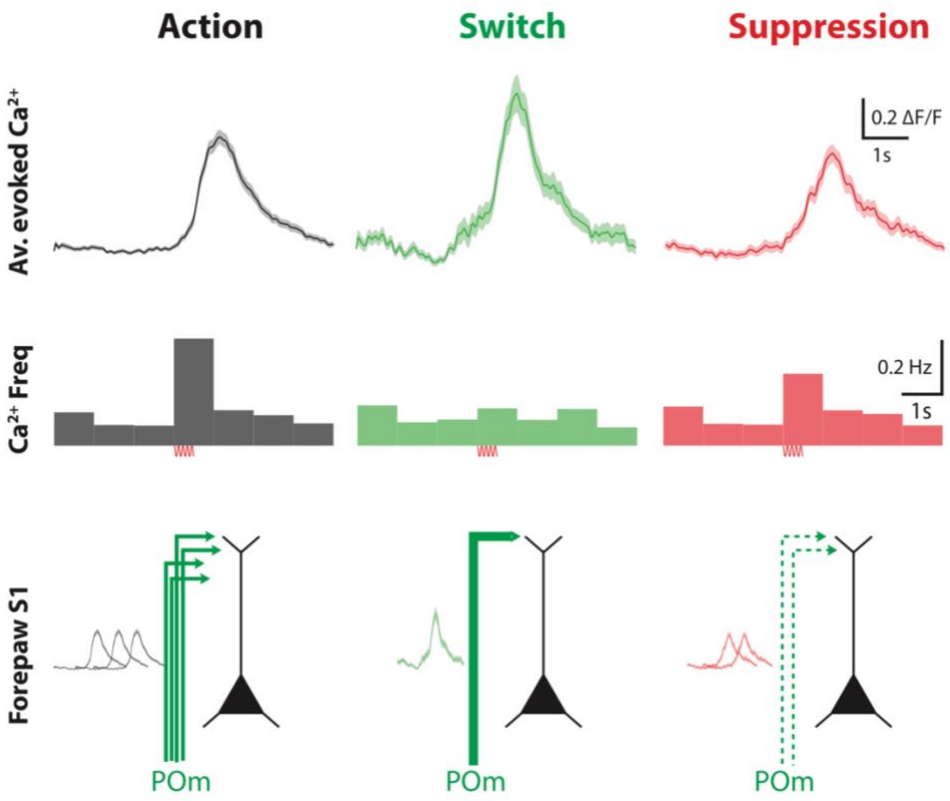

Figure 2.6| POm axons in forepaw S1 encodes correct goal-directed action and behavioral uncertainty

Top, Mass average with SEM of Ca^{2+} activity from all axons that were active in the stim/response epoch during correct performance in the 'Action' (black, n = 199), 'Switching' (green, n = 68) and 'Suppression' (red, n = 109) task. Middle, frequency of Ca^{2+} transients from all axons during correct performance in the 'Action' (black, n = 222), 'Switching' (green, n = 121) and 'Suppression' (red, n = 144) task. Summary schematic of POm input connectivity to forepaw S1 during goal-directed behavior (bottom). The number of arrows indicates the frequency, solid line the robustness and dotted line reduced robustness of POm input to forepaw S1 during expert goal directed behaviour and behavioral switching.

2.5 DISCUSSION

The results presented here highlight the role of the POm during sensory-based goal directed behavior. We illustrate that the POm contributes to the encoding of active behavior, which has been previously shown to be regulated by the anterior cingulate cortex [28], and thalamostriatal circuits [29,30]. In addition to performing appropriate motor actions, dynamic and rapid integration of sensory information is required for goal-directed behavior [31]. In agreement with previous studies [23,24], we show that POm input increases the sensory integration window in layer 2/3 pyramidal neurons of the primary sensory cortex. This effect is NMDA-channel dependent, suggesting the possible involvement of NMDA receptors in the layer 2/3 pyramidal neuron dendrites [15,32]. These results suggest that the increased POm activity during the correct goal directed behavior would enable greater sensory integration during task performance, leading to enhanced flexibility in response encoding.

Here, we probed the flexibility of POm thalamocortical projections to S1 by switching the task contingency. In accordance with thalamic function playing an important role in behavioral flexibility[8], both evoked and spontaneous activity were enhanced during switching, suggesting a shift in action potential firing in POm thalamocortical axons. Changes in firing mode have been reported in sensory higher order thalamus of behaving rodents and primates [22,33] and may underlie cortical state changes during adaptive behavior to uncertain conditions [34,35]. Furthermore, these changes in firing patterns could drive different microcircuits [36-38] as POm inputs to the cortex directly target both excitatory and inhibitory neurons [39].

Patterns of cortical activity during behavior have been associated with task engagement, attention, motivation or reward [40-42]. Using pupil tracking which has been correlated with brain state [43], we report a mismatch between pupil dilation and POm activity. In particular, despite maximal pupil dilation, POm activity was not enhanced during reward delivery. Although reward-related tuft-wide dendritic spikes occur in primary sensory cortex [42], our study suggests that this reward information is not conveyed by the POm. Since the thalamus has multiple projection targets [5] and forms numerous neural circuits [44], reward information may be processed through different circuits and remains to be investigated.

In summary, we show that the higher order thalamus plays an active role during complex cognitive functions such as goal-directed behavior. This finding expands the known roles of the higher-thalamic nuclei, from sensory selection to action selection and flexible switching. Overall, the thalamus is not a simple relay system. It encodes and drives complex behaviors which are crucial for survival in a dynamic environment.

2.6 EXTENDED DATA FIGURES

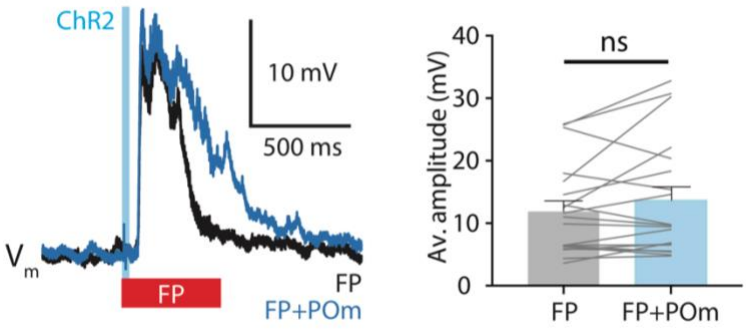

Extended Data Figure 2.1| The amplitude of the sensory evoked subthreshold voltage response in layer 2/3 pyramidal neurons is not affected by POm photo-activation

Left, representative example of average sensory evoked subthreshold voltage response in a layer 2/3 neuron following forepaw stimulation (FP; 200Hz, 500ms; black) and in combination with simultaneous photo-activation of ChR2-expressing POm axonal terminals in upper cortical layers (FP + POm; blue). Right, average peak amplitude in response to forepaw stimulus alone (FP) and paired with POm photoactivation (FP, 12.1 ± 1.67 mV, FP + POm, 13.8 ± 2.15 mV, p = 0.241; n = 19 cells). Statistical significance was determined by paired t-test. Error bars represent the mean + SEM

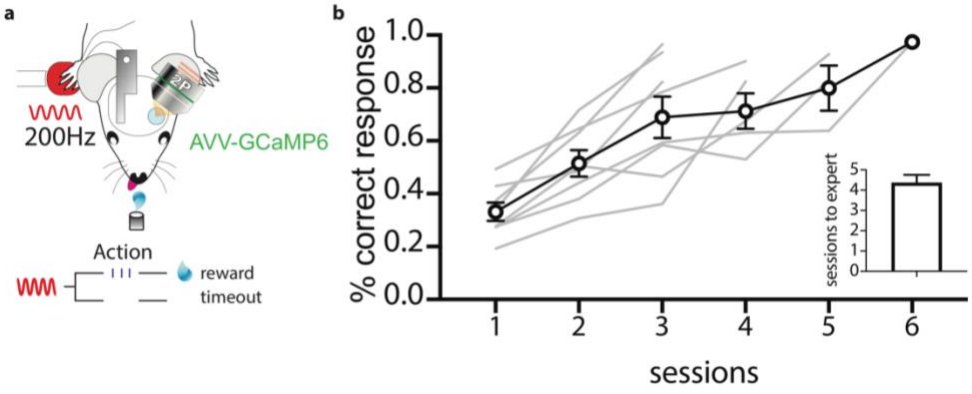

Extended Data Figure 2.2| Experimental design for two photon imaging of POm axons and learning curves for the Action goal-directed task.

a, Schematic of experimental design. Two photon imaging of POm axons was performed through a cranial window above forepaw S1 in mice injected with the Ca^{2+} indicator GCaMP6f into the POm. Mice were trained to associate forepaw tactile stimulation (200 Hz, 500 ms) with a reward. If mice correctly respond by licking a reward port within 1.5 sec after receiving the tactile stimulus, a sucrose water reward (10% sucrose water) was delivered. **b**, Learning curves for the Action goal-directed task. Mice rapidly learn this task, taking on average 4.38 ± 0.37 training sessions (bar plot, inset) to reach expert level (> 80 % correct responses to tactile stimulation) after which two photon imaging was performed. Individual learning curves (grey lines) and the average are shown. Error bars represent the mean with SEM.

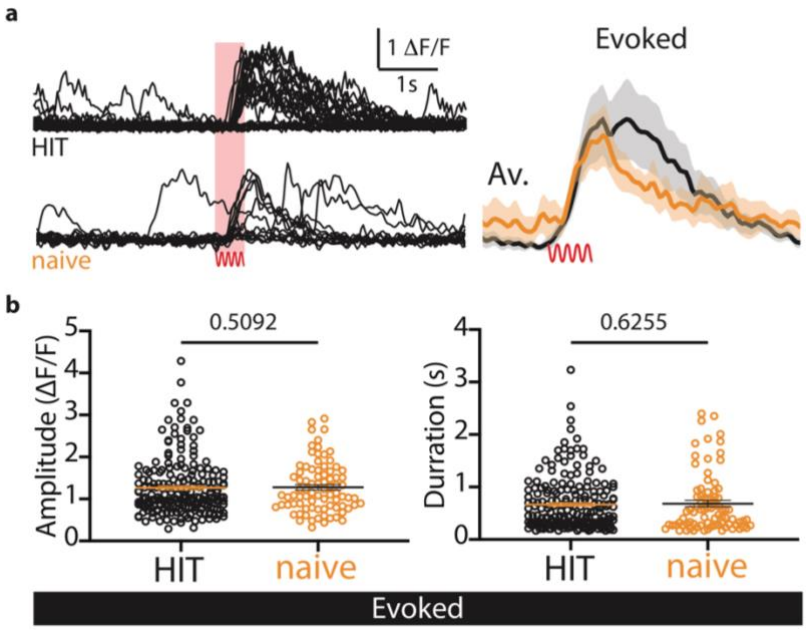

Extended Data Figure 2.3| Comparison of stimulus-evoked Ca^{2+} events in POm terminals in naïve mice and mice expert in the Action goal-directed task.

a, Left, representative example of Ca^{2+} traces for a single ROI during HIT trials (top) and naïve (bottom). Right, overlay of average evoked Ca^{2+} traces with SEM (shaded area) in naïve (orange) and during HIT trials (black) from example (left). Red shaded area, stimulus presentation. **b**, POm axonal Ca^{2+} amplitude (left) and duration (right) during forepaw stimulus in HIT (correct) trials and naïve. Amplitude, 1.26 ± 0.048 ΔF/F vs. 1.28 ± 0.06 ΔF/F; n = 199/82 axons; p = 0.5092. Duration, 665 ± 35 ms vs. 683 ± 62 ms; n = 199/82 axons; p = 0.6255. Error bars represent the mean ± SEM. Statistical significance was determined by Mann-Whitney test.

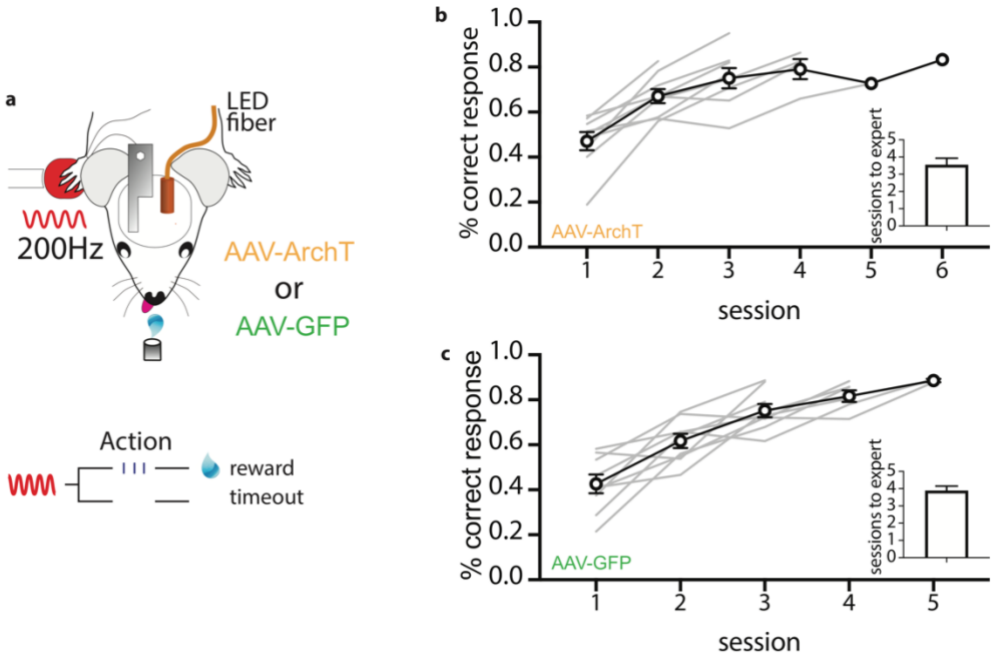

Extended Data Figure 2.4| Experimental design and learning curves for the Action-goal-directed task for optogenetic inactivation of POm complex.

a, Schematic of experimental design. The inhibitory opsin, archaerhodopsin (AAV-ArchT, 60 nl) or control opsin (AAV-GFP, 60nl), was unilaterally injected into the POm and a fiber-optic cannula was chronically inserted into the brain above the POm complex. Mice were then trained on the Action goal-directed task (see Methods) and once expert, optogenetic inactivation of the POm was performed. **b**, Learning curves for the Action goal-directed task in ArchT injected mice. Mice rapidly learnt this task, taking on average 3.55 ± 0.37 training sessions (bar plot, inset) to reach expert level (> 80 % correct responses to tactile stimulation). **c**, Learning curves for the Action goal-directed task in GFP injected mice. Mice rapidly learnt this task, taking on average 3.89 ± 0.26 training sessions (bar plot, inset) to reach expert level (> 80 % correct responses to tactile stimulation). Individual learning curves (grey lines) and the average (black line) are shown. Error bars represent the mean ± SEM.

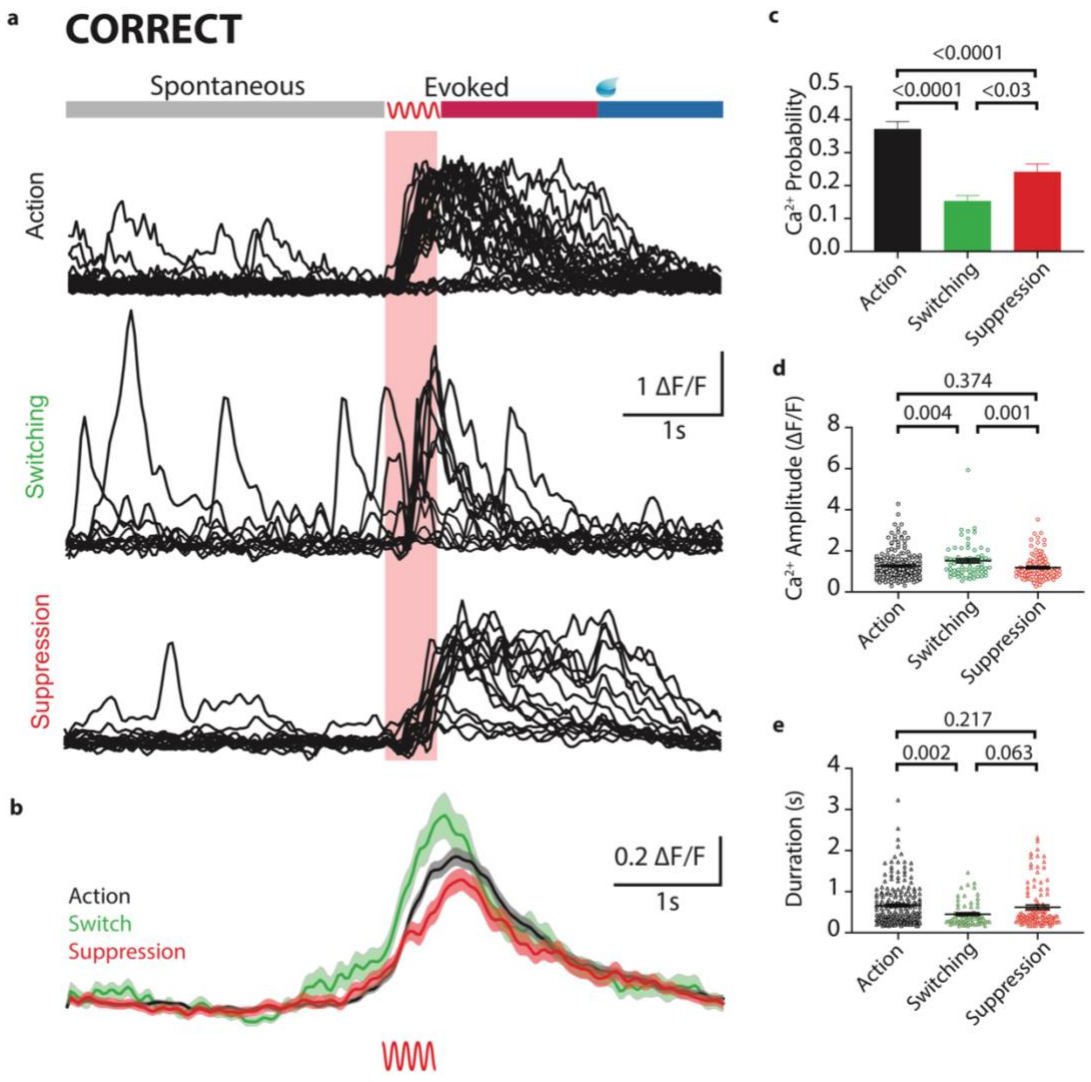

Extended Data Figure 2.5| Spontaneous and stimulus-evoked Ca^{2+} activity in POm axons during correct performance on the Action, Switching and Action-Suppression task.

a, Overlay of Ca^{2+} traces for a representative POm axon during correct responses to tactile stimulus during Action (HIT trials, top), switching (correct lick suppression trials, middle) and Suppression (correct lick suppression trials, bottom) task. **b**, Overlay of mass average of Ca^{2+} traces with SEM (shaded area) from all axons active during the evoked epoch for Action, Switching and Suppression (n = 199/68/109 axons). (**c** to **d**) Evoked Ca^{2+} activity during correct performance on the Action (black), Switching (green) and Suppression tasks (red).

c, Ca^{2+} probability (37.1 ± 0.2 vs. 15.3 ± 0.2 vs. 24.1 ± 0.2 %, n = 222/121/144 axons). **d**, Ca^{2+} amplitude (1.26 ± 0.05 vs. 1.51 ± 0.09 vs. 1.19 ± 0.06 ΔF/F, n = 199/69/109 axons). **e**, Left, Ca^{2+} duration (666 ± 35 vs. 453 ± 35 vs. 623 ± 50 ms, n = 199/69/109 axons). Statistical significance was determined by Kruskal-Wallis test with Dunn's test for Multiple comparisons. Individual p values from multiple comparisons are shown. Error bars represent the mean ± SEM.

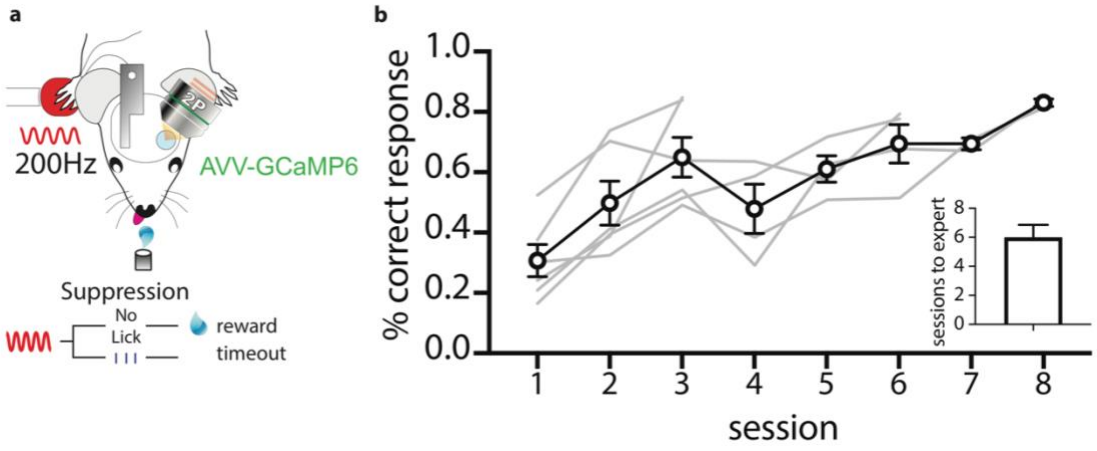

Extended Data Figure 2.6| Experimental design and learning curves for the Action-Suppression goal-directed task for two-photon imaging of POm axons.

a, Schematic of experimental design. Two-photon imaging of POm axons was performed through a cranial window above forepaw S1 in mice injected with the Ca^{2+} indicator GCaMP6f into the POm. To get a reward, mice were trained to suppress (licking) response during a 1.5 second response epoch following tactile stimulation (200 Hz, 500 ms). If mice correctly suppressed licking responses, then a sucrose water reward (10% sucrose water) was made available via a reward port. **b**, Learning curves for the Action-Suppression goal-directed task. Mice rapidly learned this task, taking on average 6 ± 0.85 training sessions (bar plot, inset) to reach expert level (> 80 % correct responses to tactile stimulation) after which two-photon imaging was performed. Individual learning curves (grey lines) and the average (black line) are shown. Error bars represent the mean ± SEM.

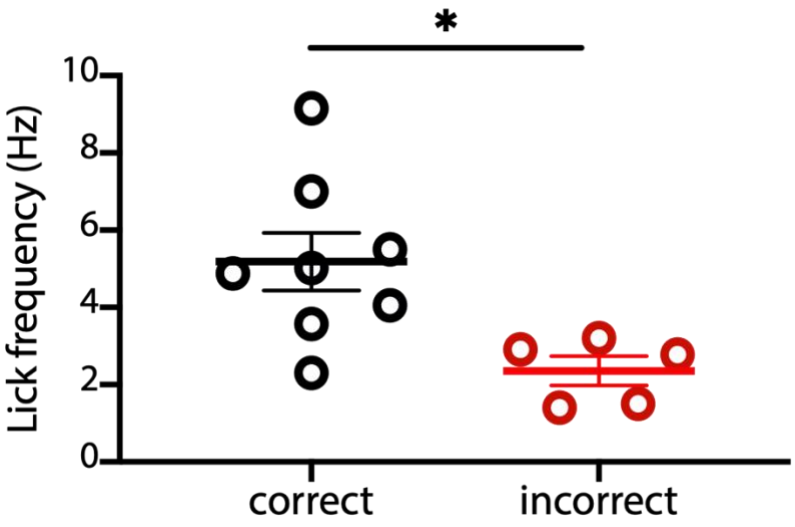

Extended Data Figure 2.7| Lick frequencies during the response epoch

Average lick frequency during the response epoch in correct hit trials at the action goal-directed task (correct, black) vs. incorrect trials at the action suppression goal directed task (incorrect, red). Statistical significance was determined with Mann Whitney test. Error bars represent the mean ± SEM.

2.7 CHAPTER REFERENCES

1 Kepecs, A., Uchida, N., Zariwala, H. A. & Mainen, Z. F. Neural correlates, computation and behavioural impact of decision confidence. *Nature* **455**, 227-231, doi:10.1038/nature07200 (2008).

2 Xu, N. L. *et al.* Nonlinear dendritic integration of sensory and motor input during an active sensing task. *Nature* **492**, 247-251, doi:10.1038/nature11601 (2012).

3 Li, N., Chen, T. W., Guo, Z. V., Gerfen, C. R. & Svoboda, K. A motor cortex circuit for motor planning and movement. *Nature* **519**, 51-56, doi:10.1038/nature14178 (2015).

4 Takahashi, N., Oertner, T. G., Hegemann, P. & Larkum, M. E. Active cortical dendrites modulate perception. *Science* **354**, 1587-1590, doi:10.1126/science.aah6066 (2016).

5 Oh, S. W. *et al.* A mesoscale connectome of the mouse brain. *Nature* **508**, 207-214, doi:10.1038/nature13186 (2014).

6 Sherman, S. M. & Guillery, R. W. Functional organization of thalamocortical relays. *J Neurophysiol* **76**, 1367-1395, doi:10.1152/jn.1996.76.3.1367 (1996).

7 Llinas, R. R., Leznik, E. & Urbano, F. J. Temporal binding via cortical coincidence detection of specific and nonspecific thalamocortical inputs: a voltage-dependent dye-imaging study in mouse brain slices. *Proc Natl Acad Sci U S A* **99**, 449-454,

doi:10.1073/pnas.012604899 (2002).

8 Wimmer, R. D. *et al.* Thalamic control of sensory selection in divided attention. *Nature* **526**, 705-709, doi:10.1038/nature15398 (2015).

9 Zhou, H., Schafer, R. J. & Desimone, R. Pulvinar-Cortex Interactions in Vision and Attention. *Neuron* **89**, 209-220, doi:10.1016/j.neuron.2015.11.034 (2016).

10 Schmitt, L. I. *et al.* Thalamic amplification of cortical connectivity sustains attentional control. *Nature* **545**, 219-223, doi:10.1038/nature22073 (2017).

11 Wilke, M., Mueller, K. M. & Leopold, D. A. Neural activity in the visual thalamus reflects perceptual suppression. *Proc Natl Acad Sci U S A* **106**, 9465-9470, doi:10.1073/pnas.0900714106 (2009).

12 Saalmann, Y. B. & Kastner, S. Cognitive and perceptual functions of the visual thalamus. *Neuron* **71**, 209-223, doi:10.1016/j.neuron.2011.06.027 (2011).

13 Casagrande, V. A., Sary, G., Royal, D. & Ruiz, O. On the impact of attention and motor planning on the lateral geniculate nucleus. *Prog Brain Res* **149**, 11-29, doi:10.1016/S0079-6123(05)49002-0 (2005).

14 Yu, J., Gutnisky, D. A., Hires, S. A. & Svoboda, K. Layer 4 fast-spiking interneurons filter thalamocortical signals during active somatosensation. *Nat Neurosci* **19**, 1647-1657, doi:10.1038/nn.4412 (2016).

15 Gambino, F. *et al.* Sensory-evoked LTP driven by dendritic plateau potentials in vivo. *Nature* **515**, 116-119, doi:10.1038/nature13664 (2014).

16 Jones, E. G. *The Thalamus.* . Vol. 2 (2007).

17 Deschenes, M., Veinante, P. & Zhang, Z. W. The organization of corticothalamic projections: reciprocity versus parity. *Brain Res Brain Res Rev* **28**, 286-308 (1998).

18 Wimmer, V. C., Bruno, R. M., de Kock, C. P., Kuner, T. & Sakmann, B. Dimensions of a projection column and architecture of VPM and POm axons in rat vibrissal cortex. *Cereb Cortex* **20**, 2265-2276, doi:10.1093/cercor/bhq068 (2010).

19 Reep, R. L., Chandler, H. C., King, V. & Corwin, J. V. Rat posterior parietal cortex: topography of corticocortical and thalamic connections. *Exp Brain Res* **100**, 67-84, doi:10.1007/bf00227280 (1994).

20 Urbain, N. & Deschenes, M. A new thalamic pathway of vibrissal information modulated by the motor cortex. *J Neurosci* **27**, 12407-12412, doi:10.1523/JNEUROSCI.2914- 07.2007 (2007).

21 Yamawaki, N. & Shepherd, G. M. Synaptic circuit organization of motor corticothalamic neurons. *J Neurosci* **35**, 2293-2307, doi:10.1523/JNEUROSCI.4023-14.2015 (2015).

22 Urbain, N. *et al.* Whisking-Related Changes in Neuronal Firing and Membrane Potential Dynamics in the Somatosensory Thalamus of Awake Mice. *Cell Rep* **13**, 647-656, doi:10.1016/j.celrep.2015.09.029 (2015).

23 Mease, R. A., Metz, M. & Groh, A. Cortical Sensory Responses Are Enhanced by the Higher-Order Thalamus. *Cell Rep* **14**, 208-215, doi:10.1016/j.celrep.2015.12.026 (2016).

24 Zhang, W. & Bruno, R. M. High-order thalamic inputs to primary somatosensory cortex are stronger and longer lasting than cortical inputs. *Elife* **8**, doi:10.7554/eLife.44158 (2019).

25 Williams, L. E. & Holtmaat, A. Higher-Order Thalamocortical Inputs Gate Synaptic Long-Term Potentiation via Disinhibition. *Neuron* **101**, 91-102 e104, doi:10.1016/j.neuron.2018.10.049 (2019).

26 Audette, N. J., Bernhard, S. M., Ray, A., Stewart, L. T. & Barth, A. L. Rapid Plasticity of Higher-Order Thalamocortical Inputs during Sensory Learning. *Neuron* **103**, 277-291 e274, doi:10.1016/j.neuron.2019.04.037 (2019).

27 Jahanshahi, M., Obeso, I., Rothwell, J. C. & Obeso, J. A. A fronto-striato-subthalamic-pallidal network for goal-directed and habitual inhibition. *Nat Rev Neurosci* **16**, 719-732, doi:10.1038/nrn4038 (2015).

28 White, M. G. *et al.* Anterior Cingulate Cortex Input to the Claustrum Is Required for Top-Down Action Control. *Cell Rep* **22**, 84-95, doi:10.1016/j.celrep.2017.12.023

(2018).

29 Nonomura, S. *et al.* Monitoring and Updating of Action Selection for Goal-Directed Behavior through the Striatal Direct and Indirect Pathways. *Neuron* **99**, 1302-1314 e1305, doi:10.1016/j.neuron.2018.08.002 (2018).

30 Kato, S. *et al.* Action Selection and Flexible Switching Controlled by the Intralaminar Thalamic Neurons. *Cell Rep* **22**, 2370-2382, doi:10.1016/j.celrep.2018.02.016 (2018).

31 Carandini, M. & Churchland, A. K. Probing perceptual decisions in rodents. *Nat Neurosci* **16**, 824-831, doi:10.1038/nn.3410 (2013).

32 Palmer, L. M. *et al.* NMDA spikes enhance action potential generation during sensory input. *Nat Neurosci* **17**, 383-390, doi:10.1038/nn.3646 (2014).

33 Ramcharan, E. J., Gnadt, J. W. & Sherman, S. M. Higher-order thalamic relays burst more than first-order relays. *Proc Natl Acad Sci U S A* **102**, 12236-12241, doi:10.1073/pnas.0502843102 (2005).

34 Bruno, R. M. & Sakmann, B. Cortex is driven by weak but synchronously active thalamocortical synapses. *Science* **312**, 1622-1627, doi:10.1126/science.1124593 (2006).

35 Poulet, J. F., Fernandez, L. M., Crochet, S. & Petersen, C. C. Thalamic control of cortical states. *Nat Neurosci* **15**, 370-372, doi:10.1038/nn.3035 (2012).

36 Morgenstern, N. A., Bourg, J. & Petreanu, L. Multilaminar networks of cortical

neurons integrate common inputs from sensory thalamus. *Nat Neurosci* **19**, 1034-1040, doi:10.1038/nn.4339 (2016).

37 Allen, W. E. *et al.* Global Representations of Goal-Directed Behavior in Distinct Cell Types of Mouse Neocortex. *Neuron* **94**, 891-907 e896, doi:10.1016/j.neuron.2017.04.017 (2017).

38 Tye, K. M. & Uchida, N. Editorial overview: Neurobiology of behavior. *Curr Opin Neurobiol* **49**, iv-ix, doi:10.1016/j.conb.2018.02.019 (2018).

39 Audette, N. J., Urban-Ciecko, J., Matsushita, M. & Barth, A. L. POm Thalamocortical Input Drives Layer-Specific Microcircuits in Somatosensory Cortex. *Cereb Cortex* **28**, 1312-1328, doi:10.1093/cercor/bhx044 (2017).

40 Kobak, D. *et al.* Demixed principal component analysis of neural population data. *Elife* **5**, doi:10.7554/eLife.10989 (2016).

41 Poort, J. *et al.* Learning Enhances Sensory and Multiple Non-sensory Representations in Primary Visual Cortex. *Neuron* **86**, 1478-1490, doi:10.1016/j.neuron.2015.05.037 (2015).

42 Lacefield, C. O., Pnevmatikakis, E. A., Paninski, L. & Bruno, R. M. Reinforcement Learning Recruits Somata and Apical Dendrites across Layers of Primary Sensory Cortex. *Cell Rep* **26**, 2000-2008 e2002, doi:10.1016/j.celrep.2019.01.093 (2019).

43 Reimer, J. *et al.* Pupil fluctuations track fast switching of cortical states during quiet

wakefulness. *Neuron* **84**, 355-362, doi:10.1016/j.neuron.2014.09.033 (2014).

44 Theyel, B. B., Lee, C. C. & Sherman, S. M. Specific and nonspecific thalamocortical connectivity in the auditory and somatosensory thalamocortical slices. *Neuroreport* **21**, 861-864, doi:10.1097/WNR.0b013e32833d7cec (2010).

45 Micallef, A. H., Takahashi, N., Larkum, M. E. & Palmer, L. M. A Reward-Based Behavioral Platform to Measure Neural Activity during Head-Fixed Behavior. *Front Cell Neurosci* **11**, 156, doi:10.3389/fncel.2017.00156 (2017).

46 Bergmann, R., Dominiak, S., Bahr, V., Kremkow, J., Mashaat, M.A., Oraby, H., Sehara, K., Larkum, M.E., Sachdev, R.N. in *Society of Neuroscience Abstracts.*

47 Paxinos, G. & Franklin, K. J. *The Mouse Brain in Stereotaxic Coordinates*. (2001).

Chapter 3
Sustained POm input drives cortical inhibition

3.1 INTRODUCTION

This chapter details my investigation of the cortical network dynamics in forepaw S1 during sustained activation of POm input.

Brain state regulates the responsiveness of neurons, such that the fraction of cells spiking in a quiet, resting animal could be very different from that in an awake, behaving animal[61]. Consistent with this notion, cortical encoding of sensory information in primary sensory areas can be either enhanced or dampened in response to attentional allocation and arousal in a behavioral-relevant and task-dependent manner[4,6,40,68,141]. In accordance with this notion, POm neurons dynamically increase spontaneous AP firing from periods of quiet to active wakefulness[95,170]. During active sensation, this on-going POm input may markedly influence cortical sensory processing as it can desynchronize S1 cortical activity[121]. Furthermore, as discussed in *Chapter 2*, our investigation of POm cortical input during goal-directed behavior demonstrated that information transfer between POm and the forepaw S1 is task dependent, increasing during active behavior and the behavioral uncertainty caused by a change in task contingency.

A prominent principle of thalamocortical networks is the feed-forward inhibition mediated by cortical interneurons[171] that is thought to control the temporal precision of cortical responses to sensory stimuli[70,172,173]. Given the intricate connectivity between the POm and its interneuron targets in S1[41], increased activity in POm is likely to have a complex effect on the cortical processing of sensory information. Studies involving the whisker system in rodents and our own investigation (*Chapter 2*) have revealed that POm has a prevalent excitatory effect on cortical activity, contributing to enhancing sensory responses in both L5 and L2/3 pyramidal neurons[166,167]. POm can directly excite VIP interneurons in the BC,

which in turn inhibit SOM interneurons releasing principal cells from inhibition. This thalamocortical circuit is involved in sensory-evoked LTP in pyramidal neurons[164]. In contrast, stimulation of the POm nucleus has also been shown to mediate cortical inhibition[150,169]. In addition, electrophysiological recordings in BC slice preparations indicate that POm drives layer specific microcircuits which show unique functional properties. While in deep layers the flow of cortical excitation is regulated by POm input directly targeting PV interneurons, in superficial layers this role is assumed by 5HT3a interneurons[41]. To shed light on the complex cortical microcircuits mediating POm excitatory vs. inhibitory influence, we used a combination of electrophysiology and optogenetics *in vivo* to probe the effect of sustained POm input on L2/3 cortical neurons in the forepaw S1 of urethane anaesthetized mice. We delivered a sustained, behaviorally-relevant[95] photo-stimulation to activate ChR2-expressing POm axons in forepaw S1. Upon sustained activation, POm input drives cortical inhibition suppressing both L2/3 neurons spontaneous and sensory evoked activity. This inhibitory effect is prevalently $GABA_A$ mediated as evidenced by cortical application of $GABA_A$ selective blocker gabazine, which abolished POm evoked inhibition. Moreover, both sustained and brief POm axons activation can evoke a long-lasting excitatory voltage response in L2/3 neurons, which is modulated by $GABA_B$-mediated inhibition. Taken together, these results demonstrate that the higher order somatosensory thalamus can both enhance and suppress cortical sensory processing in S1. The excitatory or inhibitory influence of POm input to S1 is likely behaviorally-relevant and task-specific.

3.2 MATERIAL AND METHODS

All procedures were approved by the Florey Institute of Neuroscience and Mental Health Animal Care and Ethics Committee and followed the guidelines of the Australian Code of Practice for the Care and Use of Animals for Scientific Purposes.

Mice.

Wild type C57BL/6 female mice (PN30 – PN70) were used in this study. Mice were housed in groups of 6 in a 12:12 natural light/dark cycle.

Virus injection. Similar procedures were followed for virus injections (60 nl, AAV1.hSyn.ChR2(H134R)-eYFP.WPRE.hGH; or AAV1.CAG.ArchT.GFP.WPRE.SV40;) . See chapter 2 virus injection section for details.

In vivo L2/3 pyramidal neurons recordings and optogenetic manipulation of POm axons in forepaw S1.

Similar procedures were followed for L2/3 recording and optogenetic manipulation as described in chapter 2 methods.

Pharmacology. Pharmacological modulation of cortical $GABA_A$ or $GABA_B$ receptors was performed in a cohort of mice by local application to the exposed surface of gabazine (10µM, Tocris) or CGP52432 (1µM, Tocris), respectively. Typically, the effect of the drug was observable over the time course of 4–5min, and remained stable thereafter.

In vivo whole cell recordings from POm neurons. Mice were initially anaesthetized with isoflurane (~3 % in O2, vol/vol,) before urethane anesthesia (1.3 g/kg of body weight in 20 % saline, Sigma) was administered i.p. Body temperature was maintained at ~36 °C and the depth of anesthesia was monitored throughout the experiment and, when necessary, anesthesia was topped-up with 10 % of the initial urethane dose. Once anesthetized, lidocaine (1 %, wt/vol,) was injected around the surgical site and the mouse head was stabilized in a stereotaxic frame and aligned (Wimmer et al. 2004) for precise targeting of POm. A head-plate was attached to the skull with dental cement (C&B metabond) and the region above the POm nucleus was located stereotaxically. A craniotomy then performed (~1 × 1 mm square, centered at coordinates: RC, -1.7 mm; ML, -1.25; from bregma) and the area was submerged with rat ringer solution containing (135 mM NaCl, 5.4 mM KCl, 1.8 mM CaCl2, 1 mM MgCl2, 5 mM HEPES). Using maximal pressure a glass pipette with a tip resistance between 6 - 9 MΩ, filled with intracellular solution containing (in mM): 115 K gluconate, 20 KCl, 10 HEPES, 10 phosphocreatine, 4 ATP, 0.3 GTP adjusted to pH 7.3-7.4 with NaOH, was inserted at 90$_{o}$ degree-angle into the brain and lowered to a vertical depth of 3 mm. The positive pressure was then decreased to 25-35 mbar and using test pulses (10 mV, 10 ms) in voltage clamp the pipette was advanced at steps of 1μm until a cell was encountered (initial access resistance following whole-cell were typically ~50 MΩ). In vivo whole cell patch recordings were then obtained from POm neurons. Recordings were performed from the soma using a differential amplifier (BVC-700A, Dagan) and were filtered at 10 kHz. Forepaw stimulation (500 ms, 200 Hz) was provided by a stepper motor (Precision Microdrives) coupled to a metal pole onto which the animal forepaw was taped.

Histology. Similar procedures were followed to histological analysis as described in chapter 2 methods section.

Data analysis and statistical methods.

Custom-written Igor software (WaveMetrics) were used for acquisition of electrophysiological data while analysis was carried out using custom routines in Igor pro or Python. Only cells with a tactile-evoked subthreshold response were included in the analysis. For L2/3 pyramidal neurons recordings and optogenetics, the baseline, measured as the mean membrane potential 20 ms before stimulus onset, was subtracted from the raw intracellular membrane potential traces to minimize the effect of up and down states. Normalized traces were then split according to their stimulation protocol (forepaw stimulation; POm axons photoactivation(ChR2)/inactivation(ArchT); forepaw stimulation + photoactivation(ChR2)/inactivation(ArchT)) and averaged. The magnitude of the sensory evoked response was measured as the integral of the averaged evoked subthreshold voltage envelope (between 0 and +0.5 sec relative to stimulus onset). Unless otherwise specified, the average action potential frequency was measured for spontaneous firing and evoked firing (between -4 to -2 sec and 0 to +0.5 sec, relative to stimulus onset, respectively). The average peak amplitude or negative peak amplitude and duration of the sensory evoked response were respectively measured as the local maxima, the local minima and halfwidth of the average subthreshold voltage envelope, between 0 and +0.5 sec relative to stimulus onset. For analysis of the rebound activity, the action potential frequency, peak amplitude, integral and halfwidth were measured as above between 0 and 1 sec relative to the onset of the last LED pulse.

Statistical analysis. All statistics were performed using Prism software. The significant level was set at 0.05. Normality of all value distributions was assessed by Shapiro-Wilk test (α = 0.05). Standard parametric tests were used only when data passed the normality test (p > 0.05). Non-parametric tests were used otherwise. Only two-sided tests were used. Specific statistical tests used are reported in the figure captions.

3.3 RESULTS

To directly measure sensory encoding within the POm nucleus, we performed *in vivo* patch clamp recordings in the POm of urethane (1.3g/Kg) anaesthetized mice during tactile stimulation (vibration, 200Hz, 500ms; FP) delivered to the forepaw contralateral to the recorded side (Fig. 3.1A). Recorded neurons were labelled with a fluorescent marker (Tetramethylrhodamine Biocytin; 0.1mM) enabling post hoc confirmation of the recording site and POm neuron morphology (Fig. 3.1B, C and methods). POm neurons were spontaneously active generating action potentials (APs) at an average frequency of 0.677 ± 0.123 Hz (n = 7 neurons, 5 mice; Fig. 3.1D). Overall, forepaw stimulus was sparsely encoded in POm neurons, with sensory-evoked APs occurring in only 30 % of trials (n = 90/270 trials from 7 neurons, 5 mice; Fig. 3.1E). When evoked, there was a dramatic increase in the frequency of APs above baseline, with an average sensory-evoked firing rate of 6.22 ± 0.46 Hz (n = 7 neurons, 5 mice; Fig. 3.1F). Taken together, these results indicate that POm neurons sparsely encode forepaw stimuli by increasing their action potential output.

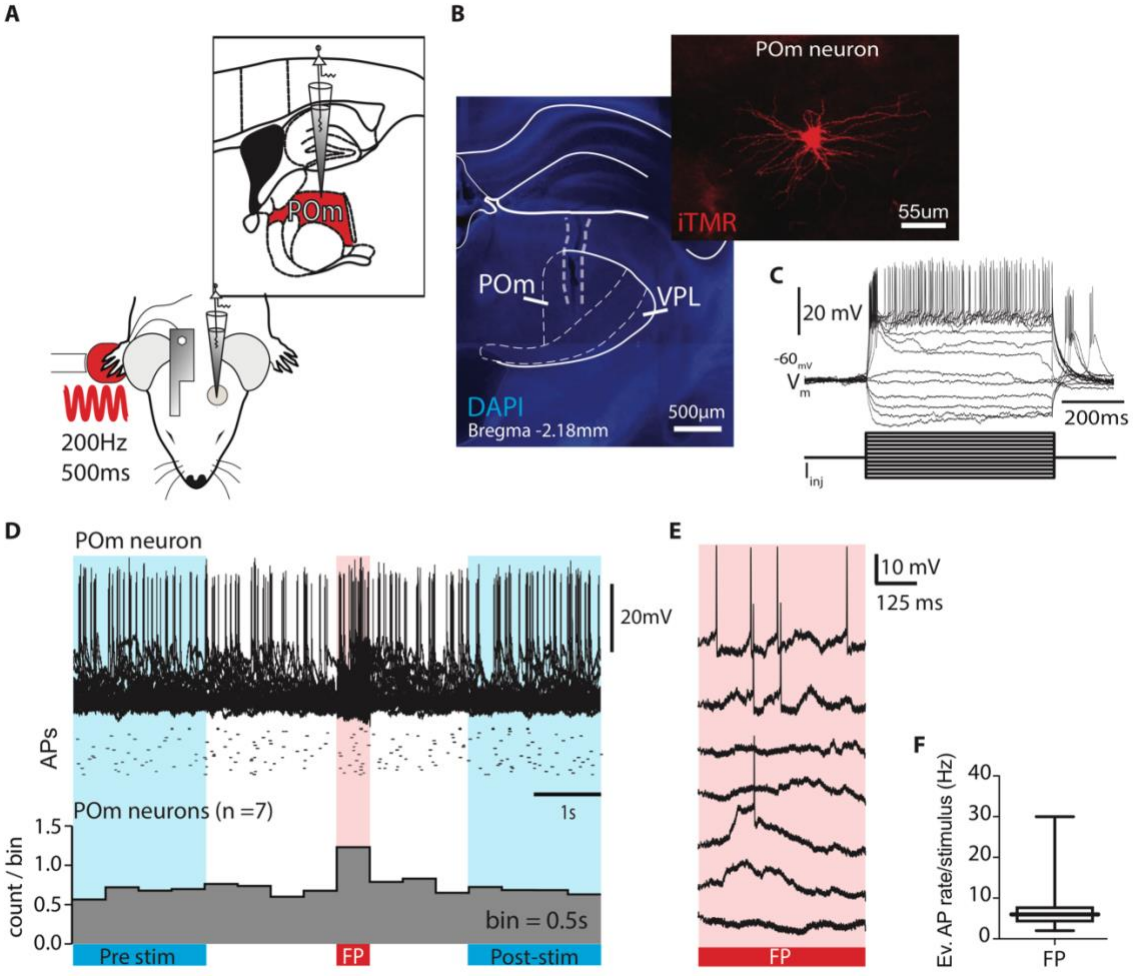

Figure 3.1| Forepaw stimuli are encoded in POm neurons

A, Schematics of experimental design. *In vivo* whole-cell patch clamp recordings were performed from POm neurons of urethane (1.3g/Kg) anaesthetized mice (n = 5) during tactile stimulation (vibration, 200Hz, 500ms; FP) delivered to the forepaw contralateral to the recorded side. **B,** Post hoc fluorescence image of coronal section at coordinates (-2.18 mm from bregma) stained with DAPI. Outline overlaid highlights the track left by the recoding pipette targeted into the POm nucleus. For comparison, the ventral posterior lateral nucleus (VPL) is also shown. Inset, POm neurons labelled with fluorescent marker Tetramethylrhodamine Biocytin (0.1mM).

C, POm neurons voltage responses to a train of current pulses. **D**, Top, Example of voltage responses in a POm neuron during forepaw stimulation (FP, red shaded area). Middle, Raster of evoked action potentials from example above. Bottom, Average spike count histogram. Bin = 0.5s long. N = 7 neurons. Forepaw stimulation increases AP firing in POm neurons. Pre and Post stimulus epochs (blue rectangles). **E**, Evoked voltage activity in POm neurons during forepaw stimulation (FP, red shaded area). POm neurons sparsely encode the stimulus, trials with and without evoked APs are interleaved. **F**, Average evoked (Ev.) APs frequency in trials with successful AP generation (n = 90/270 trials from 7 neurons).

We next investigated the influence of POm input on cortical activity. Patch clamp recordings were performed from L2/3 pyramidal neurons in the forepaw S1 of urethane anaesthetized mice which were previously injected with the excitatory opsin, ChannelRhodopsin2, in the POm nucleus (n = 23 mice; Fig. 3.2A). Post hoc fluorescence microscopy of labelled POm cortical projections showed that POm preferentially innervates L1 and L5 of forepaw S1 (Fig. 3.2B and Extended Data Fig. 3.1). To investigate the role of this POm input during sensory encoding, we designed a physiological optogenetic stimulation protocol based on both the duration of the tactile stimulus (500 ms) and the average sensory-evoked POm firing rate during this forepaw stimulus (Fig. 3.1F), which also matched the firing rates of POm neurons in awake mice during the active cortical state[95]. Six brief LED pulses (10 ms, 10 Hz; 470 nm; ChR2) were focused onto the forepaw S1 to photo-activate POm cortical axons throughout the duration of the tactile stimulation. In L2/3 pyramidal neurons within forepaw S1 (Fig. 3.2C, D), this photoactivation protocol evoked a complex somatic subthreshold voltage response with each LED pulse evoking a small excitatory postsynaptic potential followed by

hyperpolarization (Fig. 3.2E). Overall, the sustained POm photoactivation hyperpolarized the membrane potential for the duration of the light-stimulus (-1.742 ± 0.413 mV n = 27 neurons, 23 mice; Fig. 3.2F). This led to a significant decrease in the baseline firing rate of spontaneously-active L2/3 pyramidal neurons during the sustained photo-activation of superficial POm cortical projections (0.455 ± 0.150 vs 0.210 ± 0.094 Hz; p = 0.008; n = 10 neurons, 9 mice; Fig. 3.2G, H). Taken together, these results indicate that sustained POm input to S1 hyperpolarizes L2/3 pyramidal neurons, suppressing spontaneous firing rates.

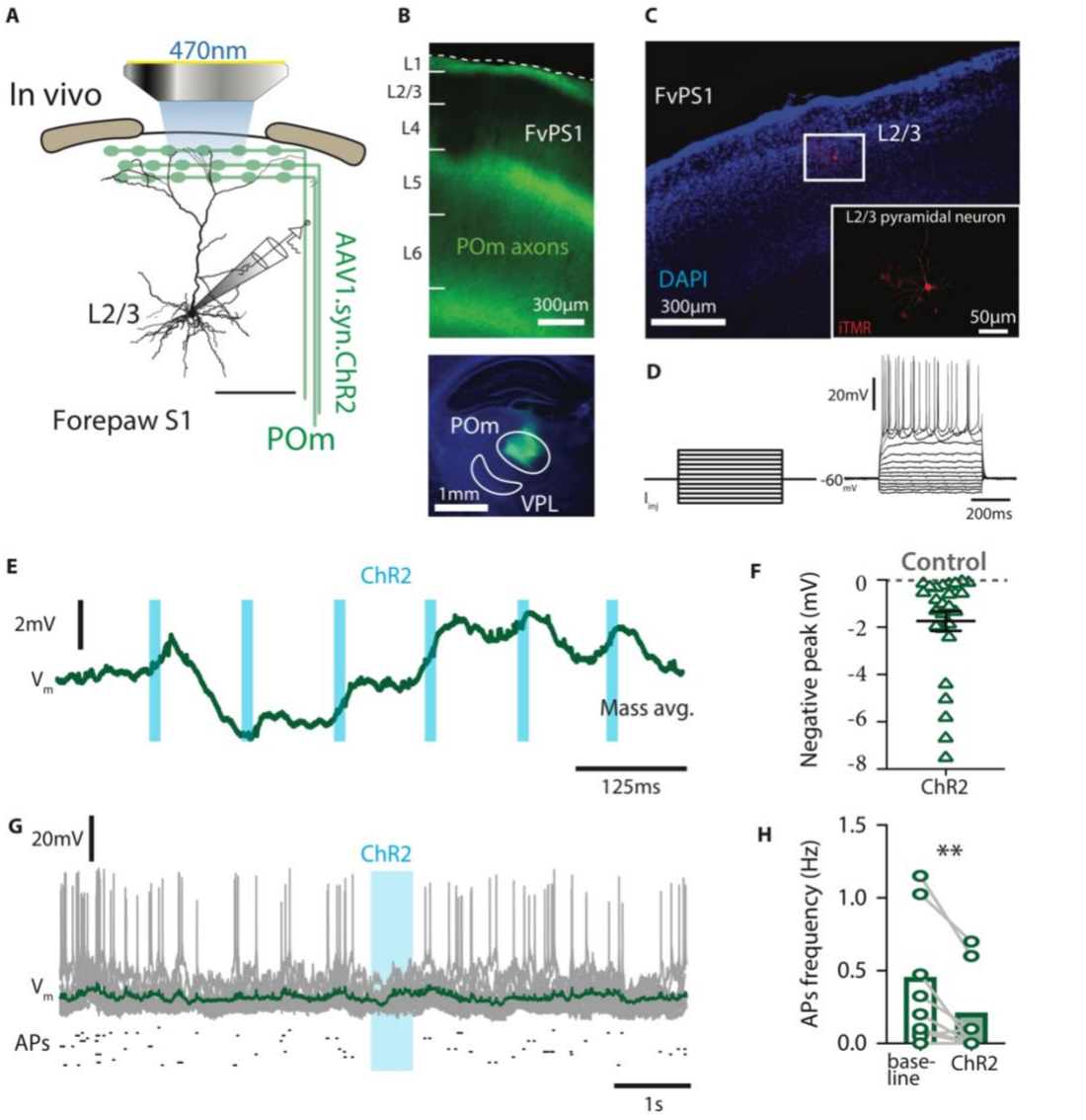

Figure 3.2| Sustained POm input drives cortical inhibition in forepaw S1

A, Experimental design. *In vivo* whole-cell patch clamp recordings were performed from L2/3 pyramidal neurons in forepaw S1 during photoactivation (6 pulses, 10 ms, 10Hz, 460 nm) of ChR2-expressing POm axons. **B**, Post hoc fluorescence images illustrating (top) that POm primarily sends axonal projections to layer 1 and layer 5 of the forepaw S1 (FvPS1) and (bottom) localized POm injection. For comparison, the ventral posterior lateral nucleus (VPL) is shown. **C**, fluorescence image of forepaw S1 (FvPS1). Highlighted (white rectangle) a recorded L2/3 neuron filled with fluorescent marker Tetramethylrhodamine Biocytin (0.1mM). Inset, 20x magnification of recorded neuron. **D**, L2/3 neuron's (from C) voltage responses to a train of current pulses. **E**, Mass average of L2/3 neurons' evoked voltage response during photo-activation of POm axons (ChR2, n = 27 neurons). **F**, Average negative peak amplitude of L2/3 neurons' membrane potential during photo-activation of POm axons. Baseline measured 20ms before stimulus onset (Control, gray dotted line). Error bar indicates the mean ± SEM. **G**, Voltage responses in an example L2/3 pyramidal neuron during photo-activation of POm axons (ChR2, top) Bottom, Raster of evoked action potentials from example above. Photo-stimulation (light-blue shaded area; ChR2). **H**, Average L2/3 neurons' AP frequency during baseline (green-hollow bar) and photo-activation of POm axons (green-filled bar). Statistical significance was determined with Wilcoxon test. $^{**}P \leq 0.01$.

We next investigated the influence of sustained POm input during the encoding of sensory information within the somatosensory cortex. To this end, tactile stimulation (vibration, 500ms, 200Hz, FP) was delivered simultaneously with sustained photo-activation of POm axonal projections in forepaw S1 (10 ms, 10 Hz, 500 ms; 470 nm). In L2/3 pyramidal neurons, forepaw stimulus evoked a large sub-threshold voltage response (amplitude, 9.258 ± 0.776 mV; half width, 189.800 ± 18.910 ms, n = 27 neurons, 23 mice; Fig. 3.3A to D). Forepaw stimulus also evoked action potentials in approximately 30 % of recorded L2/3

pyramidal neurons (10/27 neurons), leading to a significant increase in firing rate above baseline (0.478 ± 0.172 vs 1.810 ± 0.492 Hz, n = 10 neurons, 9 mice; Fig. 3.3E). When POm axons were photo-activated simultaneously with tactile stimulus (FP+POm; Fig. 3.3F), the sensory-evoked activity was strongly suppressed (Fig. 3.3G), significantly decreasing the peak amplitude of the sub-threshold voltage response (9.260 ± 0.776 vs 6.090 ± 0.560; $p < 0.0001$; n = 27 neurons, 23 mice; Fig. 3.3H) and evoked AP firing (1.810 ± 0.492 vs 1.030 ± 0.435 Hz; $p = 0.0039$; n = 10 neurons, 9 mice; Fig. 3.3I). Since the direct projection from POm to S1 is glutamatergic[41,152], these results indicate that sustained POm activity suppresses sensory processing in L2/3 pyramidal neurons by engaging a cortical inhibitory network in forepaw S1.

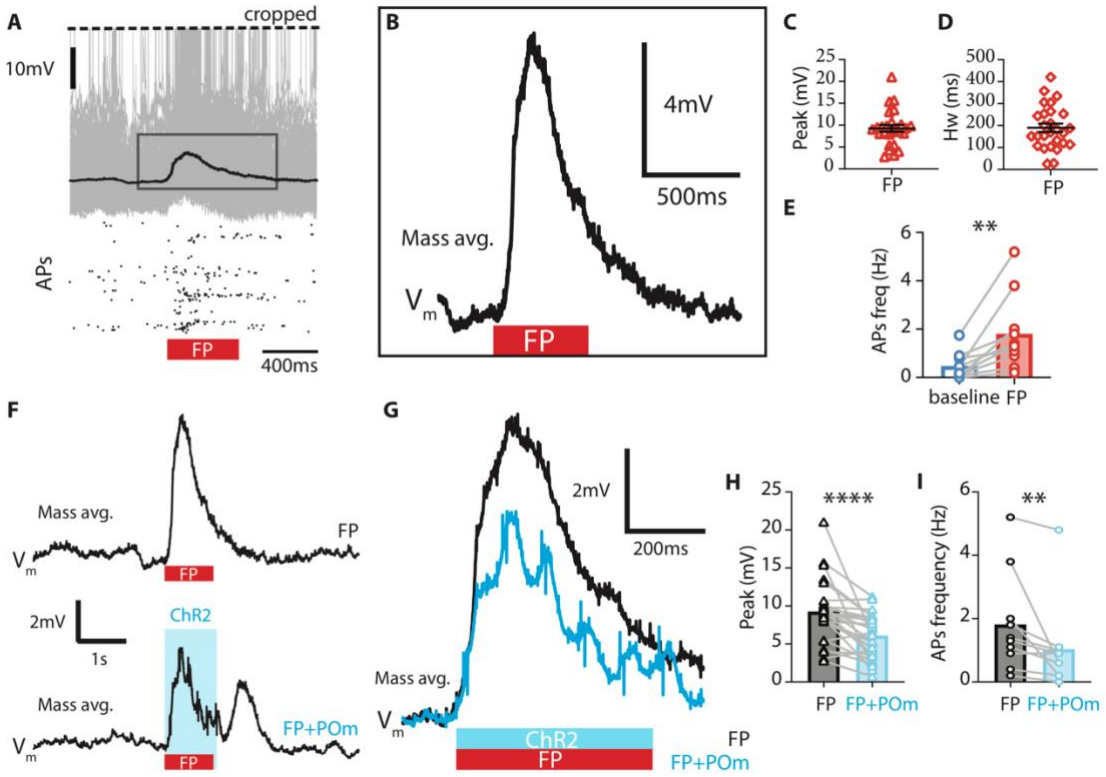

Figure 3.3| Sustained POm input inhibits sensory processing in L2/3 pyramidal neurons

A, Top, Evoked voltage responses from all L2/3 pyramidal neurons recorded (gray, n = 27) in forepaw S1, during forepaw stimulation (FP, 200Hz, 500ms). Highlighted (rectangle) the mass average of the evoked voltage response (black). Bottom, raster plot of APs from top. **B**, Mass average of voltage traces from A. Forepaw stimulus (red rectangle). **C**, Average peak amplitude of the sensory evoked voltage response in L2/3 neurons during forepaw stimulation (FP). **D**, Average half width of the sensory evoked voltage response in L2/3 neurons during forepaw stimulation (FP). **E**, Average L2/3 neurons' AP frequency during baseline (blue-hollow bar) and forepaw stimulation (FP, red-filled bar). **F**, Mass average voltage response from L2/3 neurons during forepaw stimulation (FP, n = 27 neurons, top) and simultaneous forepaw stimulation and POm axons photo-activation (FP+POm, n = 27 neurons, bottom). **G**, Overlay of mass average traces from F. Forepaw stimulation alone (FP, black trace). Forepaw stimulation + POm axons photo-activation (FP+POm, light blue trace). Forepaw stimulus (red rectangle); POm axons photo-activation (ChR2, light blue rectangle). **H**, Average L2/3 neurons' peak amplitude during forepaw stimulation (FP, dark-filled bar) and forepaw stimulation + photo-activation (FP+ POm, light blue-filled bar). **I**, Average L2/3 neurons' AP frequency during forepaw stimulation (FP, dark-filled bar) and forepaw stimulation + photo-activation (FP+ POm, light blue-filled bar). Statistical significance was determined with Wilcoxon test. Error bars indicate the mean ± SEM. **P < 0.01, ****P < 0.0001.

Since sustained POm activity leads to a robust inhibition of both spontaneous and evoked activity in L2/3 pyramidal neurons, we further investigated the cellular-mechanism of POm di-synaptic inhibition of cortical activity using pharmacological approaches. Cortical application of the $GABA_A$ receptor blocker; gabazine (gb; 10µM; Fig. 3.4A) effectively abolished the POm mediated inhibition of spontaneous activity and instead led to a

significant enhancement of the initial excitatory response (ChR2+gb: 0.908 ± 0.210 mV*s, p = 0.010, n = 6 neurons, 5 mice; Fig. 3.4B, C). During paired tactile stimulus and POm photo-activation, cortical application of gabazine effectively prevented POm suppression of the sensory-evoked activity in L2/3 pyramidal neurons (amplitude: 26.200 ± 5.740 vs 23.900 ± 4.810 mV; p = 0.437; n = 6 neurons, 5 mice; Fig. 3.4D, E). These results illustrate that POm input in forepaw S1 targets interneurons which exert GABAA-mediated inhibition onto cortical pyramidal neurons, leading to inhibition of both spontaneous and sensory-evoked activity.

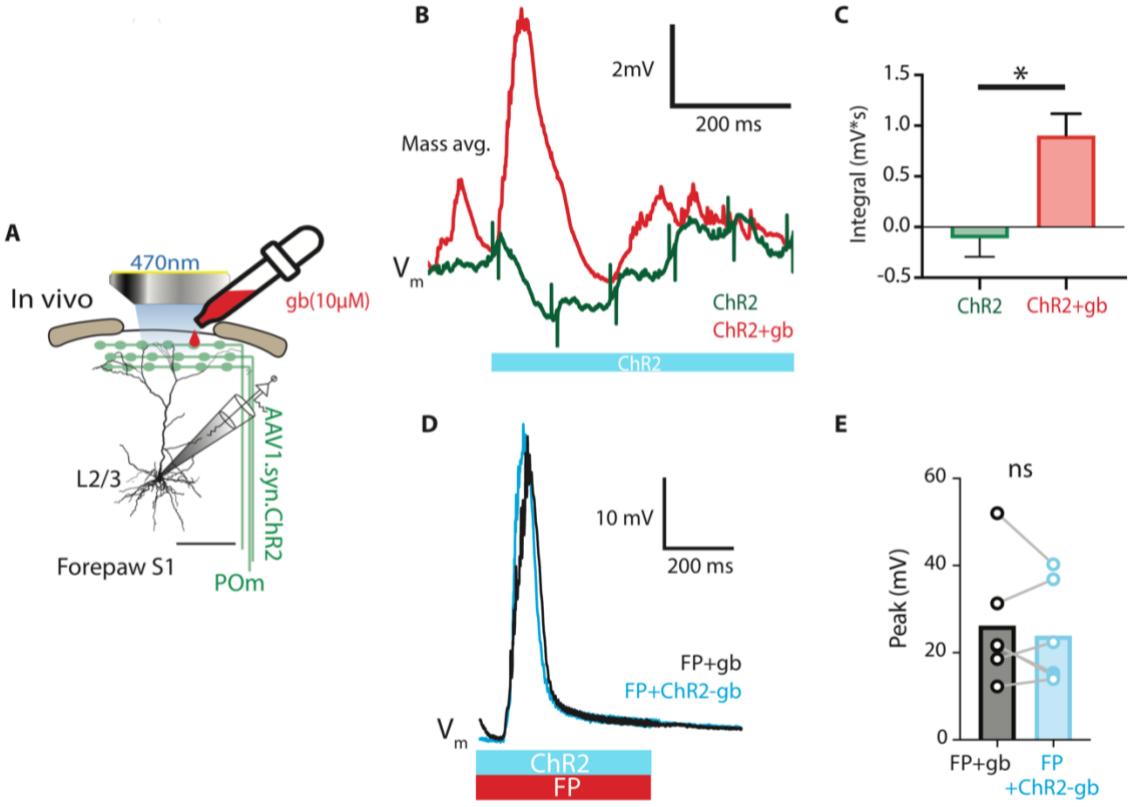

Figure 3.4| POm evoked cortical inhibition is GABAA mediated

A, Experimental design. *In vivo* whole-cell patch clamp recordings were performed from L2/3 pyramidal neurons in forepaw S1 during photoactivation (6 pulses, 10 ms, 10Hz, 460 nm) of ChR2-expressing POm axons and cortical application of gabazine (gb; GABAA receptor blocker; 10µM).

B, Mass average of L2/3 neurons' evoked voltage response during POm axons photo-activation alone (ChR2, green trace, n = 27 neurons) and with simultaneous gabazine application (ChR2+gb, red trace, n = 6 neurons). **C**, Integral of L2/3 neurons' evoked voltage response during POm axons photo-activation (ChR2, green filled bar) and with gabazine application (ChR2+gb, red filled bar). Statistical significance was determined with Mann-Whitney test. **D**, Average evoked voltage response from example L2/3 neuron during forepaw stimulation with gabazine (FP+gb, black trace) and simultaneous POm axons photo-activation (FP+ChR2+gb, light blue trace). **E**, Average L2/3 neurons' peak amplitude during forepaw stimulation + gabazine (FP+gb, black) and simultaneous forepaw stimulation + gabazine + POm axons photo-activation (FP+ChR2+gb, light blue, n = 6 neurons). Error bars indicate the mean + SEM. *P < 0.05.

Long-range projections have been previously shown to cause $GABA_B$–mediated inhibition in cortical pyramidal neurons[48]. We therefore tested whether POm input leads to $GABA_B$–mediated inhibition in L2/3 pyramidal neurons in forepaw S1. In contrast to blocking $GABA_A$ receptors, POm-mediated inhibition of spontaneous activity in L2/3 pyramidal neurons was not significantly altered during cortical application of the $GABA_B$ receptor blocker, CGP52432 (CGP; 1µM; -0.118 ± 0.175 vs. -0.645 ± 0.349 mV*s; p = 0.601; n = 27/11 neurons, n = 23/6 mice; Fig. 3.5 A-C). Likewise, inhibition of the subthreshold sensory-evoked response during paired tactile and POm axons photo-stimulation was not significantly influenced by blocking $GABA_B$ receptors (11.100 ± 1.510 vs 6.540 ± 1.690; p = 0.006; n = 11 neurons, n = 6 mice; 3.5D, E). Taken together, these results indicate that POm evoked di-synaptic inhibition of both spontaneous and sensory-evoked activity in L2/3 pyramidal neurons is primarily mediated by $GABA_A$, and not $GABA_B$, receptors.

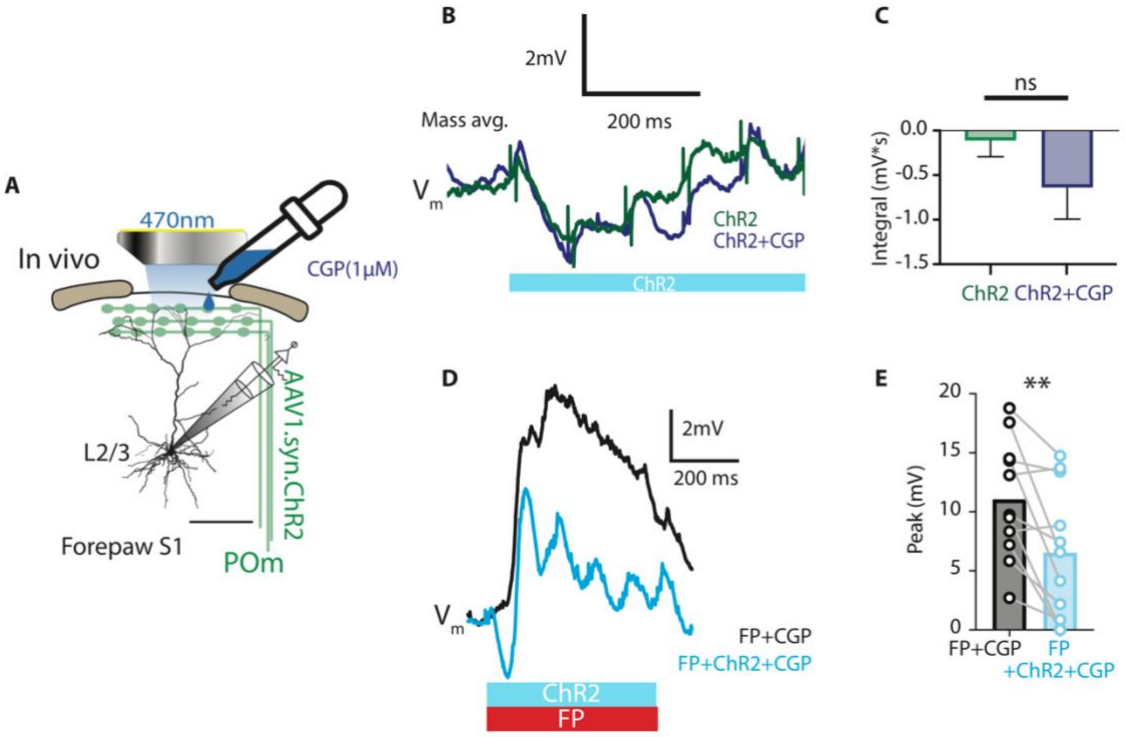

Figure 3.5| GABAB receptor blockade does not affect the POm evoked cortical inhibition

A, Experimental design. *In vivo* whole-cell patch clamp recordings were performed from L2/3 pyramidal neurons in forepaw S1 during photoactivation (6 pulses, 10 ms, 10Hz, 460 nm) of ChR2-expressing POm axons and cortical application of CGP52432 (CGP; GABAB receptor blocker; 1µM). **B**, Mass average of L2/3 neurons' evoked voltage response during POm axons photo-activation alone (ChR2, green trace, n = 27 neurons) and with simultaneous CGP application (ChR2+CGP, blue trace, n = 11 neurons). **C**, Integral of L2/3 neurons' evoked voltage response during POm axons photo-activation (ChR2, green filled bar) and with CGP application (ChR2+CGP, blue filled bar). Statistical significance was determined with Mann-Whitney test. **D**, Average evoked voltage response from example L2/3 neuron during forepaw stimulation with CGP (FP+CGP, black trace) and simultaneous POm axons photo-activation (FP+ChR2+CGP, light blue trace). **E**, Average L2/3 neurons' peak amplitude during forepaw stimulation + CGP (FP+CGP, black) and simultaneous forepaw stimulation + CGP + POm axons photo-activation (FP+ChR2+CGP, light blue, n = 11 neurons). Error bars indicate the mean + SEM. **P < 0.01.

In addition to driving an inhibitory network in forepaw S1, POm input activation also led to a delayed increase in L2/3 pyramidal neuron activity (Fig. 3.6A, B). Following the robust hyperpolarization, sustained activation of POm input to forepaw S1 caused a long-lasting depolarizing sub-threshold voltage response, which significantly increased AP generation above baseline (0.506 ± 0.157 vs 1.10 ± 0.281 Hz; p = 0.0195; n = 9 neurons, 8 mice; p = 0.0195; Fig. 3.6C). The persistent voltage response of L2/3 pyramidal neurons was also elicited by brief activation of POm input to forepaw S1 (1 pulse ,10ms, 470nm, ChR2-single; Fig. 3.6D). Interestingly, the amplitude of this persistent-voltage response to brief POm input was significantly greater than during sustained POm input (ChR2 vs ChR2-single; 5.620 ± 0.743 vs 13.100 ± 1.760 mV; p = 0.0003; n = 27/7 neurons, n = 23/5 mice; Fig. 3.6E, F). However, the onset of the peak voltage response measured from the last LED pulse was not changed (411 ± 30.100 vs 500 ± 50.7 ms; p = 0.116; n = 27/7 neurons, n = 23/5 mice; Fig. 3.6G), suggesting that the persistent-voltage response to both brief and sustained POm input involves similar mechanisms.

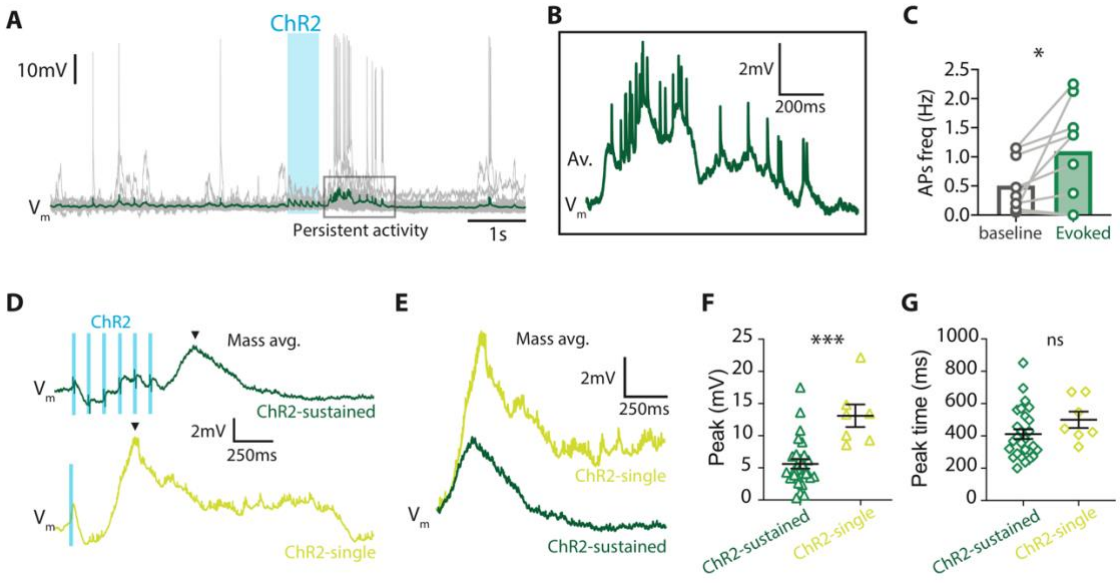

Figure 3.6| POm stimulation evokes a post-inhibitory persistent voltage response in L2/3 pyramidal neurons

A, Example of voltage responses in a L2/3 pyramidal neuron (gray) and average (green) during POm axons photo-activation. The post-inhibitory persistent voltage response of the membrane potential is highlighted (rectangle). **B**, Average voltage response in L2/3 pyramidal neuron during persistent depolarization from example (A). **C**, Average AP frequency in L2/3 neurons during baseline (baseline, gray-hollow bar) and persistent voltage response (Evoked, green-filled bar). Statistical significance was determined with Wilcoxon test. **D**, Mass average of voltage responses in L2/3 neurons during sustained (6 pulses, 10 ms, 10Hz, 460 nm) POm axons photo-activation (ChR2-sustained, green, n = 27 neurons, top) and brief POm axons photo-activation (ChR2-single; 1 pulse; 10ms; light-green; n = 7 neurons; bottom). Arrow heads indicate the persistent voltage response. **E**, Overlay from voltage responses in D. **F**, Average peak amplitude of the persistent voltage response in L2/3 neurons evoked by sustained-POm axons photo-activation (ChR2-sustained; green) and single pulse photo-activation (ChR2-single, light green). **G**, Average peak onset time of the persistent voltage response in L2/3 neurons evoked by sustained-POm axons photo-activation (ChR2-sustained; green) and single pulse photo-activation (ChR2-single, light green). Statistical significance was determined with Mann-Whitney test. Error bars indicate the mean ± SEM. *P < 0.05, ***P < 0.001.

To further investigate the mechanisms driving the POm-evoked persistent-voltage response in L2/3 pyramidal neurons, we inhibited the cortical inhibitory network by blocking either $GABA_A$ or $GABA_B$ receptors (Fig. 3.7A). Here, in contrast to the dramatic increase in the EPSP evoked in response to direct POm input (Fig. 3.4B), local application of the $GABA_A$ receptor agonist gabazine had no significant effect on the peak amplitude (5.620 ± 0.743 vs 5.78 ± 1.130 mV; p > 0.999; Fig. 3.7B, C) nor the integral (1.19 ± 0.254 vs 0.857 ± 0.140 mV*s; p > 0.999; n = 27/6 neurons, 23/5 mice; Fig. 3.7D) of the persistent voltage

response. Therefore, these results illustrate that the persistent-voltage response is not modulated directly by $GABA_A$-mediated inhibition.

The reduction in the amplitude of the persistent-voltage response following sustained POm activation suggests the involvement of a long-lasting inhibition of L2/3 pyramidal neuron activity. To investigate this, $GABA_B$ receptors were blocked by cortical application of CGP (1µM) during sustained POm activation. Here, the persistent-voltage response was significantly increased in peak amplitude (10.500 ± 2.020 mV; p = 0.019; n =11 neurons, 6 mice; Fig. 3.7B, C) and integral (3.300 ± 0.884 mV*s; p = 0.011; n =11 neurons, 6 mice; Fig. 3.7D). Interestingly, the peak of the persistent-voltage response during local block of $GABA_B$ receptors was not significantly different from that evoked by the brief POm activation (ChR2-single; 13.100 ± 1.760 mV; p = 0.151; n = 7 neurons, n = 5 mice; 3.7E to G), illustrating that the sustained POm activation recruited long-lasting $GABA_B$-mediated inhibition which modulated the persistent-voltage response in L2/3 pyramidal neurons. In summary, local cortical block of inhibitory receptors suggests that the POm-evoked persistent-voltage response in L2/3 pyramidal neurons is not affected by fast $GABA_A$ inhibition but can instead be modulated by a long-lasting $GABA_B$ inhibitory circuit.

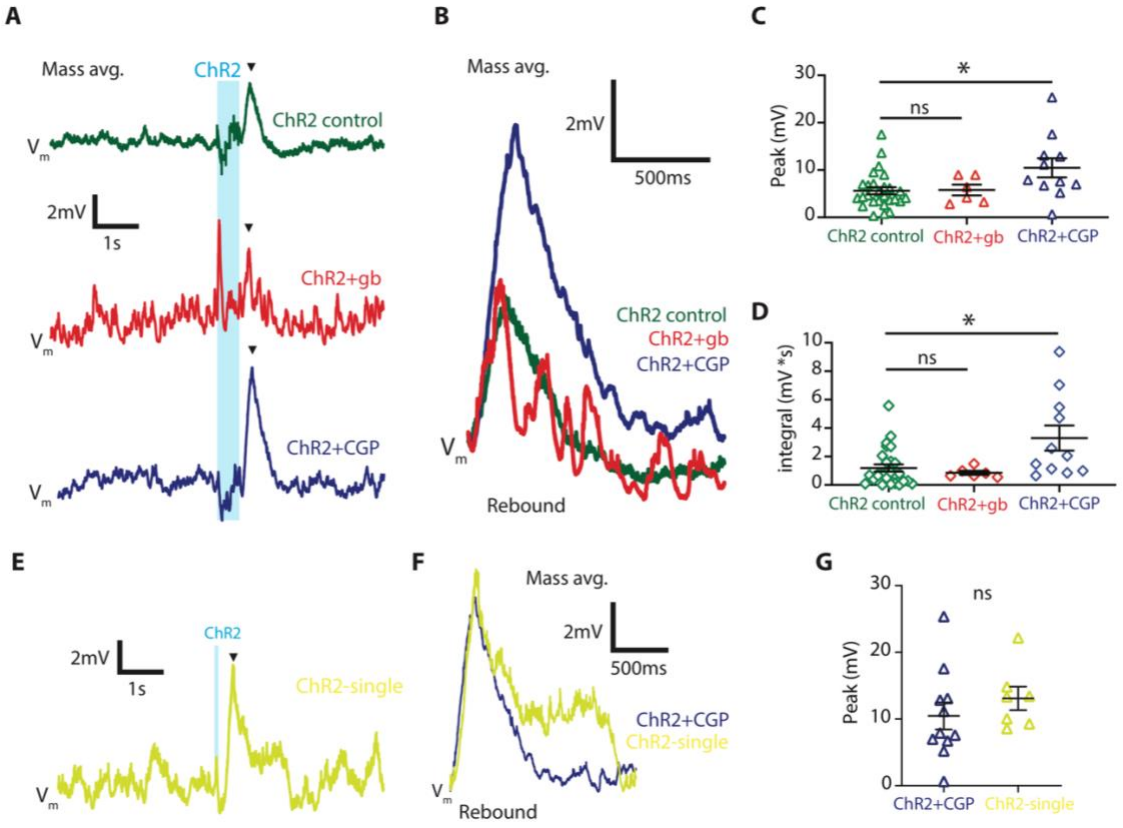

Figure 3.7| GABAB dependent modulation of POm-evoked persistent voltage response

A, Mass average of voltage responses in L2/3 neurons during sustained POm axons photo-activation alone (ChR2 control, green trace, n = 27 neurons, top), during application of gabazine (ChR2+gb, red trace, n = 6 neurons, middle) and during application of CGP (ChR2+CGP, blue trace trace, n = 11 neurons, bottom). Arrow heads indicate the persistent voltage response. Photo-activation (ChR2, light-blue shaded area). **B**, Overlay of mass average traces from A showing the POm-evoked persistent voltage response in L2/3 neurons. ChR2 control (green) and during gabazine (ChR2+gb, red) and CGP (ChR2+CGP, blue) application. **C**, Average peak amplitude of the persistent voltage response in L2/3 neurons evoked by sustained-POm axons photo-activation (ChR2 control; green) and during gabazine (ChR2+gb, red) or CGP application (ChR2+CGP, blue). Statistical significance was determined with Kruskal

D, Average integral of the persistent voltage response in L2/3 neurons evoked by sustained-POm axons photo-activation (ChR2 control; green) and during gabazine (ChR2+gb, red) or CGP application (ChR2+CGP, blue). Statistical significance was determined with Kruskal Wallis test. **E**, Mass average of voltage responses in L2/3 neurons during brief POm axons photo-activation (ChR2-single; 1 pulse; 10ms; light-green, n = 7 neurons). **F**, Overlay of mass average traces from A and F showing the POm-evoked persistent voltage response in L2/3 neurons evoked by brief (ChR2-single, light green) and sustained+CGP POm axons activation (ChR2+CGP, blue). **G**, Average peak amplitude of the persistent voltage response in L2/3 neurons evoked by brief (ChR2-single, light green) and sustained+CGP POm axons photo-activation (ChR2+CGP, blue). Statistical significance was determined with Mann-Whitney test. Error bars indicate the mean ± SEM. *P < 0.05.

3.4 EXTENDED DATA FIGURES

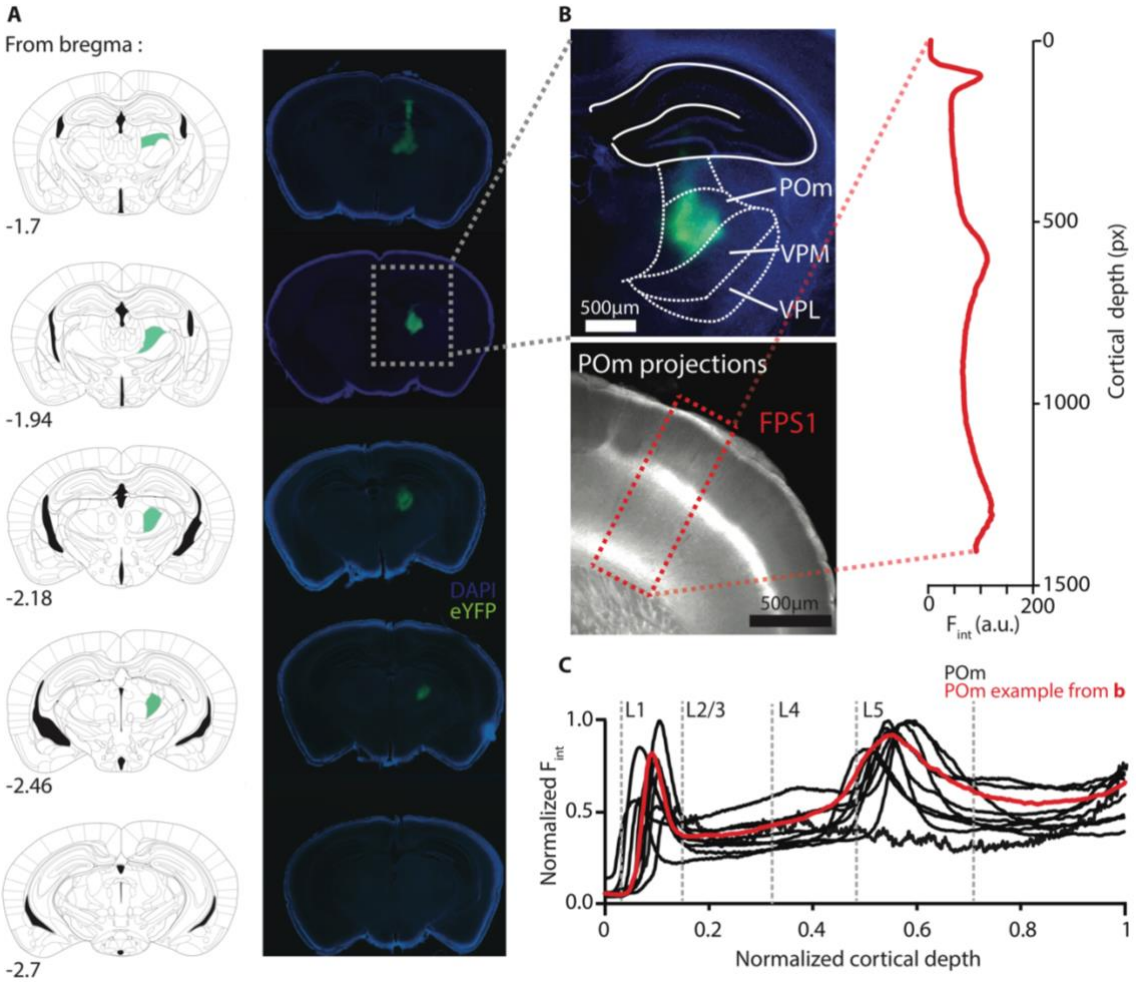

Extended Data Figure 3.1| AAV mediated expression of ChR2-eYFP in the POm nucleus of the thalamus and its axonal projections in forepaw S1.

A, Representative example of ChR2-eYFP in the mouse thalamus illustrating localized viral expression in the POm nucleus. Left, outline of cortical slices at different rostra-caudal locations indicating the POm nucleus (green) from Paxinos and Franklin, 2001. Right, Corresponding brain sections showing the virus expression profile in the thalamus. **B**, Top, enlarged fluorescence image showing ChR2-eYFP expression profile in POm nucleus from example in A. The location of the ventral posteromedial nucleus (VPM) and ventral posterior lateral nucleus (VPL) are illustrated for comparison.

Bottom, POm axonal projection profile in the forepaw area of S1 (FPS1) from example in A. Inset, Fluorescence intensity (Fint) measured as a function of cortical depth (in pixels (px)) in FPS1 (rectangle). **C**, Plot comparing the intensity profiles of 10 different animals with injections localized in the POm nucleus.

3.5 DISCUSSION

The activity of the POm nucleus increases during states of arousal and attention[95,170]. The impact this increased thalamic input has on cortical activity *in vivo* has remained largely unaddressed. In this study, we investigated the effect of sustained POm input on cortical network dynamics and discovered that POm can exert a strong inhibitory influence in superficial layers of the forepaw S1, effectively suppressing both spontaneous and sensory evoked activity of L2/3 pyramidal neurons. This finding adds to the well-characterized POm enhancing effect of cortical sensory responses reported elsewhere[166,167] and demonstrated by our own investigation (*Chapter 2*). The POm mediated enhancement and suppression of cortical activity are therefore two complementary mechanisms supported by a complex thalamocortical circuit whose modulation is likely dependent on the frequency and duration of POm input. Supporting this view, we show that forepaw stimulation evokes a wide range of responses in POm neurons. During active sensation, this thalamocortical input could have important consequences for sensory processing as animals are required to discriminate between somatosensory signals generated by self-movement and touch[40].

Primary thalamic relays exert a tight control of neural activity in sensory cortices via strong feed-forward inhibition mediated by cortical interneurons[171,70,172,173]. Our findings indicate that the higher order thalamus can similarly mediate inhibition of cortical activity in forepaw S1. In agreement with this, a previous report has shown that the nucleus MD, a higher order thalamic nucleus that does not receive direct input from the periphery, can drive feed-forward inhibition in a sub-region of the mPFC[174]. This study and the results reported here are particularly important because they suggest a circuit motif by which the

higher order thalamus could control cortical activity recruiting cortical interneurons and thus modulating not only sensory processing but also higher cognitive functions such as attentional allocation and cortical state[113,121].

Pharmacological blockade of cortical $GABA_A$ receptors abolished POm inhibitory effect. Since POm input to S1 is excitatory glutamatergic[41,152], this result indicates that POm-evoked inhibition is achieved via the recruitment of a cortical inhibitory network in forepaw S1. In superficial layers of S1, POm axonal projections form monosynaptic contacts with and preferentially excite 5HT3a inhibitory interneurons[41]. These interneurons could potentially mediate POm inhibitory effect via feed-forward inhibition. However, POm input also directly excites pyramidal neurons which could in turn excite neighboring connected interneurons leading to recurrent inhibition. This hypothesis should not be ruled out.

Photoactivation of POm input evoked a persistent-voltage response in L2/3 pyramidal neurons which led to a delayed increase in evoked AP firing. In a recent study, Zhang et al (2019) employing a similar optogenetic approach to ours (i.e. brief photo-activation of ChR2 expressing POm axons), made a similar observation in the mouse barrel cortex[166]. In agreement with this study, we found that a persistent voltage response in L2/3 neurons could be evoked not only by sustained POm photo-activation but also using a single brief (10ms) LED pulse. In the barrel cortex, the POm-evoked depolarization of L2/3 neurons exhibits oscillations in the alpha/beta range[166]. In agreement with this, we show that pharmacological manipulation of the inhibitory cortical network, which is heavily involved in the generation of cortical oscillations[31,175,176], can modulate the persistent depolarization of L2/3 neurons in forepaw S1. Pharmacological blockade of $GABA_B$, but not $GABA_A$

receptors, significantly increased the magnitude of the persistent-voltage response evoked by sustained POm input. This result suggests the recruitment of a long-lasting inhibition triggered by sustained POm input. Long-range projections have been previously shown to cause $GABA_B$–mediated inhibition in cortical pyramidal neurons of S1[48] and $GABA_B$-mediated cortical inhibition is known to underlie important functions such as regulation of fine motor control[50], visuo-spatial attention[51] and somatosensory processing[52]. Taken together, these findings further highlight the important modulatory role played by the higher order thalamus.

In conclusion, the results reported here describe a complex thalamocortical circuit capable of tightly regulating the cortical somatosensory flow. While brief POm input leads to cortical excitation in superficial layers of S1, during a sustained barrage of APs the net effect is inhibitory leading to suppression of cortical signals in L2/3 pyramidal neurons.

Chapter 4
General Discussion

4.1 SUMMARY OF MAIN RESULTS

The work presented in this thesis examined the functional contribution of the higher order somatosensory thalamus in cortical sensory processing and goal-directed behavior. In *Chapter 2*, we demonstrated that POm axons are active during stimulus presentation, generating a NMDA-dependent response in layer 2/3 pyramidal neurons within forepaw S1 which extends the sensory integration window. However, as shown in *Chapter 3*, sustained POm input can also initiate a GABAergic-dependent inhibition of L2/3 neurons sensory responses. Therefore, the work presented here suggests that both excitatory and inhibitory mechanisms can be supported by the higher order thalamocortical circuit and are contingent on the timing and duration of POm cortical input. In *Chapter 2*, we further demonstrated that the effective connectivity between POm and S1 is drastically enhanced during goal-directed behavior, with more robust signaling during correct responses, suggesting that POm plays a pivotal role during the execution of a correct goal-directed action. This finding is further corroborated by our optogenetic investigation, which revealed that photoinhibition of ArchT-expressing POm neurons decreased the overall behavioral success. Moreover, POm axonal activity in forepaw S1 was profoundly altered during the acquisition of a novel task contingency, with larger but less frequent evoked Ca^{2+} transients. Both evoked and spontaneous POm activity were enhanced during switching of the task rule, suggesting a shift in action potential firing in POm thalamocortical axons.

4.2 CELLULAR MECHANISM UNDERLYING POm-EVOKED EXCITATION AND INHIBITION

Pyramidal neurons in superficial cortical layers sparsely encode sensory stimuli, having low spontaneous and evoked firing rates, usually 1 spike per s[55–58]. Previous work has highlighted that POm input can depolarize L2/3 pyramidal neurons in the barrel cortex[27,166]. Although this excitatory input from the higher order thalamus is generally not sufficient to drive L2/3 cells to fire, when occurring concomitantly with sensory stimulation can enhance sensory processing of L2/3 pyramidal neurons increasing their AP output[166] and effectively contributing to sparse coding of sensory information. A similar enhancing effect has been observed in other higher order thalamocortical circuits. For example, increased AP generation in cortical pyramidal neurons has been reported in the visual system in response to pulvinar pharmacological activation[177] -the visual higher order thalamus- and in the MD-PFC thalamocortical loop[113]. In line with these findings, we show that in the forepaw S1, POm plays a similar role, whereby in response to a brief optogenetic stimulus applied to cortical POm axons (which likely elicits a single AP[178]), POm increases the net depolarization of the concomitant sensory evoked response in L2/3 neurons. Slice studies have shown that L2/3 pyramidal neurons are subject to weak and delayed inhibition from an interneuronal population located in L1 which expresses the serotonin receptor 5HT3a[41]. In comparison, the flow of excitation in L5 pyramidal neurons is more strongly and rapidly regulated by fast spiking PV interneurons[40,41]. In addition, activation of POm input was shown to silence SOM interneurons tonic inhibitory influence on pyramidal neurons[164]. It is possible that the interplay between these two circuit mechanisms, the concomitant 5HT3a interneurons delayed inhibition and the POm-mediated silencing of SOM

interneurons may underlie the increase in responsiveness of superficial pyramidal neurons to incoming somatosensory and distal projecting inputs. However, occasionally the flow of sensory information needs to be delayed or completely shut down to allocate portions of neural real estate to a specific sensory modality or to the generation of a motor command crucial for the task at hand[68,97,179]. We show that sustained POm input can suppress sensory integration in L2/3 pyramidal neurons in forepaw S1. This finding is in line with previous studies demonstrating POm-mediated inhibition in the BC *in vivo*[160,169] and *in vitro*[41]. How can these two contrasting findings be reconciled? It is worth noting that electrical micro stimulation (E-stim) of POm neurons was employed in one of the study that reports POm-evoked cortical inhibition[169], while in a second study, a long (300ms) optogenetic stimulus was used to activate ChR2-expressing POm axons in the rat BC[150]. Similar to our sustained POm input activation, it is plausible that the E-stim and the long optogenetic stimulus used in these studies more strongly excited POm neurons compared to the single brief light pulse used in other studies[166,167]. Our findings illustrate that, under these conditions, a more sustained POm input would drive inhibition of cortical activity. Interestingly, micro stimulation of BC L1 was shown to drive inhibition of sensory responses in L2/3 pyramidal neurons comparable to that evoked by POm stimulation[169]. Both the POm-evoked and the L1 stimulation-evoked inhibition was abolished by pharmacological blockade of L1 GABAergic drive using either $GABA_A$ antagonist Picrotoxin or P/Q-type voltage gated calcium channel blocker ω-agatoxin-IVa[169]. In line with these findings, we demonstrate that POm-evoked cortical inhibition is prevalently $GABA_A$-mediated. Distinct subpopulations of 5HT3a inhibitory interneurons reside in superficial layers of S1[41,43,180,181]. More specifically, a subfamily of 5HT3a interneurons which does not express

VIP, increases their firing in response to POm stimulation[41]. The response latency of this specific subgroup of L1 5HT3a interneurons matched the latency of inhibitory currents observed in nearby L2/3 pyramidal neurons. These results suggest that L1 5HT3a interneurons are a likely candidate to mediate POm-evoked di-synaptic inhibition of superficial pyramidal neurons[41]. In addition to 5HT3a interneurons, POm input also drives PV interneurons to fire in L2/3 of the barrel cortex although to a lesser degree compared to 5HT3a neurons[41]. It is also plausible that the sustained optogenetic activation of POm axons in our study was sufficient to drive these PV interneurons. Further investigations should aim to address the functional relevance of these unique local connectivity patterns the POm input forms with different interneuron populations. A potential experiment to study the effect of a particular interneuron type on pyramidal neurons activity, whilst maintaining spatial and temporal resolution *in vivo*, would require the use of transgenic mice carrying inhibitory opsins specific for that interneuronal population (e.g. PV). Using a similar electrophysiology/optogenetic approach to that used in this study to activate POm terminal, it would then be feasible to selectively inactivate those specific interneurons while simultaneously activating POm terminals and recording from pyramidal neurons. For this experimental approach to work different light sources would be needed, selective for the inhibitory and excitatory opsin respectively and these will have to be applied to the exposed brain surface simultaneously. Analysis of the different iterations of this approach (e.g. interneurons ON/POm terminals ON vs. interneurons OFF/POm terminal ON) will allow to infer causal relations between the specific interneuronal population investigated POm input and their effect on pyramidal neurons.

An important question that remains to be addressed is whether POm inhibition of cortical pyramidal neurons is achieved via feedforward inhibition or by recurrent cortical mechanisms. POm input was investigated in cortical slice preparations under recording conditions that tend to suppress recurrent network activity (i.e. including TTX and 4-AP in the recording solution). Under these conditions, Ca^{2+}dependent synaptic release is thought to be mediated by ChR2-depolarization at the terminal that directly enables opening of voltage-gated Ca^{2+} channels. Here, activation of POm-terminals expressing ChR2 was sufficient to drive specific networks of inhibitory interneurons to fire APs with a mean spike time well-aligned with the IPSC events simultaneously recorded in pyramidal neurons[41]. This result suggests that POm inhibitory influence is more likely achieved via feed-forward inhibition rather than being a recurrent network mechanism[41].

The ability of sustained POm input to delay the maximal firing rate of L2/3 neurons in response to sensory stimulation will have important consequences for the integration and propagation of sensory information within the cortical column and across connected cortical areas. *In vivo*, POm neurons fire at roughly 10-15 Hz during active touch[95]. This firing frequency matches the optogenetic activation frequency tested in our study suggesting that inhibition could occur physiologically rather being an artefact of the optogenetic stimulation. Previous work has suggested that such sustained POm input would drive depolarization of S1 pyramidal neurons[166]. In contrast, our results indicate that while POm input to S1 is strong and sustained, inhibition of cortical activity prevails, whereas a brief and synchronized POm input temporally locked with sensory stimulation would instead lead to enhanced sensory integration. How can these two thalamo-cortical mechanisms coexist in the same sensory area? One possible explanation is that the

functional influence of POm input to S1 could be even more localized and layer specific than previously thought. While POm more densely projects to L1 and L5a of S1[151], during touch, L2/3 neurons receive an ascending wave of excitatory input from the POm that is distributed relatively broadly[152]. Our findings suggest that strong and sustained POm input prevalently targeted to L1 is inhibitory whereas POm input to L2/3 might have the opposite effect, driving depolarization perhaps recruiting the known VIP to SOM interneuron dis-inhibitory network[41,164].

The functional consequences of the persistent voltage response are potentially important for both plasticity and perception. POm was recently shown to facilitate a NMDA-dependent plateau potential in the BC that can induce synaptic long-term potentiation in superficial pyramidal neurons[27]. In agreement with this finding we demonstrate that in forepaw S1 the POm-mediated persistent-voltage response in L2/3 neurons is NMDA-dependent and can extend the duration of sensory evoked responses.

Additionally, we report that sustained, but not brief, POm input activation recruited long-lasting $GABA_B$ mediated inhibition which further modulated the persistent voltage response. This finding is in line with functional mechanisms of $GABA_B$ receptors activation, which require strong and persistent firing to accumulate sufficient amounts of synaptically released GABA[182].

Presynaptic $GABA_B$ receptors can be found on many feedforward inhibitory neurons and glutamatergic terminals where they act as autoreceptors. Moreover, presynaptic $GABA_B$ receptors on glutamatergic terminals were shown to be activated by GABA spillover from neighbouring inhibitory synapses[183,184]. Albeit speculative, a potential mechanism to regulate the input flow from POm neuron at thalamocortical synapses could be mediated

by $GABA_B$ autoreceptors. This hypothesis not tested here is worth of further investigation. $GABA_B$ receptors have also been implicated in the control of cortical networks[185]. Depending on the temporal properties of network activity, $GABA_B$ receptors can directly mediate slow network activity, modulate the strength of fast network activity, and moderate the relative spike timing of individual cells during network oscillations[185]. This evidence is in line with the role played by the POm as modulator of cortical activity delineated in this study. In this framework, the higher order thalamus would act as a hub for the convergence and transfer behaviorally relevant information to S1 having a dramatic effect on sensory processing affecting sparseness and cortical state[121].

4.3 LIMITATIONS OF THE ChR2 OPTOGENETIC APPROACH

While optogenetics provides a powerful tool to investigate neural network dynamics, there are limitations to the application of this technique. More specifically, a major caveat for the interpretation of the effect of POm input on its cortical targets is the synchronized activation of all ChR2-expressing POm axons located in the illuminated area. This synchronized activation is hardly physiological. In fact, Ca^{2+} imaging of POm axons in awake naïve mice (*Chapter 1*) indicates that only a fraction of the entire POm axonal population is active at any given time in forepaw S1. Such synchronized activation will inevitably provide a stronger driving input that will bias the effect of POm activation toward the strongest responses. In addition, given that in our preparation, the field of focus was roughly the size of the entire forepaw area (1-1.5 mm), the unique local functional specificity of POm input effect could not be properly assessed. Similarly, the laminar specificity of POm input can only partially be inferred. The total blue light energy

transmitted within the cortical tissue *in vivo* decreases rapidly with distance (to around 50% by 100 μm and by 90% at 1 mm;[186,187]). Under these conditions, the effective area of ChR2 activation is restricted to few hundred microns[150]. Therefore, while it can be safely assumed that POm axons activation is strongly weighted toward L1 projections, it cannot be ruled out that broadly projecting POm terminals in L2/3 could also be activated. These limitations of the optogenetic tool should be taken into account when interpreting the findings reported here and elsewhere.

4.4 BEHAVIORAL IMPACT OF POm CORTICAL INPUT

In this study, we aimed to assess the contribution of the higher order somatosensory thalamus to goal-directed behavior. To achieve this aim, we trained mice to perform a tactile based goal-directed task and imaged POm axonal projections in superficial layers of forepaw S1. To our knowledge, this is the first attempt to investigate the role of POm cortical input during goal-directed behavior. In naive mice, POm input to forepaw S1 significantly increases during tactile stimulus presentation suggesting stimulus encoding. However, the effective connectivity between POm and S1 is drastically enhanced during goal-directed action, with a two-fold increase in Ca^{2+} transient rate and number of active POm axons during HIT behavior. This robust increase in activity during active but not passive behavior –the action-suppression task- suggests that motor or premotor activity influences POm input dynamics in forepaw S1. Indeed, the primary motor cortex (M1) forms strong and reciprocal connections with the POm nucleus [95,159] which could drive POm activity during goal-directed action. Furthermore, a trans-thalamic pathway coursing through the POm has been described to link these two cortical areas[188]. Trans-thalamic pathways reliably relay information between connected cortical areas, are generally

arranged in parallel with the direct corticocortical pathway and are a prevalent feature of higher order thalamic nuclei[94]. For example, a trans-thalamic pathway running through the pulvinar allows information transfer between primary and secondary visual areas[189]. In addition, these alternative pathways have also been found between S1 and S2 via the POm[190] and connecting primary and secondary auditory cortices via the dorsal division of the medial geniculate nucleus[189]. These parallel routes of information transfer between cortical areas are a fascinating architectural aspect of brain connectivity whose role in the global economy of brain function is still poorly understood[191]. Thus, it would of great interest to probe the functional connectivity between M1 to S1 via the POm trans-thalamic pathway during goal-directed behavior. In addition to M1 drive, the POm is also the recipient of cholinergic modulation, which could contribute to the increase in POm input to S1 observed during the active task [162].

What inferences can we make about the cortical effect of POm input during goal-directed behavior? Our optogenetic and electrophysiological experiments can help address this question. However, it is important to first highlight an important limitation due to the slow kinetics of the fluorescent reporter used GCAMP6f[192]. In order to improve signal-to-noise ratio for *in vivo* imaging, calcium fluorescent reporters have high binding affinity, resulting in fluorescence which is slower than the biological events they aim to monitor. This constraint limits the correlation that can be made between the fluorescent signal and the underlying biological events even when adopting sophisticated deconvolution strategies[193]. For this reason, it is difficult to assess the number, frequency or duration of APs underlying the Ca^{2+} signal recorded in POm axons during behavior. Bearing this in mind, as previously discussed, we observed that brief POm input to forepaw S1 extends the sensory integration

window of L2/3 pyramidal neurons in forepaw S1. During goal-directed behavior, this prolonged window of depolarization would facilitate the integration of behaviorally relevant inputs ranging from sensory, motor, reward and attentional input[166,167]. On the other hand, inhibition of cortical sensory processing could also be beneficial during the generation of a motor response. The literature on the topic is divided, while motor input can increase S1 cortical activity thus facilitating motor integration[43], during whisking, sensory voltage responses in BC neurons change from large to small amplitude[122]. Similarly, active touch was shown to heavily recruit GABAergic interneurons in the somatosensory cortex in a behavior-relevant and layer specific manner[40]. Such dichotomy of the effect of motion is observed virtually in all sensory cortices[194]. Future experiments, combining simultaneous thalamic electrophysiological recording and POm axonal imaging, will help elucidate the exact impact of POm input on S1 cortical activity during a goal-directed action.

4.5 PLASTICITY OF POm INPUT DURING SWITCHING

During switching of the task contingency POm axonal activity in forepaw S1 was drastically altered, with larger but less frequently evoked Ca^{2+} transients. Both evoked and spontaneous activity were enhanced during switching of the task rule, suggesting an overall shift in action potential firing in POm thalamocortical axons. This finding is noteworthy for multiple reasons: first it suggests that activity in the POm nucleus may encode the action-outcome association. This aspect of POm function is unheard-of and requires extensive investigation, for example measuring POm activity during classical goal-directed behavioral paradigms followed by extinction of the learned action-outcome contingency.

Second, it suggests a state change in information transfer between the POm and the cortex. An important feature of thalamic neurons is their ability to fire in two distinct modes (called tonic and burst)[195].

A key mechanism underlying the generation of burst firing is the low threshold activation and delayed inactivation of voltage-gated, T-type Ca^{2+}channels in the membranes of soma and dendrites[196], which strongly affects the nature of the signal that is relayed to the cortex[195]. For example, compared with tonic mode, burst mode produces much more nonlinear distortions in the relay of information, but the information being relayed has greater detectability and generates stronger activation of postsynaptic cortical targets[195]. During the acquisition and reversal of a goal-directed behavior, imaging of POm axonal projections in the target cortex should be paired with direct electrophysiological investigation at thalamic level to assess whether a behaviorally-correlated transition from tonic to burst mode occurs in POm neurons and when this signal is relayed to the target cortex. Finally, this finding provides further support to the body of research indicating that POm-mediated plasticity changes in S1 are crucial for perceptual learning[27,42,164]. Opto/chemo-genetic silencing of POm cortical input during the training phase of a behavioral task would help elucidate if this is indeed the case.

4.6 CONCLUSION

Several studies have shown the role of the higher order somatosensory thalamus in sensory processing and learning. The work presented here expands on this previous knowledge demonstrating that POm input can have a powerful inhibitory action on sensory processing and engage a long-lasting $GABA_B$-mediated disynaptic circuit. In addition, our findings

show that the POm encodes goal-directed behavior and behavioral switching demonstrating that activity in the higher order thalamus tightly correlates with cognitive behavior. As discussed above, this study and the previous body of research alike, have primarily focused on the role of POm input to S1 and to a lesser extent to M1. Nevertheless, POm cortical projections are widespread, encompassing higher order association areas such as the premotor and the posterior parietal cortex[146–149]. What information the POm relays to these cortical areas? and what information is relayed back to the higher order thalamus? The POm nucleus is a strategic hub for the integration and relay of cortical information. Elucidating the unique connectivity patterns between these higher order cognitive centers and their functional role during behavior should be the focus of future research.

While investigators have recognized for many decades that the thalamus has functions beyond the relay of ascending sensory signals, it has been difficult to specify and quantify these beyond-relay functions. One reason is that such functions are likely much more prominent in behaving animals, which are difficult to study. Overall, with this thesis, I aimed to add further evidence to the body of research which has already revealed a far richer contribution of thalamic activity to cognition with roles ranging from learning and memory to attentional allocation and flexible adaptation. Hopefully, I have achieved this goal and these notions will make a small but tangible contribution to the understanding of circuit function and most importantly dysfunction in the brain.

4.7 THESIS REFERENCES

1. Romo, R., Lemus, L. & de Lafuente, V. Sense, memory, and decision-making in the somatosensory cortical network. *Curr. Opin. Neurobiol.* **22**, 914–919 (2012).
2. Gilbert, C. D. & Sigman, M. Brain states: top-down influences in sensory processing. *Neuron* **54**, 677–696 (2007).
3. Shuler, M. G. & Bear, M. F. Reward timing in the primary visual cortex. *Science* **311**, 1606–1609 (2006).
4. Jaramillo, S. & Zador, A. M. The auditory cortex mediates the perceptual effects of acoustic temporal expectation. *Nat. Neurosci.* **14**, 246–251 (2011).
5. Reynolds, J. H. & Heeger, D. J. The normalization model of attention. *Neuron* **61**, 168–185 (2009).
6. Saleem, A. B., Ayaz, A., Jeffery, K. J., Harris, K. D. & Carandini, M. Integration of visual motion and locomotion in mouse visual cortex. *Nat. Neurosci.* **16**, 1864–1869 (2013).
7. Petreanu, L. *et al.* Activity in motor-sensory projections reveals distributed coding in somatosensation. *Nature* **489**, 299–303 (2012).
8. Deschênes, M., Veinante, P. & Zhang, Z. W. The organization of corticothalamic projections: reciprocity versus parity. *Brain Res. Brain Res. Rev.* **28**, 286–308 (1998).
9. Jones, E. G. *The Thalamus*. (Springer Science & Business Media, 2012).
10. Bickford, M. E. Thalamic Circuit Diversity: Modulation of the Driver/Modulator Framework. *Front. Neural Circuits* 86 (2016) doi:10.3389/fncir.2015.00086.

11. Sherman, S. M. & Guillery, R. W. On the actions that one nerve cell can have on another: Distinguishing “drivers” from “modulators”. *Proc. Natl. Acad. Sci.* **95**, 7121–7126 (1998).

12. Groh, A. *et al.* Convergence of Cortical and Sensory Driver Inputs on Single Thalamocortical Cells. *Cereb. Cortex N. Y. NY* **24**, 3167–3179 (2014).

13. Larkum, M. A cellular mechanism for cortical associations: an organizing principle for the cerebral cortex. *Trends Neurosci.* **36**, 141–151 (2013).

14. Shipp, S. Structure and function of the cerebral cortex. *Curr. Biol.* **17**, R443–R449 (2007).

15. Reznikov, D. K. Y. Hippocampal Formation in the Mouse and Rat — Structural Organization and Development: A Review. in *Cell Proliferation and Cytogenesis in the Mouse Hippocampus* 1–11 (Springer Berlin Heidelberg, 1991). doi:10.1007/978-3-642-76447-9_1.

16. Constantinople, C. M. & Bruno, R. M. Deep Cortical Layers Are Activated Directly by Thalamus. *Science* **340**, 1591–1594 (2013).

17. DeFelipe, J. & Fariñas, I. The pyramidal neuron of the cerebral cortex: Morphological and chemical characteristics of the synaptic inputs. *Prog. Neurobiol.* **39**, 563–607 (1992).

18. Rubio-Garrido, P., Pérez-de-Manzo, F., Porrero, C., Galazo, M. J. & Clascá, F. Thalamic Input to Distal Apical Dendrites in Neocortical Layer 1 Is Massive and Highly Convergent. *Cereb. Cortex* **19**, 2380–2395 (2009).

19. Cauller, L. J., Clancy, B. & Connors, B. W. Backward cortical projections to primary somatosensory cortex in rats extend long horizontal axons in layer I. *J. Comp. Neurol.* **390**, 297–310 (1998).

20. Felleman, D. J. & Van Essen, D. C. Distributed hierarchical processing in the primate cerebral cortex. *Cereb. Cortex N. Y. N 1991* **1**, 1–47 (1991).

21. Grienberger, C., Chen, X. & Konnerth, A. Dendritic function in vivo. *Trends Neurosci.* **38**, 45–54 (2015).

22. Bean, B. P. The action potential in mammalian central neurons. *Nat. Rev. Neurosci.* **8**, 451–465 (2007).

23. Rall, W. Distinguishing theoretical synaptic potentials computed for different soma-dendritic distributions of synaptic input. *J. Neurophysiol.* **30**, 1138–1168 (1967).

24. Llinás, R., Nicholson, C., Freeman, J. A. & Hillman, D. E. Dendritic Spikes and Their Inhibition in Alligator Purkinje Cells. *Science* **160**, 1132–1135 (1968).

25. Major, G., Larkum, M. E. & Schiller, J. Active properties of neocortical pyramidal neuron dendrites. *Annu. Rev. Neurosci.* **36**, 1–24 (2013).

26. Palmer, L. M. Dendritic integration in pyramidal neurons during network activity and disease. *Brain Res. Bull.* **103**, 2–10 (2014).

27. Gambino, F. *et al.* Sensory-evoked LTP driven by dendritic plateau potentials in vivo. *Nature* **515**, 116–119 (2014).

28. Palmer, L. M. *et al.* NMDA spikes enhance action potential generation during sensory input. *Nat. Neurosci.* **17**, 383–390 (2014).

29. Takahashi, N., Oertner, T. G., Hegemann, P. & Larkum, M. E. Active cortical dendrites modulate perception. *Science* **354**, 1587–1590 (2016).

30. Swanson, O. K. & Maffei, A. From Hiring to Firing: Activation of Inhibitory Neurons and Their Recruitment in Behavior. *Front. Mol. Neurosci.* **12**, (2019).

31. Isaacson, J. S. & Scanziani, M. How Inhibition Shapes Cortical Activity. *Neuron* **72**, 231–243 (2011).

32. Higley, M. J. Localized GABAergic inhibition of dendritic Ca2+ signalling. *Nat. Rev. Neurosci.* **15**, 567–572 (2014).

33. Chalifoux, J. R. & Carter, A. G. GABAB receptor modulation of synaptic function. *Curr. Opin. Neurobiol.* **21**, 339–344 (2011).

34. Rudy, B., Fishell, G., Lee, S. & Hjerling-Leffler, J. Three groups of interneurons account for nearly 100% of neocortical GABAergic neurons. *Dev. Neurobiol.* **71**, 45–61 (2011).

35. Di Cristo, G. *et al.* Subcellular domain-restricted GABAergic innervation in primary visual cortex in the absence of sensory and thalamic inputs. *Nat. Neurosci.* **7**, 1184–1186 (2004).

36. Pouille, F. & Scanziani, M. Enforcement of temporal fidelity in pyramidal cells by somatic feed-forward inhibition. *Science* **293**, 1159–1163 (2001).

37. Wang, Y. *et al.* Anatomical, physiological and molecular properties of Martinotti cells in the somatosensory cortex of the juvenile rat. *J. Physiol.* **561**, 65–90 (2004).

38. Kapfer, C., Glickfeld, L. L., Atallah, B. V. & Scanziani, M. Supralinear increase of recurrent inhibition during sparse activity in the somatosensory cortex. *Nat. Neurosci.* **10**, 743–753 (2007).

39. Batista-Brito, R. *et al.* Developmental dysfunction of VIP interneurons impairs cortical circuits. *Neuron* **95**, 884-895.e9 (2017).

40. Yu, J., Hu, H., Agmon, A. & Svoboda, K. Recruitment of GABAergic Interneurons in the Barrel Cortex during Active Tactile Behavior. *Neuron* (2019) doi:10.1016/j.neuron.2019.07.027.

41. Audette, N. J., Urban-Ciecko, J., Matsushita, M. & Barth, A. L. POm Thalamocortical Input Drives Layer-Specific Microcircuits in Somatosensory Cortex. *Cereb. Cortex N. Y. N 1991* **28**, 1312–1328 (2018).

42. Audette, N. J., Bernhard, S. M., Ray, A., Stewart, L. T. & Barth, A. L. Rapid Plasticity of Higher-Order Thalamocortical Inputs during Sensory Learning. *Neuron* (2019) doi:10.1016/j.neuron.2019.04.037.

43. Lee, S., Kruglikov, I., Huang, Z. J., Fishell, G. & Rudy, B. A disinhibitory circuit mediates motor integration in the somatosensory cortex. *Nat. Neurosci.* **16**, 1662–1670 (2013).

44. Fu, Y. *et al.* A cortical circuit for gain control by behavioral state. *Cell* **156**, 1139–1152 (2014).

45. Prönneke, A. *et al.* Characterizing VIP Neurons in the Barrel Cortex of VIPcre/tdTomato Mice Reveals Layer-Specific Differences. *Cereb. Cortex N. Y. N 1991* **25**, 4854–4868 (2015).

46. Kamigaki, T. & Dan, Y. Delay activity of specific prefrontal interneuron subtypes modulates memory-guided behavior. *Nat. Neurosci.* **20**, 854–863 (2017).

47. Garcia-Junco-Clemente, P. *et al.* An inhibitory pull-push circuit in frontal cortex. *Nat. Neurosci.* **20**, 389–392 (2017).

48. Palmer, L. M. *et al.* The cellular basis of GABA(B)-mediated interhemispheric inhibition. *Science* **335**, 989–993 (2012).

49. Gazzaniga, M. S. Forty-five years of split-brain research and still going strong. *Nat. Rev. Neurosci.* **6**, 653–659 (2005).

50. Geffen, G. M., Jones, D. L. & Geffen, L. B. Interhemispheric control of manual motor activity. *Behav. Brain Res.* **64**, 131–140 (1994).

51. Cazzoli, D., Wurtz, P., Müri, R. M., Hess, C. W. & Nyffeler, T. Interhemispheric balance of overt attention: a theta burst stimulation study. *Eur. J. Neurosci.* **29**, 1271–1276 (2009).

52. Forss, N., Hietanen, M., Salonen, O. & Hari, R. Modified activation of somatosensory cortical network in patients with right-hemisphere stroke. *Brain J. Neurol.* **122 (Pt 10)**, 1889–1899 (1999).

53. Williams, L. E. & Holtmaat, A. Higher-order thalamocortical inputs gate synaptic long-term potentiation via disinhibiton. *bioRxiv* 281477 (2018) doi:10.1101/281477.

54. Landisman, C. E. & Connors, B. W. VPM and PoM nuclei of the rat somatosensory thalamus: intrinsic neuronal properties and corticothalamic feedback. *Cereb. Cortex N. Y. N 1991* **17**, 2853–2865 (2007).

55. O'Connor, D. H., Peron, S. P., Huber, D. & Svoboda, K. Neural activity in barrel cortex underlying vibrissa-based object localization in mice. *Neuron* **67**, 1048–1061 (2010).

56. Niell, C. M. & Stryker, M. P. Highly Selective Receptive Fields in Mouse Visual Cortex. *J. Neurosci.* **28**, 7520–7536 (2008).

57. de Kock, C. P. J., Bruno, R. M., Spors, H. & Sakmann, B. Layer- and cell-type-specific suprathreshold stimulus representation in rat primary somatosensory cortex. *J. Physiol.* **581**, 139–154 (2007).

58. Sakata, S. & Harris, K. D. Laminar structure of spontaneous and sensory-evoked population activity in auditory cortex. *Neuron* **64**, 404–418 (2009).

59. Harris, K. D. & Mrsic-Flogel, T. D. Cortical connectivity and sensory coding. *Nature* **503**, 51–58 (2013).

60. Wolfe, J., Houweling, A. R. & Brecht, M. Sparse and powerful cortical spikes. *Curr. Opin. Neurobiol.* **20**, 306–312 (2010).

61. Barth, A. L. & Poulet, J. F. A. Experimental evidence for sparse firing in the neocortex. *Trends Neurosci.* **35**, 345–355 (2012).

62. Olshausen, B. A. & Field, D. J. Sparse coding of sensory inputs. *Curr. Opin. Neurobiol.* **14**, 481–487 (2004).

63. Bruno, R. M. & Sakmann, B. Cortex Is Driven by Weak but Synchronously Active Thalamocortical Synapses. *Science* **312**, 1622–1627 (2006).

64. Lennie, P. The cost of cortical computation. *Curr. Biol. CB* **13**, 493–497 (2003).

65. Attwell, D. & Laughlin, S. B. An energy budget for signaling in the grey matter of the brain. *J. Cereb. Blood Flow Metab. Off. J. Int. Soc. Cereb. Blood Flow Metab.* **21**, 1133–1145 (2001).

66. Barth, A. L. & Poulet, J. F. A. Experimental evidence for sparse firing in the neocortex. *Trends Neurosci.* **35**, 345–355 (2012).

67. Silberberg, G. & Markram, H. Disynaptic inhibition between neocortical pyramidal cells mediated by Martinotti cells. *Neuron* **53**, 735–746 (2007).

68. Otazu, G. H., Tai, L.-H., Yang, Y. & Zador, A. M. Engaging in an auditory task suppresses responses in auditory cortex. *Nat. Neurosci.* **12**, 646–654 (2009).

69. Poo, C. & Isaacson, J. S. Odor representations in olfactory cortex: 'sparse' coding, global inhibition, and oscillations. *Neuron* **62**, 850–861 (2009).

70. Daw, M. I., Ashby, M. C. & Isaac, J. T. R. Coordinated developmental recruitment of latent fast spiking interneurons in layer IV barrel cortex. *Nat. Neurosci.* **10**, 453–461 (2007).

71. Carandini, M. & Churchland, A. K. Probing perceptual decisions in rodents. *Nat. Neurosci.* **16**, 824–831 (2013).

72. Dickinson, A. Actions and Habits: The Development of Behavioural Autonomy. *Philos. Trans. R. Soc. B Biol. Sci.* **308**, 67–78 (1985).

73. Adams, C. D. & Dickinson, A. Instrumental responding following reinforcer devaluation. *Q. J. Exp. Psychol. Sect. B* **33**, 109–121 (1981).

74. Dickinson, A. & Pérez, O. D. Chapter 1 - Actions and Habits: Psychological Issues in Dual-System Theory. in *Goal-Directed Decision Making* (eds. Morris, R., Bornstein, A. & Shenhav, A.) 1–25 (Academic Press, 2018). doi:10.1016/B978-0-12-812098-9.00001-2.

75. Raab, H. A. & Hartley, C. A. CHAPTER 13 c 0013 The Development of Goal-Directed Decision-Making. in (2018).

76. Tricomi, E., Balleine, B. W. & O'Doherty, J. P. A specific role for posterior dorsolateral striatum in human habit learning. *Eur. J. Neurosci.* **29**, 2225–2232 (2009).

77. Dickinson, A. Omission Learning after Instrumental Pretraining. *Q. J. Exp. Psychol. Sect. B* **51**, 271–286 (1998).

78. Simmler, L. D. & Ozawa, T. Neural circuits in goal-directed and habitual behavior: Implications for circuit dysfunction in obsessive-compulsive disorder. *Neurochem. Int.* **129**, 104464 (2019).

79. Robbins, T. W. & Costa, R. M. Habits. *Curr. Biol.* **27**, R1200–R1206 (2017).

80. Balleine, B. W. & O'Doherty, J. P. Human and Rodent Homologies in Action Control: Corticostriatal Determinants of Goal-Directed and Habitual Action. *Neuropsychopharmacology* **35**, 48–69 (2010).

81. Jahanshahi, M., Obeso, I., Rothwell, J. C. & Obeso, J. A. A fronto–striato–subthalamic–pallidal network for goal-directed and habitual inhibition. *Nat. Rev. Neurosci.* **16**, 719–732 (2015).

82. Gremel, C. M. & Costa, R. M. Orbitofrontal and striatal circuits dynamically encode the shift between goal-directed and habitual actions. *Nat. Commun.* **4**, 2264 (2013).

83. Daw, N. D., O'Doherty, J. P., Dayan, P., Seymour, B. & Dolan, R. J. Cortical substrates for exploratory decisions in humans. *Nature* **441**, 876–879 (2006).

84. Hampton, A. N., Bossaerts, P. & O'Doherty, J. P. The role of the ventromedial prefrontal cortex in abstract state-based inference during decision making in humans. *J. Neurosci. Off. J. Soc. Neurosci.* **26**, 8360–8367 (2006).

85. Haber, S. N., Kim, K.-S., Mailly, P. & Calzavara, R. Reward-related cortical inputs define a large striatal region in primates that interface with associative cortical connections, providing a substrate for incentive-based learning. *J. Neurosci. Off. J. Soc. Neurosci.* **26**, 8368–8376 (2006).

86. Pickens, C. L. *et al.* Different Roles for Orbitofrontal Cortex and Basolateral Amygdala in a Reinforcer Devaluation Task. *J. Neurosci.* **23**, 11078–11084 (2003).

87. Rudebeck, P. H., Saunders, R. C., Lundgren, D. A. & Murray, E. A. Specialized Representations of Value in the Orbital and Ventrolateral Prefrontal Cortex: Desirability versus Availability of Outcomes. *Neuron* **95**, 1208-1220.e5 (2017).

88. Corbit, L. H. & Janak, P. H. Posterior dorsomedial striatum is critical for both selective instrumental and Pavlovian reward learning. *Eur. J. Neurosci.* **31**, 1312–1321 (2010).

89. Yin, H. H., Knowlton, B. J. & Balleine, B. W. Inactivation of dorsolateral striatum enhances sensitivity to changes in the action-outcome contingency in instrumental conditioning. *Behav. Brain Res.* **166**, 189–196 (2006).

90. Russo, S. J. & Nestler, E. J. The brain reward circuitry in mood disorders. *Nat. Rev. Neurosci.* **14**, 609–625 (2013).

91. Corbit, L. H. & Balleine, B. W. Double Dissociation of Basolateral and Central Amygdala Lesions on the General and Outcome-Specific Forms of Pavlovian-Instrumental Transfer. *J. Neurosci.* **25**, 962–970 (2005).

92. Schultz, W. Multiple reward signals in the brain. *Nat. Rev. Neurosci.* **1**, 199–207 (2000).

93. Llinás, R. R., Leznik, E. & Urbano, F. J. Temporal binding via cortical coincidence detection of specific and nonspecific thalamocortical inputs: A voltage-dependent dye-imaging study in mouse brain slices. *Proc. Natl. Acad. Sci. U. S. A.* **99**, 449–454 (2002).

94. Sherman, S. M. Thalamus plays a central role in ongoing cortical functioning. *Nat. Neurosci.* **19**, 533–541 (2016).

95. Urbain, N. *et al.* Whisking-Related Changes in Neuronal Firing and Membrane Potential Dynamics in the Somatosensory Thalamus of Awake Mice. *Cell Rep.* **13**, 647–656 (2015).

96. Guo, Z. V. *et al.* Maintenance of persistent activity in a frontal thalamocortical loop. *Nature* **545**, 181–186 (2017).

97. Wimmer, R. D. *et al.* Thalamic control of sensory selection in divided attention. *Nature* **526**, 705–709 (2015).

98. Rikhye, R. V., Gilra, A. & Halassa, M. M. Thalamic regulation of switching between cortical representations enables cognitive flexibility. *Nat. Neurosci.* **21**, 1753–1763 (2018).

99. Saalmann, Y. B., Pinsk, M. A., Wang, L., Li, X. & Kastner, S. Pulvinar regulates information transmission between cortical areas based on attention demands. *Science* **337**, 753–756 (2012).

100. Komura, Y. *et al.* Retrospective and prospective coding for predicted reward in the sensory thalamus. *Nature* **412**, 546–549 (2001).

101. Do-Monte, F. H., Minier-Toribio, A., Quiñones-Laracuente, K., Medina-Colón, E. M. & Quirk, G. J. Thalamic Regulation of Sucrose Seeking during Unexpected Reward Omission. *Neuron* **94**, 388-400.e4 (2017).

102. Govindaiah, G., Wang, Y. & Cox, C. L. Dopamine enhances the excitability of somatosensory thalamocortical neurons. *Neuroscience* **170**, 981–991 (2010).

103. García-Cabezas, M. Á., Martínez-Sánchez, P., Sánchez-González, M. Á., Garzón, M. & Cavada, C. Dopamine Innervation in the Thalamus: Monkey versus Rat. *Cereb. Cortex N. Y. NY* **19**, 424–434 (2009).

104. Papadopoulos, G. C. & Parnavelas, J. G. Distribution and synaptic organization of dopaminergic axons in the lateral geniculate nucleus of the rat. *J. Comp. Neurol.* **294**, 356–361 (1990).

105. Wilson, J. *et al.* Literary reviews. *Third World Q.* **11**, 279–310 (1989).

106. Castro, A. J. The effects of cortical ablations on digital usage in the rat. *Brain Res.* **37**, 173–185 (1972).

107. Darling, W. G., Pizzimenti, M. A. & Morecraft, R. J. Functional recovery following motor cortex lesions in non-human primates: experimental implications for human stroke patients. *J. Integr. Neurosci.* **10**, 353–384 (2011).

108. Lawrence, D. G. & Kuypers, H. G. The functional organization of the motor system in the monkey. I. The effects of bilateral pyramidal lesions. *Brain J. Neurol.* **91**, 1–14 (1968).

109. Díaz-Hernández, E. *et al.* The Thalamostriatal Projections Contribute to the Initiation and Execution of a Sequence of Movements. *Neuron* **100**, 739-752.e5 (2018).

110. Ito, M. & Doya, K. Distinct Neural Representation in the Dorsolateral, Dorsomedial, and Ventral Parts of the Striatum during Fixed- and Free-Choice Tasks. *J. Neurosci.* **35**, 3499–3514 (2015).

111. Yin, H. H. & Knowlton, B. J. The role of the basal ganglia in habit formation. *Nat. Rev. Neurosci.* **7**, 464–476 (2006).

112. Halassa, M. M. & Kastner, S. Thalamic functions in distributed cognitive control. *Nat. Neurosci.* **20**, 1669–1679 (2017).

113. Schmitt, L. I. *et al.* Thalamic amplification of cortical connectivity sustains attentional control. *Nature* **545**, 219–223 (2017).

114. Daum, I. & Ackermann, H. Frontal-type memory impairment associated with thalamic damage. *Int. J. Neurosci.* **77**, 187–198 (1994).

115. Van der Werf, Y. D., Witter, M. P., Uylings, H. B. & Jolles, J. Neuropsychology of infarctions in the thalamus: a review. *Neuropsychologia* **38**, 613–627 (2000).

116. Van der Werf, Y. D. *et al.* Deficits of memory, executive functioning and attention following infarction in the thalamus; a study of 22 cases with localised lesions. *Neuropsychologia* **41**, 1330–1344 (2003).

117. Saalmann, Y. B. & Kastner, S. Cognitive and perceptual functions of the visual thalamus. *Neuron* **71**, 209–223 (2011).

118. Shipp, S. The functional logic of cortico-pulvinar connections. *Philos. Trans. R. Soc. B Biol. Sci.* **358**, 1605–1624 (2003).

119. Poulet, J. F. A. & Petersen, C. C. H. Internal brain state regulates membrane potential synchrony in barrel cortex of behaving mice. *Nature* **454**, 881–885 (2008).

120. Urbain, N., Fourcaud-Trocmé, N., Laheux, S., Salin, P. A. & Gentet, L. J. Brain-State-Dependent Modulation of Neuronal Firing and Membrane Potential Dynamics in the Somatosensory Thalamus during Natural Sleep. *Cell Rep.* **26**, 1443-1457.e5 (2019).

121. Poulet, J. F. A., Fernandez, L. M. J., Crochet, S. & Petersen, C. C. H. Thalamic control of cortical states. *Nat. Neurosci.* **15**, 370–372 (2012).

122. Crochet, S. & Petersen, C. C. H. Correlating whisker behavior with membrane potential in barrel cortex of awake mice. *Nat. Neurosci.* **9**, 608–610 (2006).

123. Everitt, B. J. & Robbins, T. W. Drug Addiction: Updating Actions to Habits to Compulsions Ten Years On. *Annu. Rev. Psychol.* **67**, 23–50 (2016).

124. Godier, L. R. & Park, R. J. Compulsivity in anorexia nervosa: a transdiagnostic concept. *Front. Psychol.* **5**, (2014).

125. Gillan, C. M. *et al.* Disruption in the Balance Between Goal-Directed Behavior and Habit Learning in Obsessive-Compulsive Disorder. *Am. J. Psychiatry* **168**, 718–726 (2011).

126. Morris, R. W., Quail, S., Griffiths, K. R., Green, M. J. & Balleine, B. W. Corticostriatal Control of Goal-Directed Action Is Impaired in Schizophrenia. *Biol. Psychiatry* **77**, 187–195 (2015).

127. Albin, R. L., Young, A. B. & Penney, J. B. The functional anatomy of basal ganglia disorders. *Trends Neurosci.* **12**, 366–375 (1989).

128. DeLong, M. R. Primate models of movement disorders of basal ganglia origin. *Trends Neurosci.* **13**, 281–285 (1990).

129. Kringelbach, M. L. & Rolls, E. T. Neural correlates of rapid reversal learning in a simple model of human social interaction. *NeuroImage* **20**, 1371–1383 (2003).

130. Cools, R., Lewis, S. J. G., Clark, L., Barker, R. A. & Robbins, T. W. L-DOPA disrupts activity in the nucleus accumbens during reversal learning in Parkinson's disease. *Neuropsychopharmacol. Off. Publ. Am. Coll. Neuropsychopharmacol.* **32**, 180–189 (2007).

131. Brennan, B. P., Rauch, S. L., Jensen, J. E. & Pope, H. G. A Critical Review of Magnetic Resonance Spectroscopy Studies of Obsessive-Compulsive Disorder. *Biol. Psychiatry* **73**, 24–31 (2013).

132. Menzies, L. *et al.* Integrating evidence from neuroimaging and neuropsychological studies of obsessive-compulsive disorder: The orbitofronto-striatal model revisited. *Neurosci. Biobehav. Rev.* **32**, 525–549 (2008).

133. Saxena, S. & Rauch, S. L. FUNCTIONAL NEUROIMAGING AND THE NEUROANATOMY OF OBSESSIVE-COMPULSIVE DISORDER. *Psychiatr. Clin. North Am.* **23**, 563–586 (2000).

134. Welch, J. M. *et al.* Cortico-striatal synaptic defects and OCD-like behaviours in *Sapap3*-mutant mice. *Nature* **448**, 894–900 (2007).

135. Brown, R. G. & Pluck, G. Negative symptoms: the 'pathology' of motivation and goal-directed behaviour. *Trends Neurosci.* **23**, 412–417 (2000).

136. Kaye, W. H. *et al.* Does a shared neurobiology for foods and drugs of abuse contribute to extremes of food ingestion in anorexia and bulimia nervosa? *Biol. Psychiatry* **73**, 836–842 (2013).

137. Huber, D. *et al.* Multiple dynamic representations in the motor cortex during sensorimotor learning. *Nature* **484**, 473–478 (2012).

138. Lacefield, C. O., Pnevmatikakis, E. A., Paninski, L. & Bruno, R. M. Reinforcement Learning Recruits Somata and Apical Dendrites across Layers of Primary Sensory Cortex. *Cell Rep.* **26**, 2000-2008.e2 (2019).

139. Sensation, movement and learning in the absence of barrel cortex | Nature. https://www.nature.com/articles/s41586-018-0527-y.

140. Diamond, M. E., Heimendahl, M. von, Knutsen, P. M., Kleinfeld, D. & Ahissar, E. 'Where' and 'what' in the whisker sensorimotor system. *Nat. Rev. Neurosci.* **9**, 601–612 (2008).

141. Kleinfeld, D., Ahissar, E. & Diamond, M. E. Active sensation: insights from the rodent vibrissa sensorimotor system. *Curr. Opin. Neurobiol.* **16**, 435–444 (2006).

142. Prsa, M., Morandell, K., Cuenu, G. & Huber, D. Feature-selective encoding of substrate vibrations in the forelimb somatosensory cortex. *Nature* **567**, 384–388 (2019).

143. Micallef, A. H., Takahashi, N., Larkum, M. E. & Palmer, L. M. A Reward-Based Behavioral Platform to Measure Neural Activity during Head-Fixed Behavior. *Front. Cell. Neurosci.* **11**, 156 (2017).

144. Vallbo, A. B. & Johansson, R. S. Properties of cutaneous mechanoreceptors in the human hand related to touch sensation. *Hum. Neurobiol.* **3**, 3–14 (1984).

145. Woolsey, T. A. & Van der Loos, H. The structural organization of layer IV in the somatosensory region (SI) of mouse cerebral cortex. The description of a cortical field composed of discrete cytoarchitectonic units. *Brain Res.* **17**, 205–242 (1970).

146. Oh, S. W. *et al.* A mesoscale connectome of the mouse brain. *Nature* **508**, 207–214 (2014).

147. Reep, R. L., Chandler, H. C., King, V. & Corwin, J. V. Rat posterior parietal cortex: topography of corticocortical and thalamic connections. *Exp. Brain Res.* **100**, 67–84 (1994).

148. Urbain, N. & Deschênes, M. A New Thalamic Pathway of Vibrissal Information Modulated by the Motor Cortex. *J. Neurosci.* **27**, 12407–12412 (2007).

149. Yamawaki, N. & Shepherd, G. M. G. Synaptic Circuit Organization of Motor Corticothalamic Neurons. *J. Neurosci.* **35**, 2293–2307 (2015).

150. Casas-Torremocha, D., Clascá, F. & Núñez, Á. Posterior Thalamic Nucleus Modulation of Tactile Stimuli Processing in Rat Motor and Primary Somatosensory Cortices. *Front. Neural Circuits* **11**, (2017).

151. Wimmer, V. C., Bruno, R. M., de Kock, C. P. J., Kuner, T. & Sakmann, B. Dimensions of a projection column and architecture of VPM and POm axons in rat vibrissal cortex. *Cereb. Cortex N. Y. N 1991* **20**, 2265–2276 (2010).

152. Petreanu, L., Mao, T., Sternson, S. M. & Svoboda, K. The subcellular organization of neocortical excitatory connections. *Nature* **457**, 1142–1145 (2009).

153. Ohno, S. *et al.* A Morphological Analysis of Thalamocortical Axon Fibers of Rat Posterior Thalamic Nuclei: A Single Neuron Tracing Study with Viral Vectors. *Cereb. Cortex* **22**, 2840–2857 (2012).

154. Diamond, M. E., Armstrong-James, M., Budway, M. J. & Ebner, F. F. Somatic sensory responses in the rostral sector of the posterior group (POm) and in the ventral posterior medial nucleus (VPM) of the rat thalamus: Dependence on the barrel field cortex. *J. Comp. Neurol.* **319**, 66–84.

155. Diamond, M. E., Armstrong-James, M. & Ebner, F. F. Somatic sensory responses in the rostral sector of the posterior group (POm) and in the ventral posterior medial nucleus (VPM) of the rat thalamus. *J. Comp. Neurol.* **318**, 462–476.

156. Mease, R. A., Sumser, A., Sakmann, B. & Groh, A. Corticothalamic Spike Transfer via the L5B-POm Pathway in vivo. *Cereb. Cortex N. Y. NY* **26**, 3461–3475 (2016).

157. Veinante, P., Jacquin, M. F. & Deschênes, M. Thalamic projections from the whisker-sensitive regions of the spinal trigeminal complex in the rat. *J. Comp. Neurol.* **420**, 233–243 (2000).

158. Groh, A. *et al.* Convergence of Cortical and Sensory Driver Inputs on Single Thalamocortical Cells. *Cereb. Cortex N. Y. NY* **24**, 3167–3179 (2014).

159. Jeong, M. *et al.* Comparative three-dimensional connectome map of motor cortical projections in the mouse brain. *Sci. Rep.* **6**, 20072 (2016).

160. Casas-Torremocha, D. *et al.* Posterior thalamic nucleus axon terminals have different structure and functional impact in the motor and somatosensory vibrissal cortices. *Brain Struct. Funct.* **224**, 1627–1645 (2019).

161. Escudero, G. & Nuñez, A. Medial Prefrontal Cortical Modulation of Whisker Thalamic Responses in Anesthetized Rats. *Neuroscience* (2019) doi:10.1016/j.neuroscience.2019.01.059.

162. Masri, R., Trageser, J. C., Bezdudnaya, T., Li, Y. & Keller, A. Cholinergic Regulation of the Posterior Medial Thalamic Nucleus. *J. Neurophysiol.* **96**, 2265–2273 (2006).

163. Gharaei, S., Honnuraiah, S., Arabzadeh, E. & Stuart, G. J. Superior colliculus modulates cortical coding of somatosensory information. *bioRxiv* (2019) doi:10.1101/715847.

164. Williams, L. E. & Holtmaat, A. Higher-order thalamocortical inputs gate synaptic long-term potentiation via disinhibiton. (2018) doi:10.1101/281477.

165. Mease, R. A., Metz, M. & Groh, A. Cortical Sensory Responses Are Enhanced by the Higher-Order Thalamus. *Cell Rep.* **14**, 208–215 (2016).

166. Zhang, W. & Bruno, R. M. High-order thalamic inputs to primary somatosensory cortex are stronger and longer lasting than cortical inputs. *eLife* **8**,.

167. Mease, R. A., Metz, M. & Groh, A. Cortical Sensory Responses Are Enhanced by the Higher-Order Thalamus. *Cell Rep.* **14**, 208–215 (2016).

168. Hong, Y. K., Lacefield, C. O., Rodgers, C. C. & Bruno, R. M. Sensation, movement and learning in the absence of barrel cortex. *Nature* **561**, 542–546 (2018).

169. Castejon, C., Barros-Zulaica, N. & Nuñez, A. Control of Somatosensory Cortical Processing by Thalamic Posterior Medial Nucleus: A New Role of Thalamus in Cortical Function. *PLoS ONE* **11**, (2016).

170. Moore, J. D., Lindsay, N. M., Deschênes, M. & Kleinfeld, D. Vibrissa Self-Motion and Touch Are Reliably Encoded along the Same Somatosensory Pathway from Brainstem through Thalamus. *PLOS Biol* **13**, e1002253 (2015).

171. Swadlow, H. A. Fast-spike interneurons and feedforward inhibition in awake sensory neocortex. *Cereb. Cortex N. Y. N 1991* **13**, 25–32 (2003).

172. Cruikshank, S. J., Lewis, T. J. & Connors, B. W. Synaptic basis for intense thalamocortical activation of feedforward inhibitory cells in neocortex. *Nat. Neurosci.* **10**, 462–468 (2007).

173. Sun, Q.-Q., Huguenard, J. R. & Prince, D. A. Barrel cortex microcircuits: thalamocortical feedforward inhibition in spiny stellate cells is mediated by a small number of fast-spiking interneurons. *J. Neurosci. Off. J. Soc. Neurosci.* **26**, 1219–1230 (2006).

174. Delevich, K., Tucciarone, J., Huang, Z. J. & Li, B. The Mediodorsal Thalamus Drives Feedforward Inhibition in the Anterior Cingulate Cortex via Parvalbumin Interneurons. *J. Neurosci.* **35**, 5743–5753 (2015).

175. Cobb, S. R., Buhl, E. H., Halasy, K., Paulsen, O. & Somogyi, P. Synchronization of neuronal activity in hippocampus by individual GABAergic interneurons. *Nature* **378**, 75–78 (1995).

176. Whittington, M. A., Traub, R. D. & Jefferys, J. G. R. Synchronized oscillations in interneuron networks driven by metabotropic glutamate receptor activation. *Nature* **373**, 612–615 (1995).

177. Purushothaman, G., Marion, R., Li, K. & Casagrande, V. A. Gating and control of primary visual cortex by pulvinar. *Nat. Neurosci.* **15**, 905–912 (2012).

178. Boyden, E. S., Zhang, F., Bamberg, E., Nagel, G. & Deisseroth, K. Millisecond-timescale, genetically targeted optical control of neural activity. *Nat. Neurosci.* **8**, 1263–1268 (2005).

179. Lee, S., Carvell, G. E. & Simons, D. J. Motor modulation of afferent somatosensory circuits. *Nat. Neurosci.* **11**, 1430–1438 (2008).

180. Jiang, X. *et al.* Principles of connectivity among morphologically defined cell types in adult neocortex. *Science* **350**, aac9462 (2015).

181. Oláh, S. *et al.* Output of neurogliaform cells to various neuron types in the human and rat cerebral cortex. *Front. Neural Circuits* **1**, 4 (2007).

182. Lambert, N. A. & Wilson, W. A. Temporally distinct mechanisms of use-dependent depression at inhibitory synapses in the rat hippocampus in vitro. *J. Neurophysiol.* **72**, 121–130 (1994).

183. Thompson, S. M., Capogna, M. & Scanziani, M. Presynaptic inhibition in the hippocampus. *Trends Neurosci.* **16**, 222–227 (1993).

184. Vigot, R. *et al.* Differential Compartmentalization and Distinct Functions of GABAB Receptor Variants. *Neuron* **50**, 589–601 (2006).

185. Kohl, M. M. & Paulsen, O. The roles of GABAB receptors in cortical network activity. *Adv. Pharmacol. San Diego Calif* **58**, 205–229 (2010).

186. Aravanis, A. M. *et al.* An optical neural interface: in vivo control of rodent motor cortex with integrated fiberoptic and optogenetic technology. *J. Neural Eng.* **4**, S143-156 (2007).

187. Azimipour, M. *et al.* Extraction of optical properties and prediction of light distribution in rat brain tissue. *J. Biomed. Opt.* **19**, 75001 (2014).

188. Mo, C. & Sherman, S. M. A Sensorimotor Pathway via Higher-Order Thalamus. *J. Neurosci.* **39**, 692–704 (2019).

189. Thalamocortical Processing : Understanding the Messages That Link the Cortex to the World | Rent 9780262019309 | 0262019302. https://www.valorebooks.com/textbooks/thalamocortical-processing-understanding-the-messages-that-link-the-cortex-to-the-world/0262019302.

190. Theyel, B. B., Llano, D. A. & Sherman, S. M. The corticothalamocortical circuit drives higher-order cortex in the mouse. *Nat. Neurosci.* **13**, 84–88 (2010).

191. Sherman, S. M. Functioning of Circuits Connecting Thalamus and Cortex. *Compr. Physiol.* **7**, 713–739 (2017).

192. Chen, T.-W. *et al.* Ultrasensitive fluorescent proteins for imaging neuronal activity. *Nature* **499**, 295–300 (2013).

193. Sabatini, B. L. The impact of reporter kinetics on the interpretation of data gathered with fluorescent reporters. *bioRxiv* 834895 (2019) doi:10.1101/834895.

194. Busse, L. *et al.* Sensation during Active Behaviors. *J. Neurosci.* **37**, 10826–10834 (2017).

195. Sherman, S. M. Tonic and burst firing: dual modes of thalamocortical relay. *Trends Neurosci.* **24**, 122–126 (2001).

196. Steriade, M. & Llinás, R. R. The functional states of the thalamus and the associated neuronal interplay. *Physiol. Rev.* **68**, 649–742 (1988).